Fall 12-6-2010

# Soil Behavior under Blast Loading

Jichong An
*University of Nebraska*, jan@unomaha.edu

# SOIL BEHAVIOR UNDER BLAST LOADING

by

Jichong An

A DISSERTATION

Presented to the Faculty of

The Graduate College at the University of Nebraska

In Partial Fulfillment of Requirements

For the Degree of Doctor of Philosophy

Major: Engineering

(Civil Engineering)

Under the Supervision of Professor Christopher Y. Tuan

Lincoln, Nebraska

December, 2010

# SOIL BEHAVIOR UNDER BLAST LOADING

Jichong An, Ph.D.

University of Nebraska, 2010

Advisor: Christopher Y. Tuan

Understanding the behavior of soil under blast loading is very important to engineers in mining, tunneling, and military construction. Due to the very complex structure of a soil mass it is very difficult to describe its constitutive relation, especially when it has different water contents and it is under blast loading conditions. New protective system designs subjected to blast loading need to be proved its validation prior to predict effect of explosive before implementation. Full-scale, buried explosive tests are costly. Finite element simulations play a significant role in the design of protective systems, for example a bottom platform of lightweight vehicles, against underground explosion.

The Perzyna viscoplastic cap model has been shown to be a valid model for use in the simulations of dry soil behavior under both static and dynamic loading. This model is a dramatic improvement over the inviscid cap model for soil behavior under high strain rate loading, such as from an explosion. However, soil should be modeled as a three-

phase porous media to accommodate various degrees of water saturation. This is especially true for the soil mass surrounding the source of energy release, as each of the three phases responds differently to shock loading. To improve the model accuracy, a revised model comprising a Gruneisen equation of state (EOS) for each of the three phases has been developed. These equations of state for solid, water and air have been integrated with a viscoplastic cap model to simulate behaviors of soil with different degrees of water saturation.

These EOS models as well as the viscoplastic cap model are implemented into LS-DYNA as user-supplied subroutines for numerical simulation of six explosive tests in dry soil as well as in saturated soil. The shock front time of arrival, the air pressure directly above the buried explosive, and the ejecta heights predicted by the revised cap model agree fairly well with the experimental data. Four elements from finite element mash are selected to observe three phases volume fractions change. There is noticeable improvement in the prediction of saturated soil behavior than dry soil behavior under blast loading. It is concluded that the revised model is adequate for blast loading behavior simulations for soil with different degrees of water saturation.

## ACKNOWLEDGEMENTS

I would like to record my heartfelt gratitude to one and all that helped and encouraged me during the course of my doctoral program at UNL.

First, I would like to thank my advisor, Dr. Christopher Y. Tuan. He initiated my doctoral program at UNL in 2006 and he has been very patient with me during my working with him. His thoughtful advice has saved me from stepping onto the wrong path. His enthusiasm towards every tiny accomplishment has encouraged my completing this research work. I am indebted to him for the time he has given in guiding me in the research and editing my dissertation. I feel myself privileged to have known him closely and to have worked under him.

My wife, Jianping Liu, has always been my constant source of inspiration throughout my educational career at UNL. Jianping was instrumental in my coming to the United States for higher studies. She is always patient and understanding. Without her love, help and support, I could not have completed my doctoral program. I am proud of her.

My parents back home in China have always blessed me in my endeavor. They are in my thoughts and prayers. Their unconditional love, blessings and moral support provided a lot of comfort at times of frustration and stress during the course of my doctoral program.

I would like to record my thankfulness to my supervisory committee members, Drs. Maher K. Tadros, Andrzej S. Nowak, Ece Erdogmus, John Rohde and Mingsheng Liu for their help and guidance during the course of my dissertation. Dr. Ece Erdogmus and Dr. John Rohde provided me valuable input as reading committee members. I thank them for their critical comments and review of the dissertation. I thankfully acknowledge the help and support that I received from Dr. Mohammed Dahab and Dr. John Rohde who offered me teaching assistantship for the Foundation Engineering class. I also thank our departmental Secretary, Ms. Arlys Blakey for all her assistance during my doctoral program at UNL.

I would also like to thank Dr. David Swanson, Mr. Tom Harvill for their kind help during finite element simulations using the Research Computing Facilities.

And I would also like to thank Mr. Xiaoli Tong, formerly a graduate research assistant to Dr. Tuan, who is a great source of help during my Ph.D. program.

Finally, I would like to thank Dr. Bryan Cheeseman and Dr. Chian-Fong Yen and Dr. Arizon at the U.S. Army Research Laboratory(ARL), Aberdeen Proving Ground, Maryland, for providing valuable information about LS-DYNA and related literature to me. Their collaborations and feedbacks are invaluable for improving this research. I gratefully acknowledge the financial support received from ARL for this research.

I would once again acknowledge the help and encouragement offered to me by all my teachers, friends, family and well wishers. Thank you so much. Your guidance, constructive criticism, help and encouragement really made the difference.

# TABLE OF CONTENTS

# LIST OF FIGURES

# LIST OF TABLES

# CHAPTER ONE INTRODUCTION

## 1.1 BACKGROUND

Many commercial and military endeavors, such as defense, construction, earthquake prevention, disaster mitigation, and mining, involve soil dynamics. Soil behavior under blast loading have been studied by engineers and researchers (Wang and Lu 2003; Tong and Tuan 2007; Grujicic et al. 2008). Soil is an assemblage of individual particles, rather than a continuum, that soil may have various degrees of water saturation. A rapid release of energy from a buried explosion causes a sudden rise of pressure or a shock front propagating through a soil medium, it is very challenging to accurately predict soil behavior under blast loading. Therefore, to date common practice in modeling soil behavior under blast loading is mainly based on empirical formulae from field tests (Wang et al. 2004). Since conditions varied in those test sites, predictions using those empirical formulae scatter significantly. Discrepancy at the same scaled distance could be more than two orders of magnitude between dry and saturated soils (Drake and Little 1983).

Soil is composed of solid particles with different sizes and shapes that form a skeleton and the voids are filled with water and air. The soil is saturated if all the voids are filled with water. Otherwise, the soil is partially saturated. If all the voids are filled with air, the soil is said to be dry. It is a common practice in soil mechanics to assume that the solid particles do not deform and the water phase is incompressible. Hence, external loading is supported by the skeleton and the water. The “effective stress” is the

average stress on a plane through the soil mass, rather than the contact stress between the solid particles. The stress on the water and the air is called “pore pressure.” The principle of effective stress was first recognized by Terzaghi in the mid-1920s during his research in soil consolidation (Budhu 2007). Soils cannot sustain significant tension, and thus the effective stress cannot be tensile. Pore water pressures, however, may be positive or negative (i.e., suction). For unsaturated soils, the effective stress (Bishop 1959) is expressed as

$$\sigma' = \sigma - u_a + \chi(u_a - u_w) \quad \text{.....(1.1)}$$

where $\sigma$ is the total stress, $u_a$ is the pore air pressure, $u_w$ is the pore water pressure, and $x$ is a factor depending on the degree of saturation. For dry soil, $x$=0; for saturated soil, $x$=1 (Loret and Khalili 2000; Budhu 2007). For instance, values of $x$ for silts are shown in FIG. 1-1.

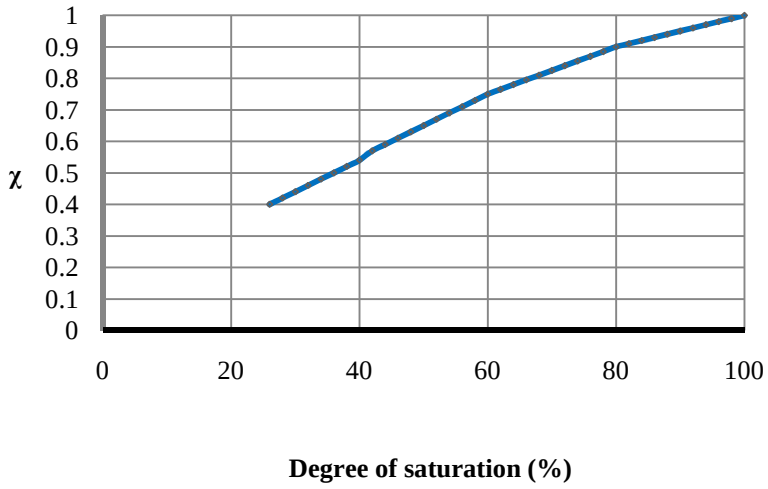


FIG. 1- 1 Values of for a silt at different degrees of saturation

A number of investigators have clearly demonstrated the effective stress hypothesis under static and quasi-static loading because the deformation of the soil skeleton depends on the effective stress caused by the structural configuration of the solid particles, while the moisture and air are assumed to flow through the skeleton driven by the pore pressure. The effective stress approach becomes invalid under shock loading. This is due to the fact that solid particles will deform under shock loading, while moisture and air are trapped in soil pores, providing additional load support.

For simulation accuracy in finite element analysis reasonable constitutive models for the involved materials are critical. Three materials, explosive, air and soil, are essential to define an underground explosion. The constitutive models for explosive and air have been reasonably described and are available for explosion simulation (Dobratz and Crawford 1985, "LS-DYNA" 2001), but soil models not be adequately have implemented into finite element programs for explosion simulations.

## 1.2 OBJECTIVES OF THE RESEARCH

The objective of this research is to develop a soil model developed for finite element simulations of explosions in soil with various degrees of saturation. Equation of state (EOS) models are developed for the three phases of the soil based on Kandaur's concept (Henrych, 1979). These EOS models are integrated with the viscoplastic cap model previously developed by Tong and Tuan (2007), and then incorporated into LS-DYNA as user-defined subroutines for soil constitutive relationship. This revised cap model is then validated by comparing simulation results against experimental data.

Explosive tests conducted by Materials Sciences Corporation (2006), in saturated soil as well as in dry soil, were used to validate the revised cap model.

## 1.3 CONTENTS

This thesis is organized as follows.

*Chapter One*: The background, objective and contents of this study are described.

*Chapter Two*: The Perzyna type viscoplastic cap model is prepared incorporating the viscoplastic cap models into LS-DYNA finite element code as user-defined material models.

*Chapter Three*: Two formulations of equation of state based on Kandaur conceptual method are described. An equation of state for soil is established and incorporated the equation of state into LS-DYNA finite element code as user-defined equation of state model.

*Chapter Four*: The models' performance is evaluated using soil viscoplastic cap model with equation of state in finite element simulation of a series of mine explosion tests. Four elements from finite element mash are selected to observe three phases volume fractions change.

*Chapter Five*: Conclusions of the research project are presented as well as suggestions and recommendations for future study.

# CHAPTER TWO VISCOPLASTIC CAP MODELS

## 2.1 INTRODUCTION

Soil has generally a complex structure consisting of mineral particles which form a soil skeleton. The interstertices between the solid particles are filled with air and/or moisture. In general, components of soil are solid, water and air and called three-phase soil. A soil element is illustrated in FIG. 2-1.

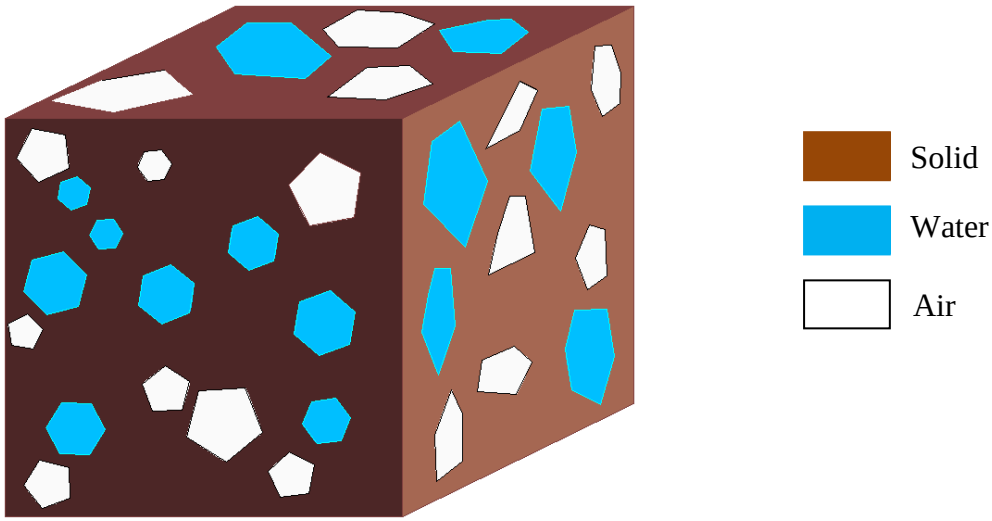


FIG. 2- 1 A schematic element

The soil skeleton can transmit normal stresses and shear stresses through the inter particle contacts. This skeleton of grains behaves in a very complex manner that depends on a large number of factors, among which void ratio, partial shape, distribution of partial

size and confining pressure are the most important (Lade 2005). When the pores between the solid particles are filled with air, the soil is referred to dry soil. When the pores are filled with water containing a small fraction of air the soil is called saturated. The relative volume fractions of the three constituent materials in the soil are generally quantified by the porosity, $\alpha$, and the degree of saturation, $\beta$, which are respectively defined as:

$$\alpha = \frac{V_p}{V} \quad \text{.....(2.1)}$$

and

$$\beta = \frac{V_w}{V_p} \quad \text{.....(2.2)}$$

Where $V_p$ is the volume of void (pores), $V_w$ is the volume of water and $V$ is the total volume of the three phase material.

For many low load rate processes, the overall macroscopic behavior of the soil skeleton may be defined within the principles of continuum mechanics, making it possible to simplify the modeling and apply the theories and methods of continuum mechanics.

For rapid loading conditions, soil models incorporate constitutive models of the three phases all required to define soil behavior.

## 2.2 DEVELOPMENT OF SOIL MODELS

### 2.2.1 SOIL BEHAVIOR

In this section, different characteristics of soil behavior are discussed.

(1) **Shear strength and deformation characteristics**: The energy applied to a soil through external loads may both overcome the frictional resistance between the soil particles and also to expand the soil against the confining pressure. The soil grains are highly irregular in shape and have to be lifted over one another for sliding to occur (Das, 1983). The relationship between the shear strength of a soil and its deformation characteristics depends mainly on how the volume changes during the shearing process. This behavior is called dilatancy. An increase in volume, or expansion, is known as positive dilation; while a decrease in volume, or contraction, is known as negative dilation. A typical curve of the soil dilatation under shear loading is shown in FIG. 2-2. In the case of sands, the degree of interlocking between particles is greater when the soil is densely packed. An initial expansion or dilation is necessary in order for the soil particles to more past each other. Thus the shear stress will first rise sharply to a peak value at a relatively low value of displacement, with a corresponding increase in volume. At this new volume the interlocking is reduced and consequently, as the displacement is continued, the shear stress falls back and finally levels off at an ultimate residual value (Whitlow, 1995).

(2) **Plasticity**: An increase in applied stress usually brings about some irrecoverable deformation, without any signs of cracking or disruption (unloading, see FIG. 2-2).

Most soils only have a very small elastic region and show plasticity from the onset of loading.

(3) **Strain-hardening/softening**: After an initial extension, the soil behaves as if it had acquired better elastic properties and a higher elastic limit, while at the same time it had lost a great part of the plastic strain. And yield surface changes with plastic strain development during loading (Maugin, 1992). Associated with strain-softening behavior is the tendency of dense granular and overconsolidated clays to dilate when sheared strain-hardening is associated with compaction of such materials as loose sand or normally consolidated clays experience strain-hardening (FIG. 2-2).

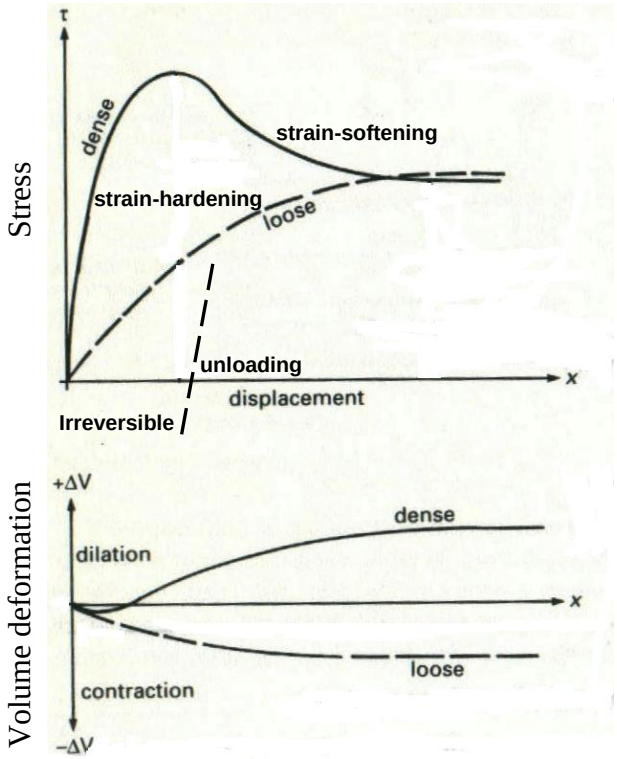


FIG. 2- 2 Response of soil with respect to shearing

(Whitlow 1995)

(4) **High Strain Rate Behaviors**: Soil with different varying water contents show different behaviors under high strain rate loading. Test data using a Split Hopkinson Pressure Bar (SHPB) (Bragov et al. 2005; Proud et al. 2007) showed that the density of soil and the shock velocity are increased with moisture content increasing. A schematic SHPB test setup is shown in FIG. 2-3.

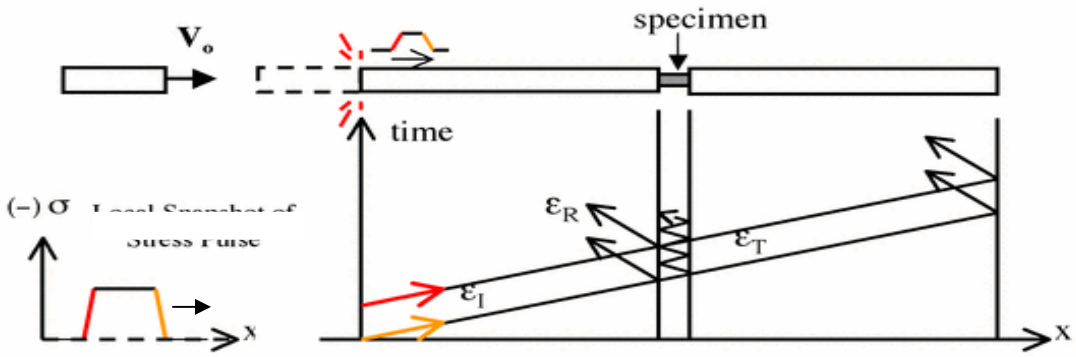


FIG. 2- 3 Split Hopkinson Pressure Bar test setup

A compressive stress pulse is induced in the incident bar by a striker, and the incident strain $\varepsilon_I$ , reflected strain $\varepsilon_R$, and transmitted strain $\varepsilon_T$ in the bars are measured. The stress-strain relation of the soil specimen and the strain rate can be determined from the elastic modulus of the bars and the recorded strain data. The confined axial stress-strain curves of the soil specimens from SHPB tests at three different strain rates are presented in FIG. 2-4.

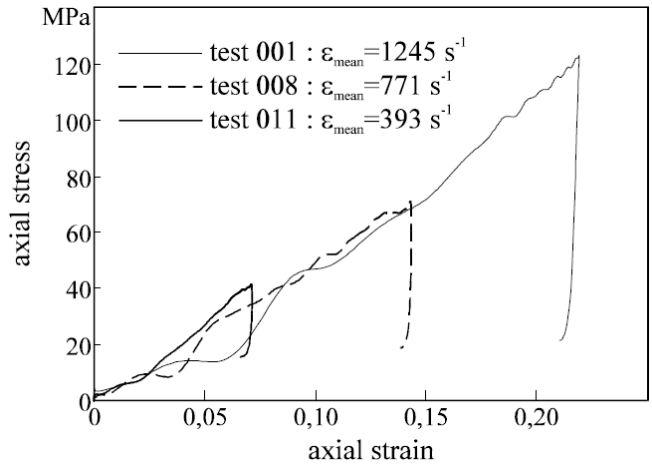


FIG. 2- 4 Split Hopkinson Pressure Bar test data

(5) **Tensile strength**: In granular media, tensile strength is a result of various interparticle physicochemical forces such as a.) van der Waals attraction, b.) electrical double layer repulsion or attraction, c.) cementation due to solute precipitation, d.) capillary stress due to the negative pore water pressure, and e.) capillary stress due to the surface tension of liquid (Lu and Likos, 2006). The macroscopic manifestation of these forces is the cohesive behavior shown widely in granular media. This strength can play an important role in stress and strain behavior. Experimental tensile strength results for the silty sand, fine sand, and medium sand are plotted in FIG 2-5, FIG 2-6 and FIG 2-7, respectively, as a function of saturation (Lu, Wu and Tan, 2007).

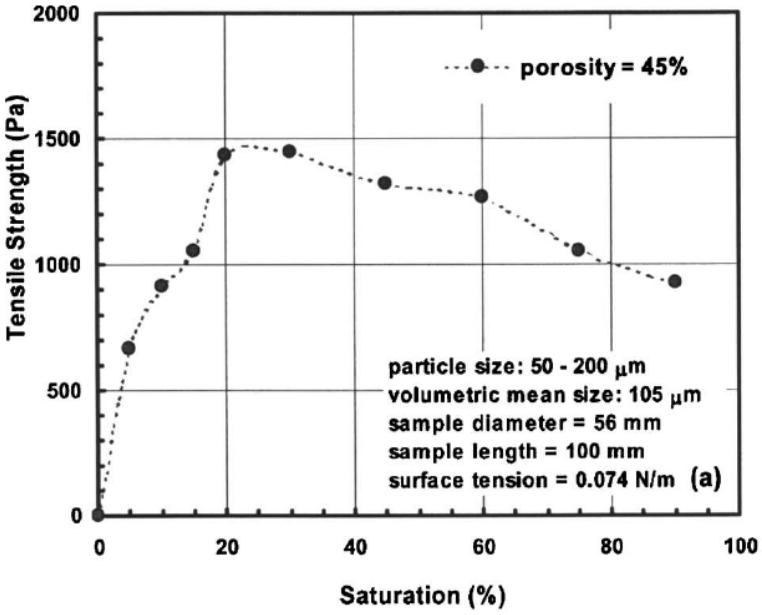


FIG. 2- 5 Tensile strength curve — silt sand

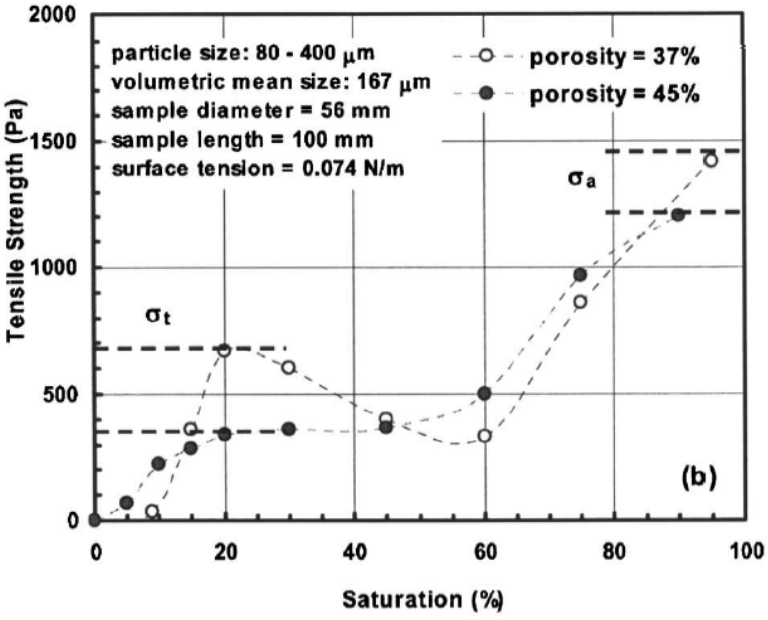


FIG. 2- 6 Tensile strength curve — fine sand

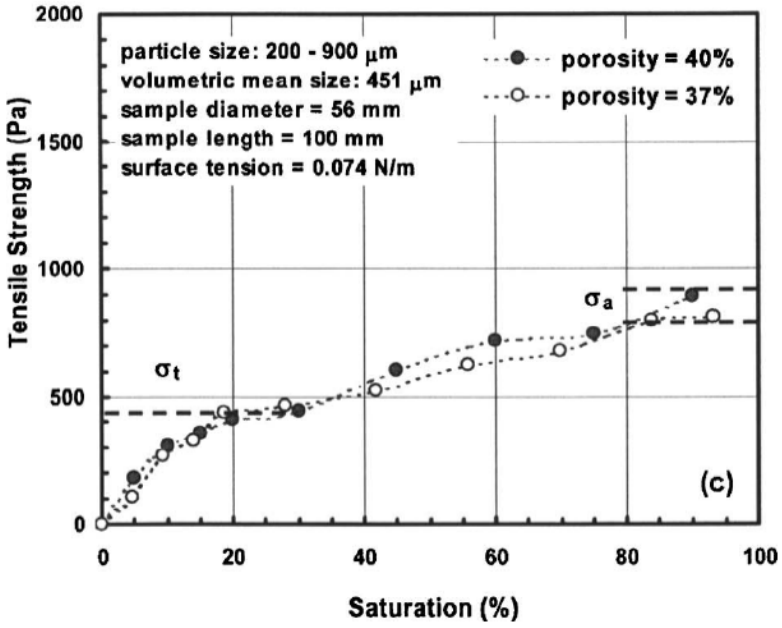


FIG. 2- 7 Tensile strength curve — medium sand

(6) **Effects of drainage and volume change**: In a saturated soil mass, an increase in applied compressive stress of creep loading causes the pore water pressure to increase. If drainage is possible an outflow of water then takes place into surrounding regions where the pore water pressure is lower. The rate of outflow depends on the permeability of the soil, in gravels and sands it is relatively rapid, but in silts and clays it is slow. As the excess pore water pressure is dissipated, the applied stress is transferred from pore pressure to effective stress. Undrained conditions occur when either drainage is prevented or when the rate of application of load is too rapid to allow significant outflow of water. The deformation of an undrained soil mass is related to the stiffness of both the pore water and the solids. When loading is applied slowly, such that the water drains away without any

increase in pore water pressure, the volume will decrease and stress-strain behavior must be defined in terms of effective stresses (Whitlow, 1995).

It should be mentioned that there are also other characteristics of soil behavior such as creep and temperature-dependency. Those aspects are not discussed here because they are beyond the scopes in this study.

### 2.2.2 SOIL MODELS

The mechanical behavior of soils may be modeled at many levels. Hooke's law of linear, isotropic elasticity may be thought of as the simplest available stress-strain relationship, but this is generally too crude to capture the essential features of soil behavior (Brinkgreve, 2005). On the other hand, a large number of constitutive models have been proposed by several researchers to describe various aspects of soil behavior in detail (Lade 2005, Prevost and Popescu 1996, Chen and Baladi 1985). Models that are appropriate to be implemented into finite element programs and to predict the soil behavior for geotechnical engineering applications are rather limited.

This study is focused on a limited number of frequently used soil models that can predict the soil behavior previously described. These models include elastic perfectly-plastic soil models, hardening-plastic soil models, elastic-viscoplastic soil models, three-phase soil models, viscoplasitc soil models, SFG (presented by Sheng, Fredlund and Gens) unsaturated soil model and bounding surface plasticity unsaturated soil models.

### 2.2.2.1 ELASTIC PERFECTLY-PLASTIC SOIL MODELS

The classical Mohr-Coulomb model is often used to describe soil behavior. In one dimension, the yield "surface" of Mohr-Coulomb mode is defined by a linear line between shear stress $\tau$ and normal stress $\sigma$ which is written as

$$f = |\tau| - (c - \sigma \tan\phi) = 0 \quad \text{.....(2.4)}$$

where the constant $c$ and $\phi$ are cohesion and internal friction angle. But in three dimensions, the yield surface defined by Eq. 2.5, is much more complicated.

$$f = \frac{1}{3} I_1 \sin\phi + \sqrt{J_2}\sin(\theta + \frac{\pi}{3}) + \sqrt{\frac{J_2}{3}}\cos(\theta + \frac{\pi}{3})\sin\phi - c\cos\phi = 0 \quad \text{.....(2.5)}$$

where $I_1$ = tr $\boldsymbol{\sigma}$ ($\boldsymbol{\sigma}$ = stress), the first invariant of stress tensor;

$J_2$ = 1/2 **s** : **s** (**s** = stress deviator), the second invariant of deviatoric stress tensor;

$\theta$ = the angle of similarity and defined by Eq. 2.6.

$$\cos 3\theta = \frac{3\sqrt{3}}{2}\frac{J_3}{J_2^{3/2}} \quad \text{.....(2.6)}$$

where $J_3$ = det |**s**|, the third invariant of deviatoric stress tensor. The failure surface of Mohr-Coulomb model in principal stress space, which is hexagonal, is shown in FIG. 2-8.

The Mohr-Coulomb model is certainly still the best known model for an isotropic pressure-sensitive soil, since the stress at failure through experimental studies agrees well with this model (Goldscheider, 1984). The model, however, is not mathematically convenient due to the presence of corners or singularities (see FIG. 2-8). A reasonable

smooth generalization of the Mohr-Coulomb model in three dimensional situations may be defined by the Drucker-Prager model (1952), which is a simple cone in principal stress space as shown in FIG. 2-9.

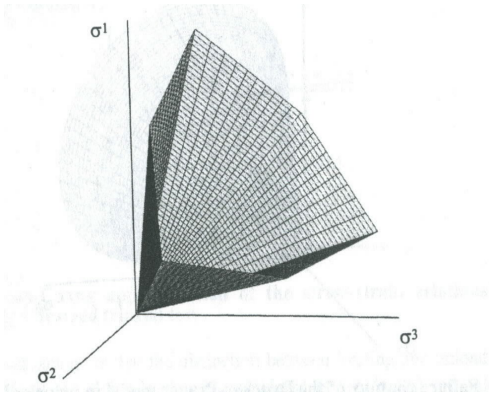


FIG. 2- 8 Mohr-Coulomb model (Brinkgreve 2005)

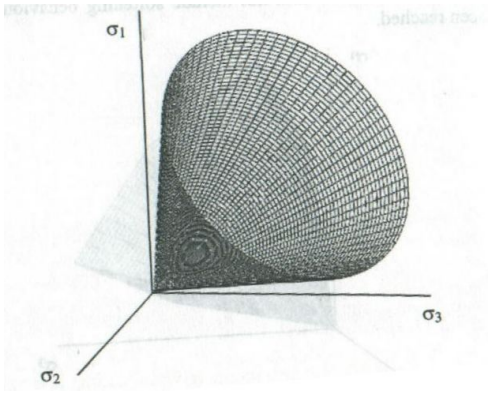


FIG. 2- 9 Drucker-Prager model (Brinkgreve 2005)

Both Mohr-Coulomb model and Drucker-Prager model capture soil plasticity behavior very well and ensure a unique solution. However, these perfectly-plastic soil models have inherent limitations and shortcomings: (1) the amount of dilatancy predicted by these models is much greater than observed experimentally; (2) tests indicate a considerable hysteresis in a hydrostatic loading-unloading which cannot be predicted using the same elastic bulk modulus of loading and unloading and a yield surface which does not cross the hydrostatic loading axis (DiMaggio and Sandler, 1971); (3) strain softening behavior cannot be reproduced; and (4) strain rate effect is not considered.

### 2.2.2.2 HARDENING-PLASTIC SOIL MODELS

Considering strain hardening/softening behavior of soil, it is logical to utilize the classical theories of work-hardening plasticity developed for metals. Drucker et al. (1957) first suggested that soil might be modeled as an elastic-plastic work-hardening material. They proposed that successive yield surfaces might resemble extended Drucker-Prager cone with convex end spherical caps as shown in FIG. 2-10 (Chen and Baladi 1985). As the soil strain hardens, both the cone and the end cap expand. This concept of cap envelope was a major step forward toward a more realistic representation of soil behavior. Based on this concept, numerous work-hardening soil models have been developed. Generally these models can be classified into two groups: modified Cam-clay model and generalized cap model.

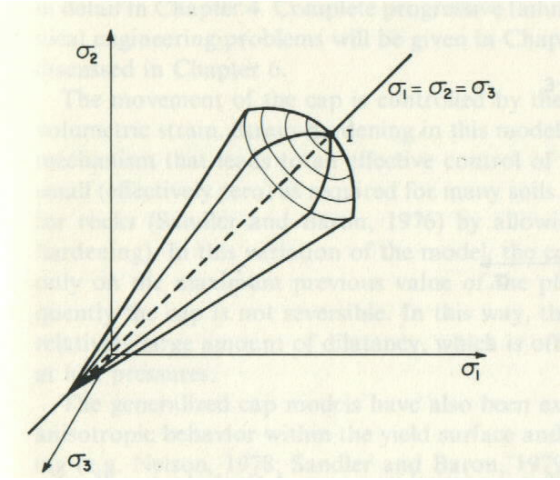


FIG. 2- 3 A Drucker-Prager type of strain-hardening cap model

(Chen and Baladi 1985)

The modified Cam-clay model was developed at Cambridge University by Roscoe et al. (1963). This model is based on critical state theory and originally meant to simulate the behavior of near-normally consolidated clays under triaxial compression test conditions. The fundamental concept of this model is that there exists a unique failure surface that defines failure of a soil irrespective of the history of loading or stress paths followed. The yield surface is assumed to be an ellipse and may be expanded with the increase of volumetric strain, as shown in FIG. 2-11 in the stress space of $I_1 \sim \sqrt{J_2}$.

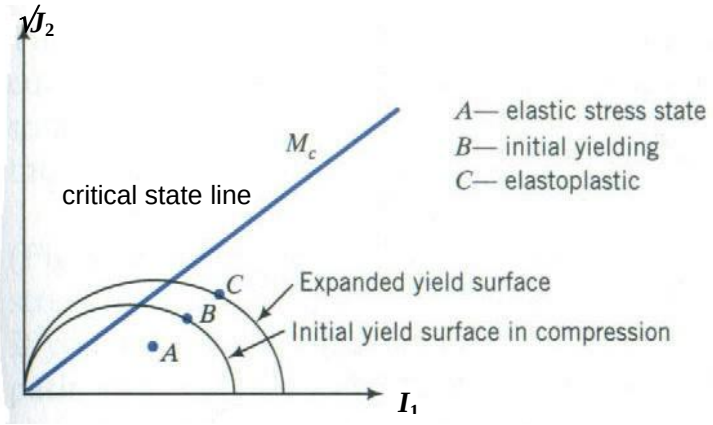


FIG. 2- 4 Modified Cam-Clay model

By taking Drucker-Prager yield surface as the critical state, the Cam-clay models can not only predict the failure behaviors very well, but also describe the nonlinear and stress-path dependent behaviors prior to failure accurately, especially for clay-type soils. This model, however, still has some disadvantages (DiMaggio and Sandler, 1971): (1) the discontinuous slope at the intersection with the $I_1$ axis predicts behavior that does not seem to be supported by experiments; (2) points on the yield surface above the critical state line do not satisfy Drucker's postulate of stability.

The generalized cap model was first proposed by DiMaggio and Sandler (1971) based on the concept of Drucker et al (1957). The yield function consists of a perfectly-plastic (failure) portion fitted to a strain-hardening elliptical cap as shown in FIG. 2-12. The movement of the cap surface is controlled by the increase or decrease of the plastic volumetric strain, strain-hardening can therefore be reversed. It is this mechanism that leads to an effective control of dilatancy, which can be kept quite small as required for many soils. Moreover, the functional forms for both the perfectly-plastic and strain-hardening portions may be quite general and allow for the fitting of a wide range of material properties. With the associated flow rule, this model may satisfy all the theoretical requirements of stability, uniqueness and continuity. The agreement between model behaviors and static experimental results for granular soils are reasonably good. As for the disadvantages for this model, one is the corners at the intersection of the yield curves which may cause mathematical problems. If the stress status happens to fall in the corners, the consistency condition may not be fulfilled.

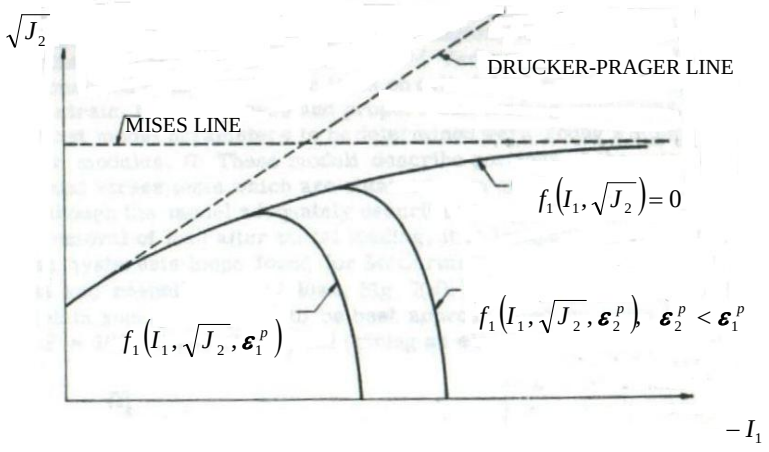


FIG. 2- 5 Yield surface of generalized cap model

(DiMaggio and Sandler 1979)

Numerous formulations have been proposed in the literature to improve the capacity of this model. Sandler et al (1976) introduced a more generalized cap model with different modulus on loading and unloading. Later Sandler and Rubin (1979) devised a cap model algorithm which permitted to obtain flexibility with respect to changes in functional forms and parameters. Simo et al (1988) proposed a new algorithm in which special attention was paid to the singular corner regions at the intersection of the yield surfaces in order to be consistent with the notion of the close-point projection method. Various smooth cap models were also proposed to eliminate the numerical problem at corners (Rubin 1991, Schwer and Murry 1994). The continuous surface cap model developed by Rubin (1991) is shown in FIG. 2-13.

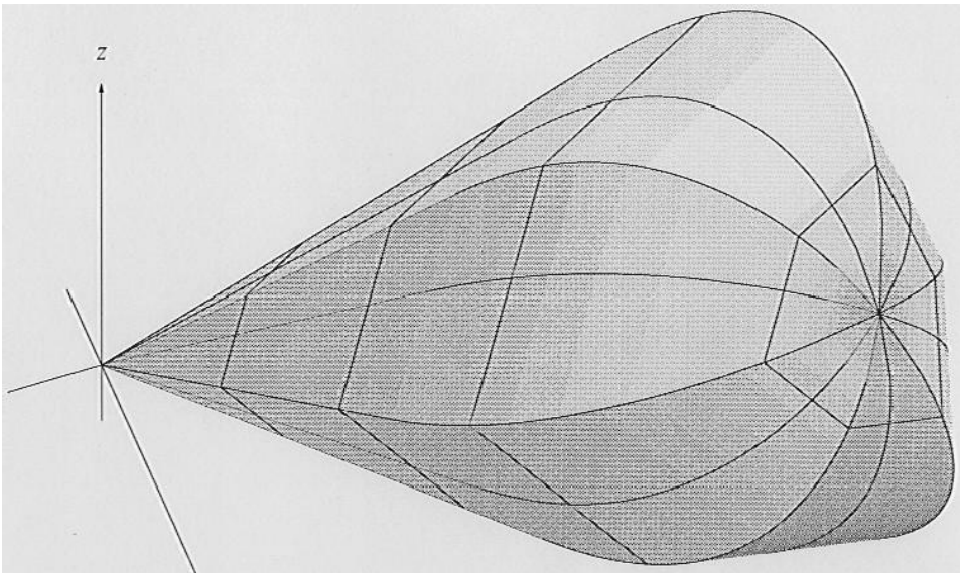


FIG. 2- 6 Stress Space View of Continuous Surface cap model

(Rubin 1991)

### 2.2.2.3 THREE-PHASE SOIL MODELS

In the early 1980s, the development of constitutive equations for saturated soils required three main components: the concept of effective stress; elastic-plastic models based on effective stress able to describe the behavior of drained soil under complex loading paths and finally, the theory of mixtures for a solid skeleton and fluid. Loret and Khalili (2000) developed a three-phase model for unsaturated soils which despite the similarity of the framework presented. There are numerous differences between the saturated and unsaturated soils. For saturated soils, the concept effective stress developed by Terzaghi is seldom questioned in its role describing the plastic behavior of saturated soils. The situation is far from being identical for unsaturated soils, which are three-phase materials. Bishop and Blight (1963) provided experimental evidence supporting the validity of Bishop's stress, they observed that the volumetric characteristics and shear-strength do not change if the effective stress for the individual components vary in such a way as to keep the net stress and suction constant. However, Jennings and Burland (1962) questioned the validity of the principle of effective stress in the deformation behavior of unsaturated soils arguing that it cannot explain the collapse phenomenon observed during wetting. On the other hand, they agree that the shear-strength depends on an effective stress of the form proposed by Bishop. Burland (1965) further resorted to arguments of theoretical nature reasoning against adding a macroscopic quantity, the net stress, and a microscopic quantity, the suction. Although this was not checked, their arguments have been widely accepted and several researchers have concluded that the behavior description of unsaturated soils should consider net stress and suction as two independent

variables. Effective stress is the key quantity that governs the material behavior, both in the elastic and plastic regimes.

The yield surface of this model is elliptical in the plane effective mean-stress $\bar{p}$ and shear-stress $q$ with the following equations.

$$\bar{p} = -\frac{1}{3} tr\bar{\sigma} \quad \text{.....(2.7)}$$

$$q = \left( \frac{3}{2} dev\bar{\sigma} : dev\bar{\sigma} \right)^{1/2} \quad \text{.....(2.8)}$$

The third invariant of the effective stress is not accounted for and the cross-sections along deviatoric planes are circular, FIG2-14,

$$f = f(\bar{p}, q, p_c) = \frac{q^2}{M^2 \bar{p}} + \bar{p} - p_c \quad \text{.....(2.9)}$$

where $M$ is the slope of the critical state line; it is assumed to be a material parameter, independent in particular of suction. The size of the yield surface can be measured by the pre-consolidation stress $P_c$.

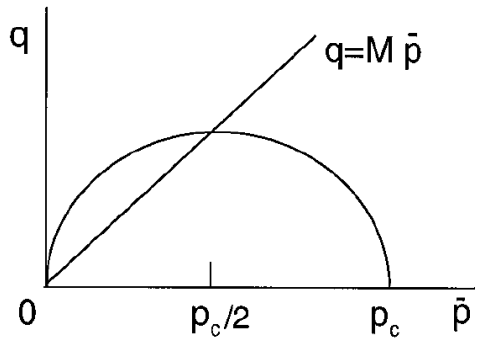


FIG. 2- 7 Yield Surface of the Modified Cam-Clay Model in terms of the Effective Mean-Stress and Shear Stress (Loret and Khalili 2000)

However, the three-phase soil model has the limitations and shortcomings: (1) experimental results are not ready available to justify the use of the complex model; and (2) the identification of material coefficients require the use of experiments ,for example, the soil-water characteristic curve is incorporated into the model.

### 2.2.2.4 VISCOPLASTIC SOIL MODELS

Viscoplastic models are expansion of plastic models which include rate effects. If the yield surfaces in viscoplastic model are taken the same as those in plastic model, a simple explanation of the difference between viscoplastic and plastic solution may be shown in FIG. 2-15. In the stress space of $I_1 \sim \sqrt{J_2}$, the plastic solution ($\bar{\boldsymbol{\sigma}}_{n+1}$) must be lie on one of the yield surfaces, this is violated. The viscoplastic solution ($\boldsymbol{\sigma}_{n+1}$) may be outside of the yield surface due to the rate effect. From the point view of numerical calculation, plasticity may be considered as a special case of viscoplasticity when strain rate is low enough to be neglected. Viscoplasicity is an improvement of plasticity in its ability to predict the soil behavior over a wide range of loading rate.

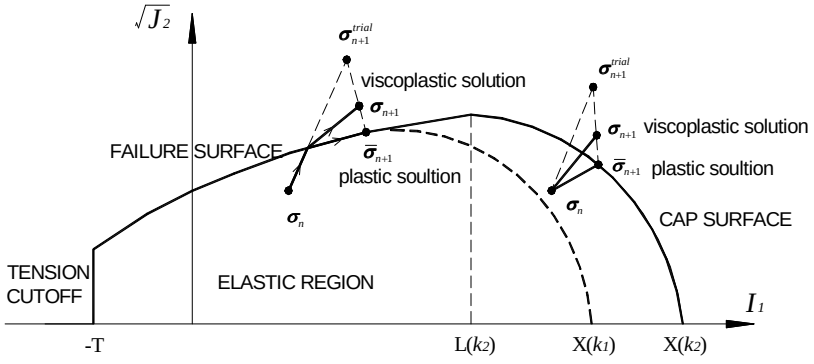


FIG. 2- 8 Viscoplasticity vs. plasticity

The most well-known formulation of viscoplasticity is based on Perzyna's theory (1966), wherein viscous behavior is modeled with a time-rate flow rule. The flow rule is assumed to be associative such that the viscoplastic potential is identical or at least proportional to the yield surface (Katona 1984, Chen and Baladi 1985, Simo et al. 1988). Perzyna (1966) pointed out that the models with rate-dependent elastic response (i.e. viscoelastic models such as Murayama and Shibata (1964)) are mathematically very complicated. In addition, rate-independent elastic response models, because of their relative mathematical simplicity and their similarities with the inviscid theory of plasticity, may be more appropriate for practical engineering applications (Perzyna 1966, Swift 1975). Also, viscous effects appear to be more evident in the plastic range for most clay. Models which explicitly incorporate time into the stress-strain relations (Matsui and Abe 1985, Sekiguchi 1984) have the drawback of predicting time-dependent deformations under zero effective stress condition. Also, it is difficult to determine the correct value of the material time parameter if the stress history is not known. Dafalias (1982), from microscopic and macroscopic observations of the structure and response of clays, has concluded the constitutive relations can best be obtained by considering the plastic strains as a combination of rate-dependent and non-rate dependent components (elastoplastic viscoplastic models such as those of Kaliakin (1985) and Broja and Kavazanjian (1985)). However, there is a difficulty in this formulation. Beyond a cetain strain rate, further increases do not affect the stress-strain relationship (Dafalias, 1982). Effects of very high strain rates cannot therefore be predicted (Whitman 1957, Richardson and Whitman 1963, Adachi, Mimura and Oka 1985). Although the viscoplastic model of the Perzyna type has been validated through simple dynamic tests,

little research work has attempted to apply this model to simulate the soil behavior under an extremely high strain-rate loading such as explosions.

Another popular format of viscoplasticity is based on Duvant-Lions' theory (1972), wherein the viscoplastic solution is simply constructed through the relavent plastic solution. The biggest advantage of the Duvant-Lions' model is its ease in numerical implementation, only a simple stress update loop is needed to add into existing plasticity algorithms. Also deterioration from viscoplastic solution to plastic solution under a low strain rate is exactly guaranteed (Simo et al 1987). Compared to the Perzyna type, the viscoplastic model of the Duvant-Lions' type has not been well validated experimently.

#### 2.2.2.5 SFG UNSATURATED SOIL MODEL

Since the pioneering work of Alonso et al. (1990), a number of elastoplastic constitutive models have been developed for modeling the behavior of unsaturated soils (Gens 1996; Jommi 2000; and Gens etal. 2006). Early models dealt only with the stress-suction-strain relationships of unsaturated soils (Kohgo et al. 1993; Wheeler and Sivakumar 1995; Bolzon et al. 1996; Cui and Delage 1996; Loret and Khalili 2002). These models are based on the same basic assumptions and largely fall in the same framework as Alonso et al. (1990), although different constitutive equations and different stress variables are used. The model by Alonso et al. (1990), generally referred to as Barcelona Basic Model, remains as one of the fundamental models for unsaturated soils. More recent models have incorporated suction-saturation relationships with hysteresis

(Wheeler 1996; Dangla et al. 1997; Vaunat et al. 2000; Gallipoli et al. 2003; Wheeler et al. 2003; Sheng et al. 2004; Santagiuliana and Schrefler 2006; Sun et al. 2007).

Usually, unsaturated soil models use a load-collapse yield surface to define the variation of the apparent pre-consolidation stress along the soil suction axis. The apparent pre-consolidation stress is usually assumed to increase with increasing suction. Under such a framework, these models are able to reproduce some basic features of unsaturated soil behavior, for example, the volume change upon wetting and the increase of shear strength with suction. However, some basic questions, like how yield stress changes with soil suction, have not been fully answered. The SFG model presents a volumetric behavior model for independent changes of mean net stress and suction. Based on this volumetric relationship, the change of the yield stress with suction and the hardening laws that govern the evolution of the yield surface are derived. Recent developments have included combining both stress-strain and suction-saturation relations of unsaturated soils are also incorporated into this model.

The SFG model is expressed in the plane mean net stress $\bar{p}$ and suction $s$ with

$$\bar{p} = p - u_a \quad \text{.....(2.10)}$$

$$s = u_a - u_w \quad \text{.....(2.11)}$$

where $u_a$ is the pore air pressure and $u_w$ is pore water pressure.

A yield surface can be expressed as,

$$\bar{p}_{yn} = \begin{cases} \bar{p}_{yn0} - s & s < s_{sa} \\ \dfrac{\bar{p}_{yn0}}{\bar{p}_{y0}}\left[\bar{p}_{y0} + s - s_{sa} - (s_{sa}+1)\ln\dfrac{s+1}{s_{sa}+1}\right] - s & s \geq s_{sa} \end{cases} \quad \text{.....(2.12)}$$

where $s_{sa}$ is the saturation suction and $\bar{p}_{yn0}$ is the new yield stress at zero suction. If $\bar{p}_{yn0}$ is known, Eq. (2-10) can be used to find the new yield surface, $\bar{p}_{yn}$. Alternatively, if the new yield stress at a given suction is known, Eq. (2-10) can be used to find $\bar{p}_{yn0}$ .

The new yield surface $\bar{p}_{yn}$ for $\bar{p}_{yn0}$ =500 kPa is shown in FIG. 2-16. The yield stress along the new yield surface does not monotonically decrease with increasing suction.

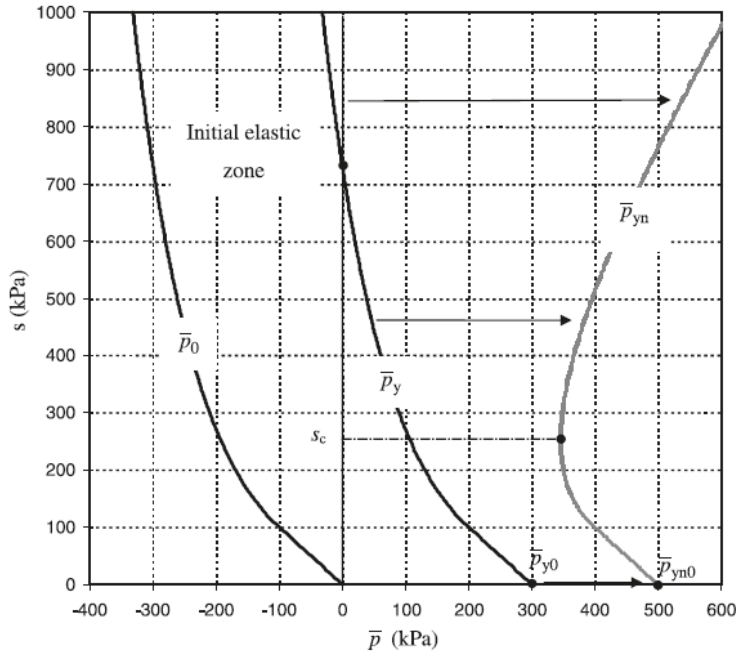


FIG. 2- 9 Initial Yield Surface for a Soil That was Consolidated to 300 kPa at Zero Suction and Its Evolution When the Soil is then Loaded at Different Suction Levels

(Sheng, D., Fredlund, D.G. and Gens, A. 2008)

However, the SFG soil model has limitation and shortcomings: (1) there are not enough experimental data at present to define precisely the suction-dependence of material parameters and (2) the yield surface function is different with different suction level.

### 2.2.2.6 BOUNDING SURFACE PLASTICITY UNSATURATED SOIL MODEL

Bounding surface plasticity was first developed for metals by Dafalias and Popov (1976), and later applied to clays by Dafalias and Herrmann (1982), to pavement base materials by McVay and Taesiri (1985), and to sands by Hashigushi and Ueno (1977), Aboim and Roth (1982) and Bardet (1985). By broadening the scope of conventional plasticity theory, bounding surface plasticity provides a flexible theoretical framework to model the cyclic behavior of engineering materials.

The bounding surface plasticity soil model represents the macroscopic behavior of soil in terms of strain and effective stress and is useful by the solution of boundary value problems with finite element or finite difference methods. The advantages of bounding surface plasticity theory over conventional plasticity have investigated for cyclic as well as monotonic loadings. The existence and direction of the irreversible strain increment, which requires non-associative the flow rule to be realistically simulated at the failure state, can be defined by only one surface in bounding surface plasticity.

Russell and Khalili (2005) developed an unsaturated soil model using bounding surface plasticity. However, this model took particle crushing into account, making it complex and difficult to apply for ordinary cases in soil mechanics. Wong, Morvan and

Branque (2009) developed a new bounding surface plasticity model for unsaturated soils with a small number of parameters based on Bardet's model (Bardet, 1985). In this model, the bounding surface itself evolves through a hardening mechanism that depends on the accumulated plastic strains.

The bounding surface of this model is elliptical in the plane effective mean-stress $p'$and shear-stress $q$ with

$$p' = \frac{1}{3}\left(\sigma_1' + \sigma_2' + \sigma_3'\right) \quad \text{.....(2.13)}$$

$$q = \sigma_1' - \sigma_2' \quad \text{.....(2.14)}$$

The bounding surface can be defined as (2-12), FIG. 2-17,

$$f(\bar{p}', \bar{q}', \varepsilon_p^p, s) = \left(\frac{\bar{p}' - A_\pi}{\rho - 1}\right)^2 - \left(\frac{\bar{q}}{M_\pi}\right)^2 - A_\pi^2 \quad \text{.....(2.15)}$$

where,

$$\bar{p}' = \gamma A_\pi \quad \text{.....(2.16)}$$

$$\bar{q}' = \gamma x M_\pi A_\pi \quad \text{.....(2.17)}$$

$$x = \frac{q}{Mp' + q_0} \quad \text{.....(2.18)}$$

$$\gamma = \frac{1 + (\rho - 1)\sqrt{1 + x^2\rho(\rho - 2)}}{1 + (\rho - 1)^2 x^2} \quad \text{.....(2.19)}$$

$M_\pi$ is the slope of the saturated soil critical state line (CSL). The size of the yield surface can be measured by the hardening variable $A_\pi$. $M_\pi$ and $A_\pi$ are assumed to be a material parameter, independent in particular of suction $s$. $\rho$ is a material parameter.

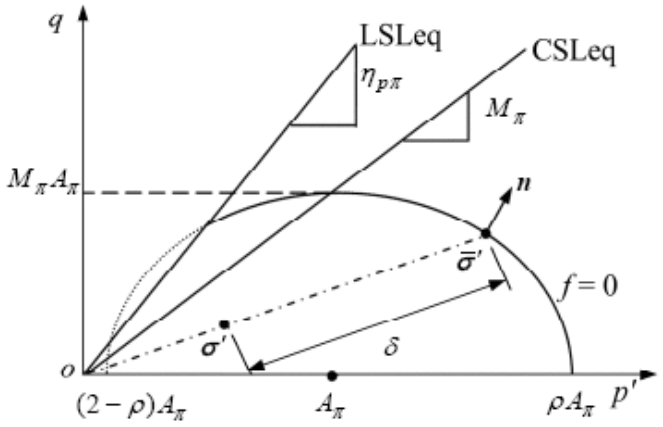


FIG. 2- 10 Yield Surface of the Modified Unsaturated Soil Model in terms of the Effective Mean-Stress and Shear Stress

(Wong, Morvan and Branque 2009)

The bounding surface plasticity soil model has the limitations and shortcomings: (1) there are not enough experimental data at present to precisely define the suction-dependence of material parameters and (2) the water retention curve in general does not define an objective relation between degree of saturation and suction.

## 2.3 VISCOPLASTIC CAP MODELS

Viscoplasticity is defined as a rate-dependent (as opposed to inviscid means rate independent) plasticity model and may be applied to the soil constitutive laws to account for the strain rate effect. A variety of viscoplastic formulations for soils have been proposed in the literature. The formulation of viscoplasticity based on Perzyna's theory (1966) is the most well-known formulation, where viscous behavior is modeled with a time-rate flow rule. The flow rule is assumed to be associative such that the viscoplastic

potential is identical or at least proportional to the yield surface (Katona 1984, Chen and Baladi 1985, Simo et al. 1988). After transition into rate-independent plasticity, this identity becomes essential although it has no great significance in viscoplasticity. The viscoplastic formulation has the following advantages: (1) the generality of the viscous flow rule offers the capability of simulating time-dependent material behavior over a wide range of loading; and (2) the extension of an inviscid cap model for viscoplasticity is relatively straightforward (Tong, 2005).

Another viscoplastic formulation of the Duvant-Lions type has been advocated by Simo et al (1988), Simo and Govindjee (1991) and Simo and Hughes (1998). The viscous behavior is constructed directly based on the difference between solutions for inviscid and the viscoplastic foumulations. The main advantage is its ease in numerical implementation, only a stress update needs to be added in an inviscid formulation in order to obtain the corresponding viscoplastic solution.

The viscoplastic cap model is an effective material model to simulate soil behavior under high strain rate loading. Tong (2005) applied viscoplastic cap model in LS-DYNA to simulate a series of explosions in soil. Comparisons with experimental results, the simulations of soil ejecta, crater and explosive clouds from landmine-explosion tests were reasonably good.

In this chapter, two type of viscoplastic cap models are proposed based on Perzyna's theory and Duvant-Lions' theory. The plastic yield functions are patterned on the generalized two-invariant cap model. Numerical algorithm is presented. The

performance of viscoplastic cap model is examined using a hypothetical uniaxial strain test and compared against experimental data under rapid loading.

In the viscoplasticity model, the total strain rate vector $\dot{\boldsymbol{\varepsilon}}$ is decomposed into an elastic component $\dot{\boldsymbol{\varepsilon}}^{e}$ and a viscoplastic component $\dot{\boldsymbol{\varepsilon}}^{vp}$

$$\dot{\boldsymbol{\varepsilon}} = \dot{\boldsymbol{\varepsilon}}^{e} + \dot{\boldsymbol{\varepsilon}}^{vp} \quad \text{.....(2.20)}$$

The elastic component is expressed as

$$\dot{\boldsymbol{\sigma}} = \mathbf{C}\,\dot{\boldsymbol{\varepsilon}} \quad \text{.....(2.21)}$$

where $\dot{\boldsymbol{\sigma}}$ = the stress rate vector and $\mathbf{C}$ = an elastic constitutive matrix.

For the viscoplastic component, it is different with the different type.

### 2.3.1 THE PERZYNA TYPE VISCOPLASTIC CAP MODEL

The viscoplastic strain rate vector is assumed to be delayed with time and is expressed as follows when assuming associated flow rule:

$$\dot{\boldsymbol{\varepsilon}}^{vp} = \eta < \phi(f) > \frac{\partial f}{\partial \boldsymbol{\sigma}} \quad \text{.....(2.22)}$$

where $\eta$ = a material constant called fluidity parameter;

The notion < > refers to the ramp function defined by $< x >= \dfrac{x + |x|}{2}$;

$f$ = plastic yield function;

$\phi(f)$ = dimensionless viscous flow function and commonly expressed in the form of

$$\phi(f) = \left(\frac{f}{f_0}\right)^N \quad \text{.....(2.23)}$$

where $N$ = an exponent; and $f_0$ = a normalizing constant with the same units as $f$.

### 2.3.1.1 STATIC YIELD FUNCTIONS

The plastic yield function $f$ is patterned in the inviscid cap model (DiMaggio and Sandler 1971, Sandler and Rubin 1979, Simo et al 1986) which is formulated in terms of the first stress invariant $I_1$ and the second deviator stress invariant $J_2$ as shown in FIG. 2-18 (Tong, 2005). The static yield surface is divided into three regions:

(a) when $I_1 \geq L$, the cap surface region $f = \sqrt{J_2} - F_c(I_1, k) = 0$

(b) when $L > I_1 > -T$ , the failure surface region $f = \sqrt{J_2} - F_e(I_1) = 0$

(c) when $I_1 \leq -T$ , the tension cutoff region $f = I_1 - (-T) = 0$

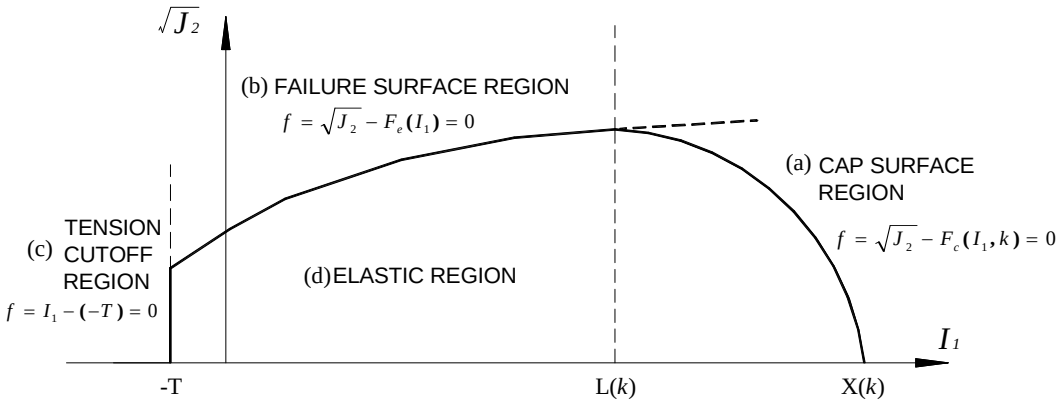


FIG. 2- 11 Static yield surface for cap model (Tong, 2005)

**(a) Cap surface portion**: the cap surface is a hardening surface in the shape of an ellipse quadrant in the stress space of $I_1$ and $J_2$. It is generally defined by

$$f\left(I_1,\sqrt{J_2},k\right)=\sqrt{J_2}-F_c(I_1,k)=\sqrt{J_2}-\frac{1}{R}\sqrt{\left(X(k)-L(k)\right)^2-\left(I_1-L(k)\right)^2}=0 \quad \text{.....(2.24)}$$

where $I_1$ = tr $\boldsymbol{\sigma}$ = $\sigma_{11}+\sigma_{22}+\sigma_{33}$; $J_2$ = 1/2 **s** : **s** =1/2 $(s_{11}^2+s_{22}^2+s_{33}^2)$ (**s** = stress deviator);

$F_c(I_1,k)$ = the loading function for cap envelope;

$R$ = a material parameter;

$k$ is a hardening parameter related to the actual viscoplastic volumetric change

$\varepsilon_v^{vp}(=\operatorname{tr}\varepsilon^{vp}=\varepsilon_{11}^{vp}+\varepsilon_{22}^{vp}+\varepsilon_{33}^{vp})$:

$$\varepsilon_v^{vp}(X(k))=W\{1-\exp[-D(X(k)-X_0)]\} \quad \text{.....(2.25)}$$

where $X(k)$ defines the intersection of the cap with the $I_1$ – axis and hence is given by

$$X(k)=k+R\cdot F_e(k) \quad \text{.....(2.26)}$$

where $F_e(k)$ =the loading function.

$L(k)$ is the value of $I_1$ at the location of the start of cap and is defined by

$$L(k)=\begin{cases}k & \text{if } k>0\\ 0 & \text{if } k\le 0\end{cases} \quad \text{.....(2.27)}$$

The cap surface may be expressed alternatively (Katona 1984) as

$$f(I_1,J_2,k)=\sqrt{\frac{(I_1-L)^2}{R^2}+J_2}-\frac{(L-X)}{R} \quad \text{.....(2.28)}$$

**(b) Failure surface portion**: the failure surface is a non-hardening, modified Drucker-Prager form with a yield function defined as

$$f\left(I_1,\sqrt{J_2}\right)=\sqrt{J_2}-F_e(I_1)=\sqrt{J_2}-\left(\alpha-\gamma\exp\left(-\beta I_1\right)+\theta I_1\right)=0 \quad \text{.....(2.29)}$$

in which $\alpha$, $\beta$, $\gamma$ and $\theta$ are material parameters.

**(c) Tension cutoff portion**: the tension cutoff surface is defined by

$$f(I_1)=I_1-(-T) \quad \text{.....(2.30)}$$

where $-T$ = tension cutoff value.

### 2.3.1.2 SOLUTION ALGORITHMS

The strain rate Eq. (2.20) and (2.21) are integrated over a time step, $\Delta t$, from $t$ to $t+\Delta t$, to yield the incremental strains and stresses:

$$\Delta\boldsymbol{\varepsilon}=\Delta\boldsymbol{\varepsilon}^{e}+\Delta\boldsymbol{\varepsilon}^{vp} \quad \text{.....(2.31)}$$

$$\Delta\boldsymbol{\sigma}=\mathbf{C}\Delta\boldsymbol{\varepsilon}^{e}=\mathbf{C}\left(\Delta\boldsymbol{\varepsilon}-\Delta\boldsymbol{\varepsilon}^{vp}\right) \quad \text{.....(2.32)}$$

where $\Delta\boldsymbol{\varepsilon}$ = the total incremental strain vector;

$\Delta\boldsymbol{\varepsilon}^{e}$ = the elastic viscoplastic incremental strain vector;

$\Delta\boldsymbol{\varepsilon}^{vp}$ = the viscoplastic incremental strain vector;

$\Delta\boldsymbol{\sigma}$ = the incremental stress vector.

Based on the Euler method, the viscoplastic incremental strain vector $\Delta\boldsymbol{\varepsilon}^{vp}$ can be approximated as

$$\Delta\boldsymbol{\varepsilon}=\left[(1-\chi)\dot{\boldsymbol{\varepsilon}}_{t}^{vp}+\chi\,\dot{\boldsymbol{\varepsilon}}_{t+\Delta t}^{vp}\right]\Delta t \quad \text{.....(2.33)}$$

in which $\chi$ is an adjustable integration parameter, $0 \le \chi \le 1$. The integration scheme is explicit if $\chi = 0$ and fully implicit if $\chi = 1$. This solution algorithm is conditionally stable

when $\chi \leq 0.5$ and unconditionally stable when $\chi > 0.5$. The fully implicit integration scheme, $\chi = 1$, is used here in the numerical algorithm just for simplification.

In the full implicit integration scheme, the viscoplastic flow (Eq. 2.33) is only determined by the gradient of the yield surface at time $t+\Delta t$. Thus, $\Delta\boldsymbol{\varepsilon}^{vp}$ may be rewritten as

$$\Delta\boldsymbol{\varepsilon}^{vp} = \Delta\dot{\boldsymbol{\varepsilon}}^{vp}\Delta t = \eta < \phi(f) > \Delta t \frac{\partial f}{\partial \boldsymbol{\sigma}} \quad \text{.....(2.34)}$$

If a plastic multiplier $\Delta\lambda$ is introduced such that

$$\Delta\lambda = \eta < \phi(f) > \Delta t \quad \text{.....(2.35)}$$

then Eq. (2.34) may be rewritten as

$$\Delta\boldsymbol{\varepsilon}^{vp} = \Delta\lambda \frac{\partial f}{\partial \boldsymbol{\sigma}} \quad \text{.....(2.36)}$$

This viscoplastic problem can be solved under the condition that the residual $\rho$, defined in Eq. (2.37), is reduced to zero during a local iteration.

$$\rho = \frac{\Delta\lambda}{\eta\Delta t} - \phi(f) \to 0 \quad \text{.....(2.37)}$$

Substituting Eq. (2.36) into Eq. (2.32) yields

$$\Delta\boldsymbol{\sigma} = \mathbf{C} : (\Delta\boldsymbol{\varepsilon} - \Delta\lambda \frac{\partial f}{\partial \boldsymbol{\sigma}}) \quad \text{.....(2.38)}$$

To compute $\Delta\lambda$, a local Newton-Raphson iteration process is applied. Note that the yield function takes the general form $f = f(\sigma, k)$. Differentiating Eq. (2.38) during iteration $i$ gives

$$\delta\boldsymbol{\sigma} = \mathbf{C} : (\delta\boldsymbol{\varepsilon} - \delta\lambda \frac{\partial f}{\partial \boldsymbol{\sigma}} - \Delta\lambda^{(i)} \frac{\partial^2 f}{\partial \boldsymbol{\sigma}^2} \delta\boldsymbol{\sigma} - \Delta\lambda^{(i)} \frac{\partial^2 f}{\partial \boldsymbol{\sigma}\, \partial\lambda} \delta\lambda) \quad \text{.....(2.39)}$$

where $\delta\boldsymbol{\sigma}$, $\delta\boldsymbol{\varepsilon}$ and $\delta\lambda$ are the iterative improvements of $\Delta\boldsymbol{\sigma}$, $\Delta\boldsymbol{\varepsilon}$ and $\Delta\lambda$, respectively, within the local iteration process.

Eq. (2.39) may be expressed alternatively as

$$\delta\boldsymbol{\sigma} = \mathbf{H} : \left[ \delta\boldsymbol{\varepsilon} - (\frac{\partial f}{\partial \boldsymbol{\sigma}} + \Delta\lambda^{(i)} \frac{\partial^2 f}{\partial \boldsymbol{\sigma}\, \partial\lambda}) \delta\lambda \right] \quad \text{.....(2.40)}$$

with a pseudo-elastic stiffness matrix **H**

$$\mathbf{H} = \left[ \mathbf{C}^{-1} + \Delta\lambda^{(i)} \frac{\partial^2 f}{\partial^2 \boldsymbol{\sigma}} \right]^{-1} \quad \text{.....(2.41)}$$

By differentiation of Eq. (2.38), the Newton-Raphson process at iteration *i* is expressed as

$$\rho^{(i)} = \left( \frac{1}{\eta \Delta t} - \frac{\partial \phi}{\partial \lambda} \right) \delta\lambda - \left( \frac{\partial \phi}{\partial \boldsymbol{\sigma}} \right)^T \delta\boldsymbol{\sigma} \quad \text{.....(2.42)}$$

Substitution of Eq. (2.40) into Eq. (2.42) yields

$$\delta\lambda = \frac{1}{\xi} \left[ \left( \frac{\partial \phi}{\partial \boldsymbol{\sigma}} \right)^T \mathbf{H}\, \delta\boldsymbol{\varepsilon} + \rho^{(i)} \right] \quad \text{.....(2.43)}$$

with

$$\xi = \left( \frac{\partial \phi}{\partial \boldsymbol{\sigma}} \right)^T \mathbf{H} \left[ \frac{\partial f}{\partial \boldsymbol{\sigma}} + \Delta\lambda^{(i)} \frac{\partial^2 f}{\partial \boldsymbol{\sigma}\, \partial\lambda} \right] + \frac{1}{\eta \Delta t} - \frac{\partial \phi}{\partial \lambda} \quad \text{.....(2.44)}$$

If a local iteration is applied, the iterative strain increment $\delta\boldsymbol{\varepsilon}$ will turn to a fixed total strain increment $\Delta\boldsymbol{\varepsilon}$ during a global iteration. The iterative algorithm for the

viscoplastic cap model of the Perzyna type, where the subscript $n$ and $n$+1 denotes the solutions at time $t$ and $t+\Delta t$ respectively, is outlined in Table 2-1.

Table 2- 1 Numerical algorithm for the Perzyna's viscoplastic model

**DATA INPUT** : $\boldsymbol{\sigma}_n, k_n, \Delta\boldsymbol{\varepsilon}$

Trial stresses : $\boldsymbol{\sigma}_{n+1}^{trial} = \boldsymbol{\sigma}_n + \boldsymbol{C}\Delta\boldsymbol{\varepsilon}$ , $k_{\mathrm{n}}$

If $f\left(\boldsymbol{\sigma}_{n+1}^{trial}, k_n\right) < 0$, elastic $\boldsymbol{\sigma}_{n+1} = \boldsymbol{\sigma}_{n+1}^{trail}$ , $k_{\mathrm{n+1}} = k_{\mathrm{n}}$ RETURN

If $f\left(\boldsymbol{\sigma}_{n+1}^{trial}, k_n\right) < 0$, viscoplastic

(a) define the initial iteration value

$$\Delta\lambda^{(0)} = 0 \ , \qquad \boldsymbol{\sigma}_{n+1}^{(0)} = \boldsymbol{\sigma}_n + \mathbf{C}\left[\Delta\boldsymbol{\varepsilon} - \Delta\lambda^{(0)}\frac{\partial f}{\partial\boldsymbol{\sigma}}\right]$$

$$\rho^{(0)} = \phi\left(\boldsymbol{\sigma}_{n+1}^{(0)}, k_n\right) - \frac{\Delta\lambda^{(0)}}{\eta\Delta t}$$

(b) do local iteration $i$

$$\mathbf{H} = \left[\mathbf{C}^{-1} + \Delta\lambda^{(i)}\frac{\partial^2 f}{\partial\boldsymbol{\sigma}^2}\right]^{-1}$$

$$\xi = \left(\frac{\partial\phi}{\partial\boldsymbol{\sigma}}\right)^T : \mathbf{H} : \left[\frac{\partial f}{\partial\boldsymbol{\sigma}} + \Delta\lambda^{(i)}\frac{\partial^2 f}{\partial\boldsymbol{\sigma}\partial\lambda}\right] + \frac{1}{\eta\Delta t} - \frac{\partial\phi}{\partial\lambda}$$

$$\Delta\lambda^{(i+1)} = \Delta\lambda^{(i)} + \frac{\rho^{(i)}}{\varsigma} \qquad \Delta k_{n+1}^{(i+1)} = \Delta\lambda^{(i+1)}\frac{\partial k}{\partial\lambda}$$

$$k_{n+1}^{(i+1)} = k_{n+1}^{(i)} + \Delta k_{n+1}^{(i+1)}$$

$$\boldsymbol{\sigma}_{n+1}^{(i+1)} = \boldsymbol{\sigma}_n + \mathbf{C} : \left[\Delta\boldsymbol{\varepsilon} - \Delta\lambda^{(i+1)}\frac{\partial f}{\partial\boldsymbol{\sigma}}\right]$$

$$\rho^{(i+1)} = \phi\left(\boldsymbol{\sigma}_{n+1}^{(i+1)}, k_{n+1}^{(i+1)}\right) - \frac{\Delta\lambda^{(i+1)}}{\eta\Delta t}$$

go back and continue until $|\rho^{(i+1)}| < \delta$

RETURN

**OUTPUT** : $\boldsymbol{\sigma}_{n+1}, k_{n+1}, \boldsymbol{\varepsilon}_{n+1}$

For the tension cutoff region, a different algorithm is needed since the yield surface for tension cutoff is independent of $J_2$. This condition is uncommon for ordinary

soil tests but must be accommodated for explosions in soil. Since very little test data is available, the following assumptions are made: (1) the viscous flow parameter under tension, $\eta_T$, may be the same as or different from that under compression; (2) the viscoplastic solution $\boldsymbol{\sigma}_{t+\Delta t}$ is presumed to be between the elastic trial stress $\boldsymbol{\sigma}^{trial}_{t+\Delta t}$ and the inviscid solution $\bar{\boldsymbol{\sigma}}_{t+\Delta t}$, and the simplest scheme is to assume that $\boldsymbol{\sigma}_{t+\Delta t}$ is on the straight line from $\boldsymbol{\sigma}^{trial}_{t+\Delta t}$ to $\bar{\boldsymbol{\sigma}}_{t+\Delta t}$, as shown in FIG. 2-19. The treatment for tension cutoff is thus proposed as follows:

(1) if $I^{trial}_{1,t+\Delta t} \le -T$ *and* $\sqrt{J^{trial}_{2,t+\Delta t}} < F_e(-T)$, then

$$I_{1,t+\Delta t} = e^{-\eta_T \Delta t} I^{trial}_{1,t+\Delta t} + (1 - e^{-\eta_T \Delta t})(-T); \quad \sqrt{J_{2,t+\Delta t}} = \sqrt{J^{trial}_{2,t+\Delta t}}$$

(2) if $I^{trial}_{1,t+\Delta t} \le -T$ *and* $\sqrt{J^{trial}_{2,t+\Delta t}} \ge F_e(-T)$, then

$$I_{1,t+\Delta t} = e^{-\eta_T \Delta t} I^{trial}_{1,t+\Delta t} + (1 - e^{-\eta_T \Delta t})(-T);$$
$$\sqrt{J_{2,t+\Delta t}} = e^{-\eta_T \Delta t} \sqrt{J^{trial}_{2,t+\Delta t}} + (1 - e^{-\eta_T \Delta t}) F_e(-T)$$

It can be shown from these conditions that the solution is plastic when $\eta_T \Delta t \to \infty$ and elastic when $\eta_T \Delta t \to 0$.

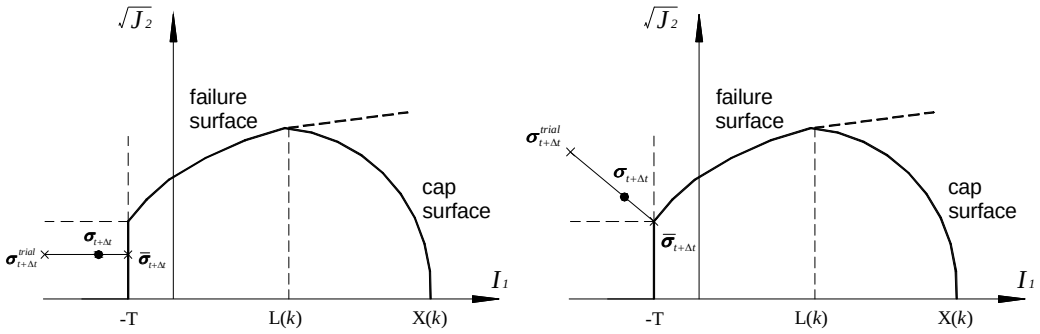


FIG. 2- 12 Treatment of tension cutoff

### 2.3.2 THE DUVANT-LIONS TYPE VISCOPLASTIC CAP MODEL

The viscoplastic strain rate vector and hardening parameter are respectively defined as:

$$\dot{\varepsilon}^{vp} = \frac{1}{\tau}\mathbf{C}^{-1}\left[\boldsymbol{\sigma} - \bar{\boldsymbol{\sigma}}\right] \quad \text{.....(2.45)}$$

$$\dot{k} = \frac{1}{\tau}\left[k - \bar{k}\right] \quad \text{.....(2.46)}$$

where $\tau$ = a material constant called the relaxation time; the pair ($\bar{\boldsymbol{\sigma}}$, $\bar{k}$) = the stress and hardening parameter of the inviscid material (a bar is used to denote the variable of the inviscid plastic model) which can be viewed as a projection of the current stress on the current yield surface; $k$ and $\dot{k}$ = hardening parameter and its differential with respect to time.

It can be seen from Eq. (2.45) that the viscoplastic strain rate is simply defined by the difference between the true stresses and the stresses obtained by the inviscid model which is quite different from that of the Perzyna type (Eq. 2.22).

### 2.3.2.1 STATIC YIELD FUNCTIONS

The Duvant-Lions type cap model plastic yield surface function $f$ is the same with the Perzyna's type.

### 2.3.2.2 SOLUTION ALGORITHMS

The strain rate Eq. (2.20) and (2.21) are integrated over a time step, $\Delta t$, from $t$ to $t+\Delta t$, to yield the incremental strains and stresses:

$$\Delta\boldsymbol{\varepsilon} = \Delta\boldsymbol{\varepsilon}^{e} + \Delta\boldsymbol{\varepsilon}^{vp} \quad \text{.....(2.47)}$$

$$\Delta\boldsymbol{\sigma} = \mathbf{C}\Delta\boldsymbol{\varepsilon}^{e} = \mathbf{C}\left(\Delta\boldsymbol{\varepsilon} - \Delta\boldsymbol{\varepsilon}^{vp}\right) \quad \text{.....(2.48)}$$

where $\Delta\boldsymbol{\varepsilon}$ = the total incremental strain vector;

$\Delta\boldsymbol{\varepsilon}^{e}$ = the elastic viscoplastic incremental strain vector;

$\Delta\boldsymbol{\varepsilon}^{vp}$ = the viscoplastic incremental strain vector;

$\Delta\boldsymbol{\sigma}$ = the incremental stress vector.

Based on the Euler method, the viscoplastic incremental strain vector $\Delta\boldsymbol{\varepsilon}^{vp}$ can be approximated as

$$\Delta\boldsymbol{\varepsilon} = \left[(1-\chi)\dot{\boldsymbol{\varepsilon}}_{t}^{vp} + \chi\,\dot{\boldsymbol{\varepsilon}}_{t+\Delta t}^{vp}\right]\Delta t \quad \text{.....(2.49)}$$

in which $\chi$ is an adjustable integration parameter, $0 \le \chi \le 1$. The integration scheme is explicit if $\chi = 0$ and fully implicit if $\chi = 1$. This solution algorithm is conditionally stable when $\chi \le 0.5$ and unconditionally stable when $\chi > 0.5$. The fully implicit integration scheme, $\chi = 1$, is used here in the numerical algorithm just for simplification.

Integrating Eq. (2.45) over a time step $\Delta t$ gives

$$\Delta \boldsymbol{\varepsilon}^{vp} = \frac{\Delta t}{\tau} \mathbf{C}^{-1} \left[ \boldsymbol{\sigma}_{n+1} - \bar{\boldsymbol{\sigma}}_{n+1} \right] \quad \text{.....(2.50)}$$

Substitution of Eq. (2.50) into Eq. (2.48) yields

$$\Delta \boldsymbol{\sigma} = \boldsymbol{\sigma}_{n+1} - \boldsymbol{\sigma}_n = \mathbf{C} : \Delta \boldsymbol{\varepsilon} - \frac{\Delta t}{\tau} \left[ \boldsymbol{\sigma}_{n+1} - \bar{\boldsymbol{\sigma}}_{n+1} \right] \quad \text{.....(2.51)}$$

By solving $\Delta \boldsymbol{\sigma}_{n+1}$ from Eq. (2.51), one obtains

$$\boldsymbol{\sigma}_{n+1} = \frac{\left( \boldsymbol{\sigma}_n + \mathbf{C} : \Delta \boldsymbol{\varepsilon} \right) + \frac{\Delta t}{\tau} \bar{\boldsymbol{\sigma}}_{n+1}}{1 + \frac{\Delta t}{\tau}} \quad \text{.....(2.52)}$$

where, $(\boldsymbol{\sigma}_n + \boldsymbol{C} \Delta \boldsymbol{\varepsilon})$ may be treated as an elastic trial stresses.

Similarly, we obtain the hardening parameter may be expressed as

$$k_{n+1} = \frac{k_n + \frac{\Delta t}{\tau} \bar{k}_{n+1}}{1 + \frac{\Delta t}{\tau}} \quad \text{.....(2.53)}$$

The numerical algorithm for the Duvant-Lions viscoplastic model is presented in Table 2-2. It is apparent that the Duvant-Lions' model is very easy implement, since the viscoplastic solution is simply an update of the inviscid solution. The ease of numerical implementation of the Duvant-Lions model is apparent compared with the Perzyna model, which requires many matrix operations.

Table 2- 2 Numerical algorithm for the Duvant-Lions's viscoplastic model

| | |
|---|---|
| **DATA INPUT** : | $\boldsymbol{\sigma}_n, k_n, \Delta\boldsymbol{\varepsilon}$ |
| Trial stresses : | $\boldsymbol{\sigma}_{n+1}^{trial} = \boldsymbol{\sigma}_n + \boldsymbol{C}\Delta\boldsymbol{\varepsilon}$ , $k_n$ |
| If $f(\boldsymbol{\sigma}_{n+1}^{trial}, k_n) < 0$, elastic | $\boldsymbol{\sigma}_{n+1} = \boldsymbol{\sigma}_{n+1}^{trail}$ , $k_{n+1} = k_n$ RETURN |
| If $f(\boldsymbol{\sigma}_{n+1}^{trial}, k_n) < 0$, viscoplastic | |
| (a) calculate the inviscid solution: $(\bar{\boldsymbol{\sigma}}_{n+1}, \bar{\boldsymbol{k}}_{n+1})$ | |
| (b) update to viscoplastic stress and hardening parameter: $\boldsymbol{\sigma}_{n+1} = \frac{(\boldsymbol{\sigma}_n + \mathbf{C} : \Delta\boldsymbol{\varepsilon}) + \frac{\Delta t}{\tau}\bar{\boldsymbol{\sigma}}_{n+1}}{1 + \frac{\Delta t}{\tau}}$; $k_{n+1} = \frac{k_n + \frac{\Delta t}{\tau}\bar{k}_{n+1}}{1 + \frac{\Delta t}{\tau}}$ RETURN | |
| **OUTPUT** : | $\boldsymbol{\sigma}_{n+1}, k_{n+1}, \boldsymbol{\varepsilon}_{n+1}$ |

## 2.4 ILLUSTRATION EXAMPLE

The simulated uniaxial strain test, presented by Kantona (1984), was used to prove the adequacy of this viscoplastic cap model under different loading/unloading strain rates.

A hypothetical uniaxial strain loading history: the axial strain of the soil under compression is increased at a constant rate ($\dot{\varepsilon}_{11}$ =0.03%/s) for 1 second, held constant ($\dot{\varepsilon}_{11}$ =0.0) for 4 seconds, unloaded at a constant rate ($\dot{\varepsilon}_{11}$ =-0.015%/s) for 0.5 second, and held constant afterwards is shown in FIG. 2-20.

The material parameters used for cap model are those for McCormick Ranch sand given by Sandler and Rubin (1979): $K$ = 66.7 ksi; $G$ = 40 ksi; $\alpha$ = 0.25 ksi; $\beta$ = 0.67 ksi$^{-1}$; $\gamma$ = 0.18 ksi; $\theta$ = 0.0; $W$ = 0.066; $D$ = 0.67 ksi$^{-1}$; $R$ = 2.5; $X_0$ = 0.189 ksi; and $T$ = 0.0 ksi.

For the Perzyna model, the two parameters, $N$ and $f_0$, were assumed to be 1.0 and 0.25ksi based on experience data, respectively. Three values of the fluidity parameter ($\eta$ = 0.0035, 0.015 and 0.032) were examined similarly. According to Eq. (2.22), when $\eta$ decreases, the viscoplastic strain decreases, and the stress is close to elastic, which implies the axial stress will increase. The stress response becomes purely elastic as $\eta \to 0$, and purely plastic as $\eta \to \infty$.

For the Duvant-Lions model, three values of the relaxation time ($\tau$ = 1.0, 0.25, 0.125) were examined to illustrate its effects on the stress response. As shown in FIG. 2-21, the stress response increases as the relaxation time $\tau$ increases. According to Eq. (2.45) and (2.50), when $\tau$ increases, the viscoplastic strain decreases, and the axial stress is close to elastic, which implies the stress response will increase. Although it is not plotted in FIG. 2-21, the stress responses will become purely elastic as $\tau \to \infty$, and purely plastic as $\tau \to 0$.

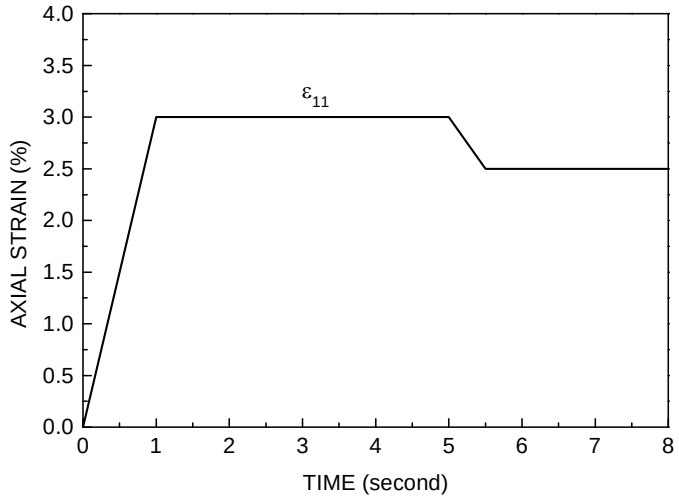


FIG. 2- 13 Axial strain history for uniaxial strain test

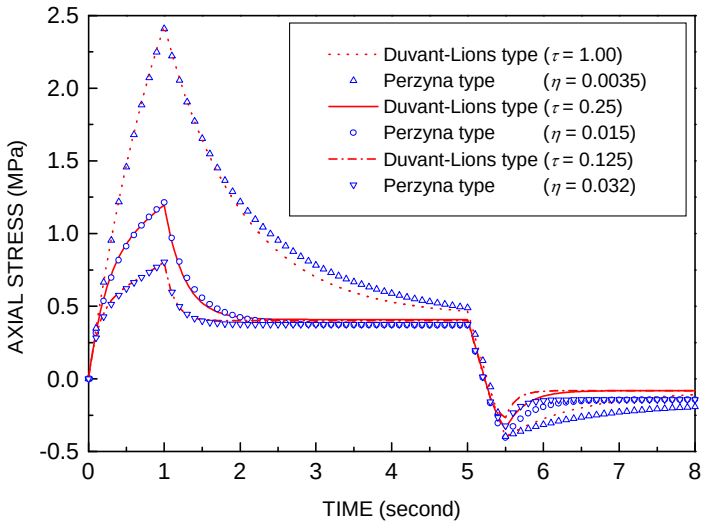


FIG. 2- 14 Axial stresses for different values of $\tau$ and $\eta$

By comparing the stresses resulting from the two models in FIG. 2-21, it can be seen that each pair of the relaxation time and fluidity parameter yields nearly the same stresses. For instance, the axial stress history with $\tau$ = 1.00 from using the Duvant-Lions model was very close to that with $\eta$ = 0.0035 from using the Perzyna model. Likewise, stresses obtained from using the Duvant-Lions model with $\tau$ = 0.25 and 0.125 are nearly the same as those obtained from using the Perzyna model with $\eta$ = 0.015 and 0.032, respectively. The ratio of the three relaxation times is 8:2:1, while that of the fluidity parameters is approximately 1:2:9. Therefore, a certain relationship between $\tau$ and $\eta$ may exist and the viscoplasticities of these two types may be equivalent for this example.

## 2.5 MODEL VALIDATOIN AGAINST EXPERIMENTAL DATA

Jackson et al. (1980) conducted a series of static and dynamic tests on a clayey sand. These tests provided data for validation of the viscoplastic cap model and the associated solution algorithms.

The first step was to calibrate the material parameters for yield functions and the elastic moduli using the static test data. The static test data consisted of the stress and strain results from a uniaxial strain test and two triaxial compression tests conducted at confining pressure of 2.07 MPa and 4.14 MPa, respectively. The material parameters obtained to fit the test data were: $K$ = 2500 MPa; $G$ = 1500 MPa; $\alpha$ = 3.654 MPa; $\beta$ = 0.003 MPa$^{-1}$; $\gamma$ = 3.500 MPa; $\theta$ = 0.263; $W$ = 0.109; $D$ = 0.05 MPa$^{-1}$; $R$ = 1.5; $X_0$ = 0.3 MPa; and $T$ = 0.0 MPa. The agreement was considered to be good both qualitatively and quantitatively.

The second step was to simulate the dynamic stress-strain relationship. The test data were obtained from dynamic uniaxial strain tests, each of which was conducted at varying strain rate. The strain-histories were obtained by choosing strain and time values from plots of vertical stress versus time, and vertical stress versus vertical strain (Schreyer and Bean 1985). The maximum strain rate in the dynamic test was approximately 200/s.

The additional viscous parameters for the Perzyna's model were: $\eta$ = 0.002msec$^{-1}$; $N$ = 1.5; $f_0$ = 1.0 MPa.

From the simulation results it is apparent that: (1) formulations are capable of predicting the dynamic soil response well; (2) the soil responses are close. For the Perzyna type, a normal constant strain rate of 0.0008/s for static tests was used. It is apparent that the soil behavior under high strain rate are very different from those obtained in static test. The confined modulus and the strength are largely increased under high strain rate loading. The viscoplastic cap models capture the strain-rate effects very well.

However, there are some slight differences between predictions of the two models. For instance, the initial soil stiffnesses under high strain rate loading, the slopes of the responses are predicted better by the Perzyna's model than those by the Duvant-Lions' model. From Eq. (2.22) and (2.45), the Perzyna's viscoplastic formulation appears to be more flexible for data fitting than the Duvant –Lions' formulation due to more viscous parameters involved (Tong, X., and Tuan, C.Y. 2007). Therefore, the Perzyna's viscoplastic cap model will be implemented into LS-DYNA finite element code to represent the soil model to analyze the strain-rate effect due to explosion.

# CHAPTER THREE EQUATION OF STATES

## 3.1 INTRODUCTION

An ideal liquid or gas is a continuous medium with neither shear or frictional forces acting between its particles. Hence the stress at a given point does not depend on the orientation of the small surface upon which it acts. In actual liquids and gases, frictional forces do act between their particles. Solid bodies differ from liquids and gases in that they transfer shear forces. When the pressure exceeds a certain magnitude, the bonds between the particles are broken so the material is compressed and the solid begins to behave like a fluid. This phase change depends only upon the magnitude of the pressure and the temperature (Grujicic et al. 2008). The state of a medium is generally defined by a combination of pressure $P$, density $\rho$, volume $\bar{V}$, temperature $T$, entropy $S$, and internal energy $E$. All these quantities are related by thermodynamic relations, and only two of these quantities are independent. The general form of $P = P(\rho, E)$ is used herein to define the state of each of the three phases of the soil.

## 3.2 DEVELOPMENT OF SOIL EQUATION OF STATES

Any equation that relates the pressure, temperature, and specific volume of a substance is called an equation of state. There are several equations of state, some simple and others very complex. Originally, equation of states were mainly used in physics and thermodynamics, an equation of state is a relation between state variables. More specifically, an equation of state is a thermodynamic equation describing the state of

matter under a given set of physical conditions. It is a constitutive equation which provides a mathematical relationship between two or more state functions associated with the matter, such as its temperature, pressure, volume, or internal energy. Gradually, equations of state are found that are useful in describing the properties of fluids, mixtures of fluids, solids, and even the interior of stars.

During the modeling of blast loading on a target or other calculations that bring materials together at high velocities, computer simulations of materials being shocked to high pressure and then releasing to low pressure are performed. Depending on the circumstances, the release to low pressure is often accompanied by release to a very low density. Numerical problems leading to very large sound speeds or to negative lagrangian volumes have been encountered during numerical simulation. These problems can be traced to the behavior of the equation of state in the limit as the density becomes much less than the normal or reference density.

Since all three phases of soil, solids, water and air, have significant volume change that lead to change pressure and density under blast loading, equations of state are considered. In this thesis, which is focused on a limited number of equation of states that can be used for solid soil finite elements. These equations of states include Mie-Gruneison equation of state, Tillotson equation of state and Kandaur conceptual equation of state.

### 3.2.1 MIE-GRUNEISON EQUATION OF STATE

The Mie-Gruneisen equation of state is a relation between the pressure and the volume of a solid at a given temperature. It is often used to determine the pressure in a shock-compressed solid.

If the pressure, in terms of energy $e$ and volume $v$ is expressed as,

$$P = f(e, v) \quad \text{.....(3.1)}$$

then a change in pressure $dP$ can be written as,

$$dP = \left(\frac{\partial P}{\partial v}\right)_e dv + \left(\frac{\partial P}{\partial e}\right)_v de \quad \text{.....(3.2)}$$

Integration of this equation allows the pressure to be expressed in terms of the volume $v$ and energy $e$ relative to the pressure at a reference volume $v_0$ and reference energy $e_0$.

$$\int dP = \int\left(\frac{\partial P}{\partial v}\right)_e dv + \int\left(\frac{\partial P}{\partial e}\right)_v de \quad \text{.....(3.3)}$$

The integration can be performed along any path desired and it is convenient to integrate first at constant energy from $v_0$ to $v$, and then at constant volume from $e_0$ to $e$, giving,

$$P = P_0 + \int\left(\frac{\partial P}{\partial v}\right)_e dv + \int\left(\frac{\partial P}{\partial e}\right)_v de \quad \text{.....(3.4)}$$

The Gruneisen Gamma is defined as,

$$\Gamma = v\left(\frac{\partial P}{\partial e}\right)_v \quad \text{.....(3.5)}$$

and if it is assumed that $\Gamma$ is a function of volume (or density), only then can the second integral above be evaluated,

$$\int\left(\frac{\partial P}{\partial e}\right)_v de = \frac{\Gamma(v)}{v}(e - e_0) \quad \text{.....(3.6)}$$

The first integral is a function only of volume and the reference energy $e_0$. If the reference state is denoted by $e_r$, then since,

$$\int\left(\frac{\partial P}{\partial v}\right)_e dv = P_r(v) - P_0 \quad \text{.....(3.7)}$$

The equation becomes,

$$P = P_r(v) + \frac{\Gamma(v)}{v}[e - e_r(v)] \quad \text{.....(3.8)}$$

This equation is generally known as the Mie-Gruneisen form of equation of state. In LS-DYNA, it can be expressed as,

$$P = \frac{\rho_0 C^2 \mu\left[1 + \left(1 - \frac{\gamma_0}{2}\right)\mu - \frac{\alpha}{2}\mu^2\right]}{\left[1 - (S_1 - 1)\mu - S_2\frac{\mu^2}{\mu+1} - S_3\frac{\mu^3}{(\mu+1)^2}\right]} + (\gamma_0 + \alpha\mu)E \quad \text{.....(3.9)}$$

Where $C$ is the intercept of the Shock velocity-Particle velocity curve; $S_1$, $S_2$ and $S_3$ are the coefficients of the slope of the Shock velocity-Particle velocity curve; $\gamma_0$ is the Gruneisen gamma; $\alpha$ is the first order volume correction to $\gamma_0$; and $\mu = \frac{v_0}{v} - 1$.

### 3.2.2 TILLOTSON EQUATION OF STATE

This form of equation of state (Tillotson 1962) was derived to provide a description of the material behavior of solid elements over the very wide range of pressure and density encountered in hypervelocity phenomena.

Not only must such an equation of state describe normal density material and its condition after shock, but also its expansion and change of phase in cases where the shock energy has been sufficient to melt or vaporize the material. The pressure range can be so large that the “low pressure” regime of this form of equation of state is defined as from 0 to 10 Mbar and “high pressure” from 10 to about 1000 Mbar. Thus any pressure and results from normal laboratory experiments cover only the “low pressure” region. For the derivation of an equation of state for the “high pressure” region, analytic forms provide best fit interpolations between Thomas-Fermi-Dirac data at high pressures (above 50 Mbar) and experimental data at low pressures. The formulation is claimed to be accurate to within 5% of the Hugoniot pressure and to within 10% of the isentrope pressures. It is therefore a very useful form of equation of state for hypervelocity impact problems.

The total range of the pressure-volume plane is divided into four regions as shown in the FIG. 3-1.

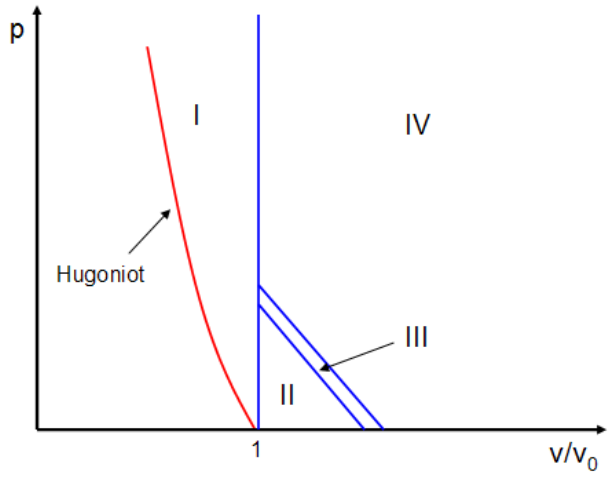


FIG. 3- 1 Regions of Interest in the (p, v) Plane

The region to the left of the Hugoniot can only be reached by adiabatic (non-shock) compression and is not relevant to impact problems. It is therefore excluded from the formulation. Region I represents the compressed phase of the material and extends vertically to shock pressures of about 1000 Mbar. Region II describes material which has been shocked to energy less than the sublimation energy and will therefore, on adiabatic release, returns to zero pressure as a solid. There is no provision in this equation of state to describe the material at pressures less than zero. Region IV is the expansion phase of material which has been shocked to energy sufficiently large to ensure that it will expand as a gas. For large specific volumes, the formulation for Region IV extrapolates to an ideal gas limit. It is desirable or even necessary, to ensure that the formulations in each region provide continuous values of the pressure and its first derivatives at the boundaries between contiguous regions. Region III lies between Regions II and IV. In this region the pressure is calculated as a mean between that calculated for Regions II and IV.

Let:

$$\eta = \frac{\rho}{\rho_0} \quad \text{.....(3.10)}$$

$$\mu = \eta - 1 \quad \text{.....(3.11)}$$

$$\omega_0 = 1 + \frac{e}{e_0 \eta^2} \quad \text{.....(3.12)}$$

where $\rho$ is the density, $\rho_0$ is the reference density, $e$ is the energy and $e_0$ is the reference energy.

For Region I $(\mu \geq 0)$ the pressure $P_1$ is given by a Mie-Gruneisen equation of state but since the formulation is to be valid for a very large range of pressure, the Gruneisen Gamma is a function of both $v$ and $e$, not just a function of $v$ alone. The constants fit the low pressure shock data but they are adjusted to fit the asymptotic Thomas-Fermi behavior for the variation of pressure at maximum compressions (like a monatomic gas). The formulation for Region II is as for Region I with a slight modification to one term to avoid difficulties as m goes increasingly negative. In Region IV the formulation is chosen to give the correct behavior both at high pressure/normal density and for very large expansion (where it must converge to an ideal gas behavior). With these constraints the different formulations are given. For region $\mathrm{I}(\mu \geq 0)$ , the pressure $P_1$ is given by,

$$P_1 = \left(a + \frac{b}{\omega_0}\right)\eta\rho_0 e + A\mu + B\mu^2 \quad \text{.....(3.13)}$$

For region II $(\mu < 0, e \le e_s)$ , the pressure $P_2$ is given by,

$$P_2 = \left(a + \frac{b}{\omega_0}\right)\eta\rho_0 e + A\mu \quad \text{.....(3.14)}$$

For region III $(\mu < 0, e_s < e < e_s^{'})$ , the pressure $P_3$ is given by,

$$P_3 = P_2 + \frac{(P_4 - P_2)(e - e_s)}{(e_s^{'} - e_s)} \quad \text{.....(3.15)}$$

For region IV $(\mu < 0, e \ge e_s^{'})$ , the pressure $P_3$ is given by,

$$P_4 = a\eta\rho_0 e + \left(\frac{b\eta\rho_0 e}{\omega_0} + A\mu e^{\beta x}\right)e^{-\alpha x^2} \quad \text{.....(3.16)}$$

where $x = 1 - \frac{1}{\eta}$. In the Tillotson equation of state, $a$, $b$, $A$, $B$, $e_0$, $e_s$, and $e_s^{'}$ are constants.

The Mie-Gruneisen equation of state and Tillotson equation of state can be used for soil behavior simulation model and ensure a unique solution. However, the limitation is soil with Mie-Gruneisen equation of state or Tillotson equation of state is defined as a unit material and leads to a simplified bulk modulus and mechanical pressure in the calculation process.

### 3.2.3 MURRAY'S EQUATION OF STATE FOR UNSATURATED SOILS

The prediction of soil behavior is intrinsically linked to the need to determine the controlling stresses in the soil. For saturated soils, Terzaghi (1936) proposed an equation

for effective stress which controls the shear resistance and volume changes. The effective stress can be written as

$$p' = p - u_w \quad \text{.....(3.17)}$$

where $p'$ is Terzaghi's mean effective stress, $p$ is the mean total stress and $u_w$ is the pore-water pressure.

The concept of the stress state variable $(p - u_w)$ controlling the behavior of saturated soils has proven very useful and has been shown to be valid in practice. For unsaturated soils, however, the search for a reliable stress state variable equation, independent of soil properties, has proven unsuccessful. As described by Fredlund and Rahardjo (1993), a number of such equations have been proposed. The original suggestion of Bishop (1959) can be written as

$$p'_B = (p - u_a) + \chi(u_a - u_w) \quad \text{.....(3.18)}$$

where $p'_B$ is Bishop's mean effective stress, $u_a$ is the pore-air pressure and $\chi$ is an empirical parameter.

A major obstacle to the use of Eq. (3.18) lies with the parameter $\chi$. This is usually ascribed the range of values $0 \le \chi \le 1$ and has been shown to be dependent on the stress path and the process to which the soil is subjected (Jennings and Burland 1962; Blight 1965; Morgenstern 1979).

Although it is desirable that the concept of effective stress for saturated soils extended to unsaturated soils and that soil properties such as the volumes of the various

phase (solid particles, water and air) are not included in any formulation of controlling stresses, experiments have demonstrated the inadequacy of any such relationship. For this reason, researchers have turned to examining the use of the independent stress state variables $(p-u_a)$, $(p-u_w)$ and $(u_a-u_w)$ to describe the mechanical behavior of soils. Fredlund and Morgenstern (1977) concluded from theoretical considerations that any two of these three stress state variables can be used to describe the behavior of an unsaturated soil. However, there are inconsistencies in experimental results not readily answered by constitutive modeling using these parameters (Wheeler and Sivakumar 1995). A logical interpretation of experimental data is essential to an appreciation of soil behavior, and a clear pricture does not always emerge using independent stress state parameters, as these interact in response to external stimuli. In this respect, it appears that the volumes of the phases play an important role in controlling the stresses in unsaturated soils, and this is demonstrated in the analysis and the comparisons with both consolidation data and critical state data which follow.

Murray (2002) examined the significance of the relative volumes of the phases, and the interactions between the phases, on the stress regime under equilibrium conditions. First, a description of the significance of enthalpy in soils relating pressures, volumes, and internal energy sources is presented, followed by an examination of Terzaghi's effective stress equation in terms of the enthalpy of a saturated system. This approach is then extended to unsaturated soils to develop an equation of state that includes the average volumetric "coupling" stress $p_c'$ . This links the stress state variables and the volumes of the phases.

The general equation of state for unsaturated soil can be expressed:

$$p = u_w n_w + b(n_w + n_s)(u_a - u_w) + u_a n_a + a u_w n_s + p'_c \quad \text{.....(3.19)}$$

$$p'_c = (p - u_a) + s(n_w + n_s) \quad \text{.....(3.20)}$$

where $n_a$ $(n_a = V_a/V)$ , $n_w$ $(n_w = V_w/V)$ and $n_s$ $(n_s = V_s/V)$ are the volume fraction of air, water and solid phase respectively, $a$ is a dimensionless parameter with a minimum value of 1, $b$ is a dimensionless number influenced by the structure and size of the saturated packets and $s$ is the suction. $(n_w + n_s)$ represents the total volume of the saturated packets per unit volume of soil. Using Eq. (3.19) it is possible to highlight the significance of the stress state variables $(p - u_a)$ , $(p - u_w)$ , and $(u_a - u_w)$ for unsaturated soils and their implicit relationship with the volumes of the phases.

FIG. 3-2 and FIG. 3-3 have been prepared based on the experimental data reported by Wheeler and Sivakumar (1995) and Toll (1990).

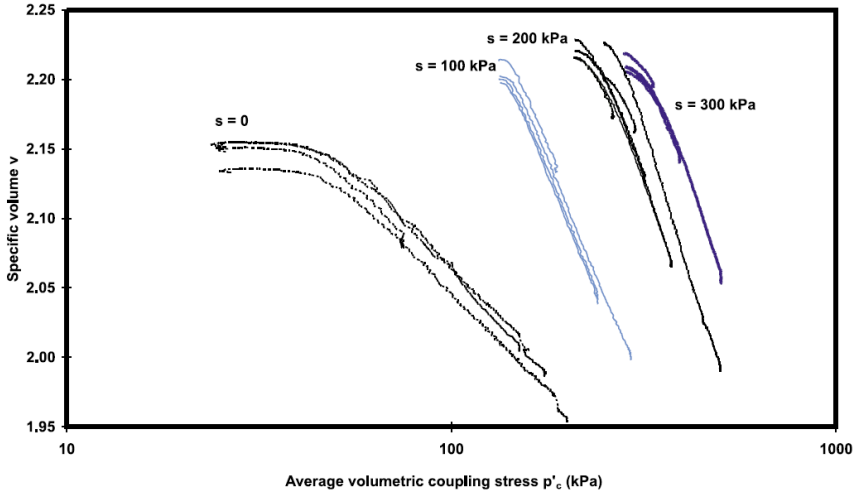


FIG. 3- 2 Variation of specific volume during ramped consolidation at different suction (Murray, 2002)

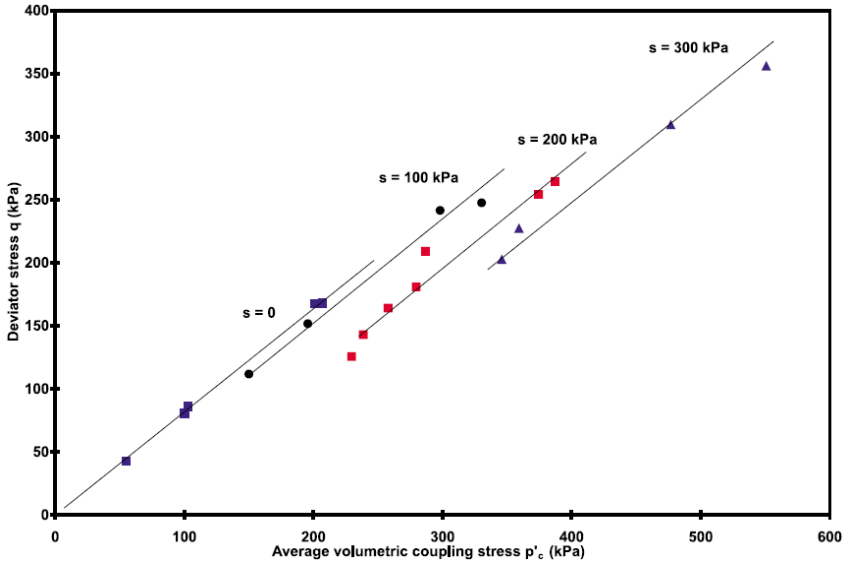


FIG. 3- 3 $q$ versus $p_c'$ at critical states

(Murray, 2002)

However, the Murray's equation of state has the limitations and shortcomings: (1) there are no enough experimental data at present to define precisely the suction-dependence of material parameters and (2) the average volumetric coupling stress $p_c'$ represents the microscopic forces between particles. Under high strain rate loading, like blasting loading, the average volumetric coupling stress doesn't play an important role.

### 3.3 KANDAUR'S CONCEPTUAL MODEL OF EOS

Soils are composed of particles of various materials- called phases. The majority of the solid mineral particles consists of silicon which can, therefore, be taken as representative, the other water and air.

Let $A_s$, $A_w$ and $A_a$ denote the relative volume of the solid particles, water and air, respectively, i.e. the volume of the corresponding phase in a unit volume of soil; then

$$A_s + A_w + A_a = 1 \quad \text{.....(3.21)}$$

The quantities $\rho_s$, $\rho_w$ and $\rho_a$ are the material densities of each phase and $\rho_0$ is the initial density of the soil as a whole. We then have

$$\rho_0 = A_s\rho_s + A_w\rho_w + A_a\rho_a \quad \text{.....(3.22)}$$

In soils, two deformation mechanisms exist:

a) at low pressures, the soil skeleton deformation is determined by the elastic deformations of bonds on the contact surfaces of grains and, at high pressures, it is determined by a failure in bond and displacements of the grains (plastic deformation);
b) the deformation of all the soil phases, determined by their volume compression. When the soil is being compressed, both mechanisms are always acting simultaneously. At certain phases of the loading process, however, one of the mechanisms predominates to such a degree that the other may be neglected.

A dry soil contains air and a small amount of water, whose compressibility considerably exceeds that of the skeleton; therefore, with static and dynamic loading, the first mechanism becomes influencial while the other is negligible; with increasing pressure, the gain bonds are deformed and displaced and the soil is compacted so that the second mechanism becomes more and more effective until it reaches a definite overbalance, while the first becomes negligible. The dependence of pressure on the

relative volume deformation is, for this case, plotted in FIG. 3-4 (Henrych 1979). The second mechanism predominates for $\sigma \geq \sigma_B$.

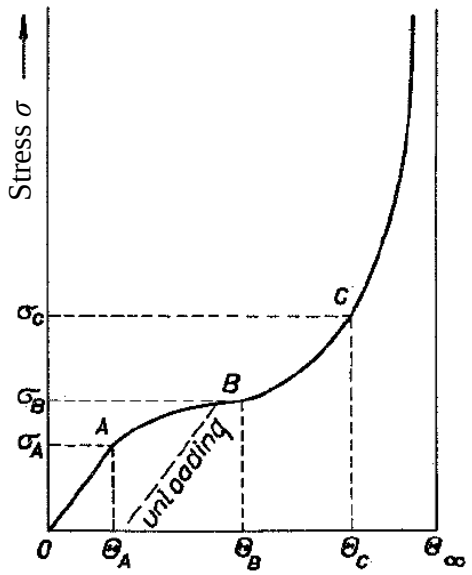


FIG. 3- 4 Relationship between stresses and relative volume deformation for solids

In a saturated soil the salts on the grain contacts are dissolved and the bonds weakened. Under a rapid dynamic loading, the water and air have a higher resistance than the contact bonds of the skeleton grain. The deformation and resistance of the soil are determined by the dominating second mechanism, particularly by the water and air deformation; the solid phase becomes effective only at high pressures (hundreds and thousands of kp/cm$^2$). The relationship between $\sigma(\Theta)$ and volume deformation under this situation is shown in FIG. 3-5. However under a slow static loading of the saturated soil, the water and air are pressed out of the void and the compressibility is mainly given by the solid skeleton compressibility.

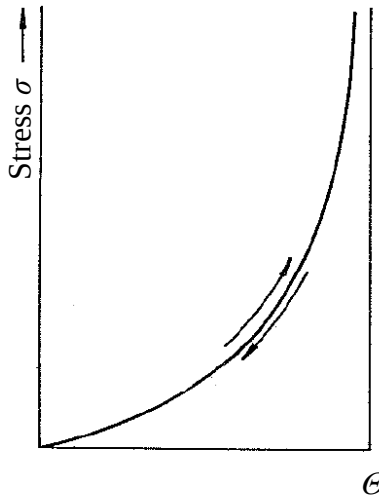


FIG. 3- 5 Relationship between stresses and relative volume deformation for liquids, gases, etc

(Henrych, 1979)

The diagram of a block grain medium, according to I.I. Kandaur (Henrych, 1979), is illustrated in FIG. 3-6. The cavities between blocks are filled with water and air. Between the corners are elastobrittle bonds. With loading, the medium deformations consist of the deformations of the elastobrittle bonds, which are disturbed with a simultaneous mutual displacement of the static blocks (first mechanism) and the void filled with water and air (second mechanism). The forces of the elastobrittle bonds and the forces of friction between the solid particles act within the scope of the first mechanism. The forces depend on the volume change of the individual phases then act within the range of the second mechanism. With fast dynamic deformation the water and air are cannot escape from the cavities through the spaces between the blocks; with a slow static deformation the water and air are forced through the spaces between the

blocks into less loaded surroundings and the dominant resistance is offered by the bonds between blocks and by the blocks themselves.

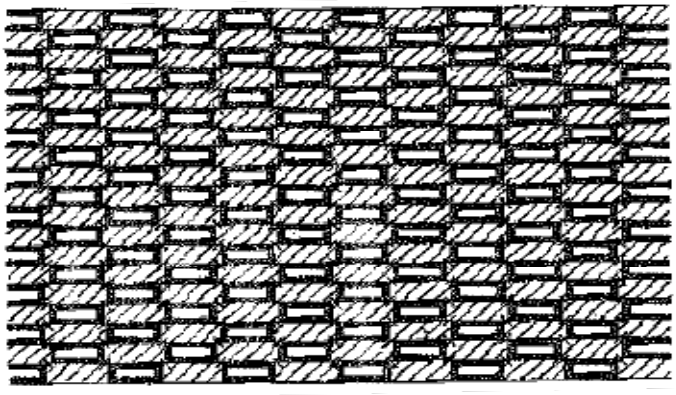

FIG. 3- 6 Schematic representation of a block grained medium with elastobrittle linkages between the blocks

(Henrych, 1979)

The medium shown in FIG. 3-6 corresponds to the rheological model illustrated in FIG. 3-7, which covers both mechanisms and applies to a dynamic loading (water and air are not forced out of the voids). This model is used to derive the equation of state for the adiabatic process. With small pressure and dry soils the first deformation mechanism is a decisive factor as it corresponds to the elements **D**, **E**, i.e. to the grain friction proportional to normal pressure, and to the resistance of the crystal bonds, which is represented by a series of filaments stretched and broken as the deformation develops.

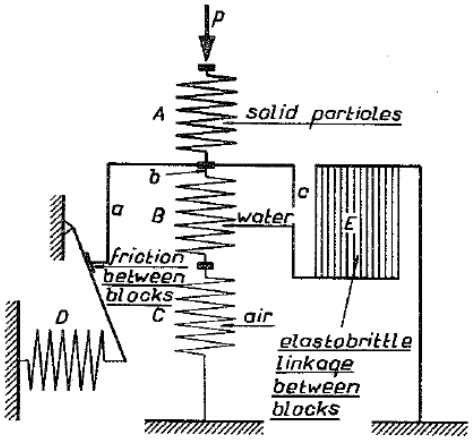


FIG. 3- 7 Schematic diagram of a rheological model of the medium (Henrych, 1979)

With water-bearing soils and for higher pressures with dry soils, the second deformation mechanism represented by the elements **A**, **B**, **C** predominates. Obviously,

$$P = P_a + P_b + P_c \quad \text{.....(3.23)}$$

$$V = V_s + V_p \quad \text{.....(3.24)}$$

$$V_p = V_w + V_a \quad \text{.....(3.25)}$$

$$V_s = A_s V_0 \quad \text{.....(3.26)}$$

$$V_w = A_w V_0 \quad \text{.....(3.27)}$$

$$V_a = A_a V_0 \quad \text{.....(3.28)}$$

where $P_a$ , $P_b$ and $P_c$ are the forces in branches a, b and c, respectively; $V$ is the soil volume, $V_0$ is the soil initial volume and $V_p$ is the void volume.

From equations (3.23) to (3.28), we obtain

$$dV = dV_s + dV_p \quad \text{.....(3.29)}$$

$$dP = \frac{\partial P_a}{\partial V_P} dV_p + \frac{\partial P_b}{\partial V_P} dV_p + \frac{\partial P_c}{\partial V_P} dV_P \quad \text{.....(3.30)}$$

$$dV_P = \frac{\partial V_w}{\partial P_b} dP_b + \frac{\partial V_a}{\partial P_b} dP_b \quad \text{.....(3.31)}$$

and hence

$$dP - \left( dV - \frac{\partial V_s}{\partial P} dP \right) \left[ \left( \frac{\partial V_w}{\partial P_b} + \frac{\partial V_a}{\partial P_b} \right)^{-1} + \frac{\partial P_a}{\partial V_p} + \frac{\partial P_c}{\partial V_p} \right] = 0 \quad \text{.....(3.32)}$$

Then dependence of the loading on deformation in phases 1 and 2 is given by the Hooke law, so that

$$\frac{\partial V_s}{\partial P_a} = -\frac{A_s V_0}{k_s^*} \quad \text{.....(3.33)}$$

$$\frac{\partial V_w}{\partial P_b} = -\frac{A_w V_0}{k_w^*} \quad \text{.....(3.34)}$$

where $k_s^*$ , $k_w^*$ are the coefficients of volume deformation of the mineral skeleton particles and of water, respectively.

In element **C** holds the equation of state of a polytropic gas, which can be written in the form

$$P_b - P_0 = a_a \left( V_a \right)^{-k} \quad \text{.....(3.35)}$$

where $P_0$ is the atmospheric pressure, $a_a$ is a constant and $k$ is the coefficient of adiabaticity. Then,

$$\frac{\partial V_a}{\partial P_b} = -a_a^{-1} k^{-1} (V_a)^{1+k} \quad \text{.....(3.36)}$$

In the element **a,** the relationship between loading and deformation is determined by the dry friction produced by a force *P'* between the blocks, proportional to deformation:

$$P_a = fP' \quad \text{.....(3.37)}$$

$$P' = K_P \Delta V_P \quad \text{.....(3.38)}$$

$$\Delta V_P = V_P - (A_w + A_a) V_0 \quad \text{.....(3.39)}$$

where $f$ is the coefficient of friction of the mineral particles and $K_P$ is the coefficient of proportionality. From equations (3.37) to (3.39), follows the coefficients,

$$P_a = \varphi \Delta V_P \quad \text{.....(3.40)}$$

$$\varphi = K_P f \quad \text{.....(3.41)}$$

which are constant for a given soil and moisture, so that,

$$\frac{\partial p_a}{\partial V_P} = \varphi \quad \text{.....(3.42)}$$

The force in each filament of the element **E** obeys the Hooke law until the filament breaks. But the strength of the individual filaments is different and, therefore, the force $P_c$ in the arm *c* is expressed as,

$$P_c = E \Delta V_P \quad \text{.....(3.43)}$$

where $E$ is a variable deformation modulus, which may be written,

$$E = E_0 (1 - \Delta E) \quad \text{.....(3.44)}$$

where $E_0$ is a constant. With regard to the statistical law of disturbance,

$$\Delta E = \int e^{-x} dx \quad \text{.....(3.45)}$$

$$x = -B\Delta V_P \quad \text{.....(3.46)}$$

We obtain

$$P_c = E_0 \Delta V_P e^{B\Delta V_p} \quad \text{.....(3.47)}$$

so that,

$$\frac{\partial p_c}{\partial V_P} = -E_0 \left(1 + B\Delta V_P\right) e^{B\Delta V_p} \quad \text{.....(3.48)}$$

Substituting the equation (3.48) into equation (3.32), the equation can be obtained,

$$dP + \left( dV - \frac{dP}{k_s^*} \right) \left[ \left( a_a{}^{-1} k^{-1} \left(V_a\right)^{1+k} + \frac{A_w V_0}{k_w^*} \right)^{-1} + E_0 \left(1 + B\Delta V_P\right) e^{B\Delta V_p} - \varphi \right] = 0 \quad \text{.....(3.49)}$$

For the initial condition (3.50), it is possible to obtain the solution of equation (3.49) in the form (3.51). Because of the their inordinate complexity, neither equation (3.49) nor its solution have as yet been used for dynamic problems, even if it determines the behavior of soil with sufficient accuracy.

$$P\left(V_0\right) = P_0 \quad \text{.....(3.50)}$$

$$P\left(V\right) = P \quad \text{.....(3.51)}$$

For the solution of soil dynamics problems the equation of state, derived by G.M. Lyakhov (Henrych, 1979), is more suitable. This equation is based on the second mechanism of soil deformation, i.e. the volume compression of all phases; in deriving it Lyakhov started from the equations of state of the individual phases.

For air, the equation of state can be expressed in the form,

$$P_a = P_0\left(\frac{\rho_a}{\rho_{a0}}\right)^{k_a} \quad \text{.....(3.52)}$$

where $P_0$ is the atmospheric pressure, it can be expressed,

$$P_0 = \frac{\rho_{a0}c_{a0}^2}{k_a} \quad \text{.....(3.53)}$$

$\rho_{a0}$ is the density of air at atmospheric pressure, $c_{a0}$ is the velocity of sound, is the density of air at pressure and $k_a$ is the exponents of the specific entropy of the air.

For water, the equation of state can be expressed in the form,

$$P_w = p_0 + \frac{\rho_{w0}c_{w0}^2}{k_w}\left[\left(\frac{\rho_w}{\rho_{w0}}\right)^{k_w} - 1\right] \quad \text{.....(3.54)}$$

For solid, the equation of state can be expressed in the form,

$$P_s = P_0 + \frac{\rho_{s0}c_{s0}^2}{k_s}\left[\left(\frac{\rho_s}{\rho_{s0}}\right)^{k_s} - 1\right] \quad \text{.....(3.55)}$$

These parameters of equations of state are summarized in Table 3-1.

Table 3- 1 Equation of state parameters for saturated soil

| | $\boldsymbol{\rho_0}$ (kg/m$^3$) | $\boldsymbol{c_0}$ (km/s) | **k** |
|---|---|---|---|
| Air | 1.2($\rho_{a0}$) | 0.34 ($\boldsymbol{c_{a0}}$) | 1.4 ($k_a$) |
| Water | 1000($\rho_{w0}$) | 1.50 ($\boldsymbol{c_{w0}}$) | 7 ($k_w$) |
| Solid | 2650($\rho_{s0}$) | 4.50 ($\boldsymbol{c_{s0}}$) | 3 ($k_s$) |

For solid, water and air, the relative volume by $A_a$ , $A_w$ , $A_s$ , the density by $\rho_{a0}$ , $\rho_{w0}$ , $\rho_{s0}$ , and the velocity of sound by $c_{a0}$ , $c_{w0}$ , $c_{s0}$ , respectively, at an initial (atmospheric) pressure $p=p_0$. Because of the different compressibilities of the components, their relative content at pressure $p$ will be different from that at pressure $p=p_0$. If, at pressure $p$, the content of the components is denoted by $A_a^*$ , $A_w^*$ , $A_s^*$ , the specific volume by $V_a$ , $V_w$ , $V_s$ and the soil density by $\rho$ , it follows from equation (3.52) that,

$$\left(\frac{A_a}{A_a^*}\right)^{k_a} = \left(\frac{V_{a0}}{V_a}\right)^{k_a} \frac{P}{P_0} \quad \text{.....(3.56)}$$

It can be rewritten as,

$$A_a^* = A_a \left(\frac{P_a}{p_0}\right)^{-k_a^{-1}} \text{.....(3.57)}$$

Similarly, for water

$$A_w^* = A_w \left(\frac{k_w \left(P_w - P_0\right)}{\rho_{w0}\, c_{w0}^2} + 1\right)^{-k_w^{-1}} \text{.....(3.58)}$$

For solid particles

$$A_s^* = A_s \left(\frac{k_s \left(P_s - P_0\right)}{\rho_{s0}\, c_{s0}^2} + 1\right)^{-k_s^{-1}} \text{.....(3.59)}$$

Because the density increments have, due to compressibility, the density of a three-phase medium at pressure $p$ will be,

$$\rho = \rho_0 (A_s^* + A_w^* + A_a^*)^{-1}. \quad \text{.....(3.60)}$$

Thus, water-bearing and dry soils may, within a certain pressure range, be considered as three-phase media. The smaller the value of $A_a$ and the greater the value of $A_w$ in the soil voids, the lower the pressure $P_{\min}$ corresponding to the lower limit of applicability of this model. For water-bearing soils $P_{\min} = P_0$ when $A_a = 0$ and $P_{\min} = 500$ to 800 kp when $A_a$ = 0.04 to 0.05. For dry soils with $A_a$ = 0.3 to 0.4, the value of $P_{\min}$ increases up to several hundred to several thousands of atmospheres. The upper limit is bounded by the validity limits of the equations of state of the individual components.

### 3.4 USER DEFINED EQUATION OF STATE

To improve simulation results, an equation of state was defined for LS-DYNA dynamic simulation software.

The conservations of mass, momentum and energy in a soil medium from the initial state (denoted by the subscript *0*) to the state under shock loading (denoted by subscript *H*) are expressed by (3.61), (3.62) and (3.63), respectively:

$$\rho_0 U_S = \rho (U_S - u_P) \quad \text{.....(3.61)}$$

$$P_H = \rho_0 U_S u_P \quad \text{.....(3.62)}$$

$$E_H - E_0 = \frac{P_H}{2} (V_0 - V_H) \quad \text{.....(3.63)}$$

where $U_S$ is the shock velocity, and $u_P$ is the particle velocity.

A series of plate impact experiments were performed on a soil at various levels of water saturation by Chapman et al. (2006). The Hugoniot was determined using a reverberation technique. The Hugoniot is presented in terms of the measured shock velocity and particle velocity in FIG. 3-8, and in terms of stress and particle velocity in FIG. 3-9. The densities, degrees of saturation and shock wave velocities in the soil specimens are summarized in Table 3-2.

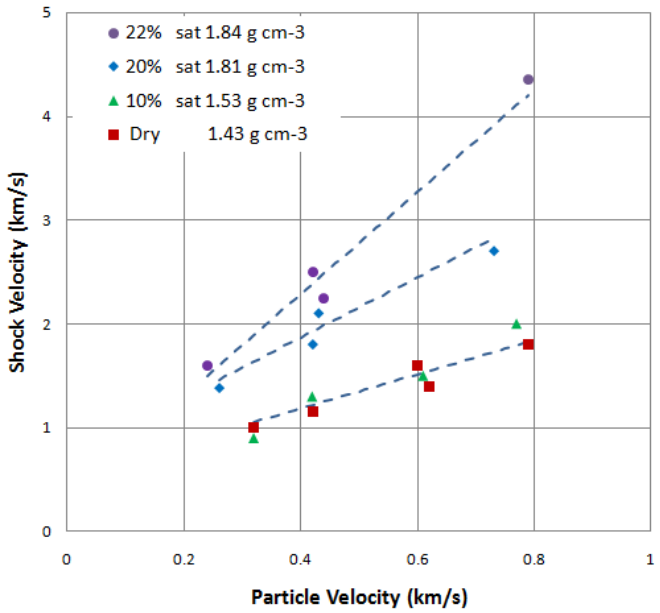


FIG. 3- 8 Shock-velocity vs. particle-velocity (Chapman et al. 2006)

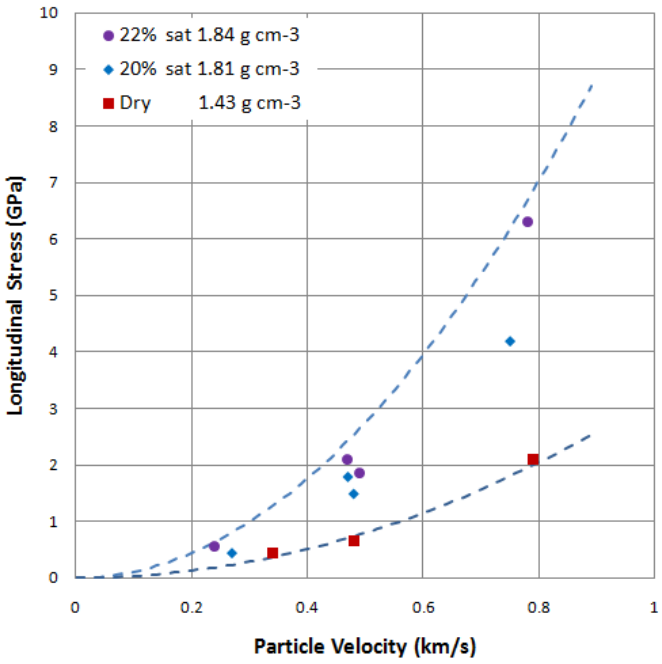


FIG. 3- 9 Stress vs. particle-velocity

(Chapman et al. 2006)

Table 3- 2 Plate impact test data

| Moisture, % | 0 | 10 | 20 | 22 |
|---|---|---|---|---|
| Saturation, % | 0 | 32 | 64 | 70 |
| Density, kg m-3 | 1430 | 1530 | 1810 | 1840 |
| Shock velocity, km/s | 1.44 | 1.45 | 1.90 | 2.68 |

Hugoniot curves are often expressed as a relation between shock velocity and particle velocity by least-square curve fitting the shock loading data (Zukas 1990). For many materials, the Hugoniot can be expressed as a linear relation between shock velocity $U_S$ and particle velocity $u_P$:

$$U_S = C_0 + s\,u_P \quad \text{.....(3.64)}$$

where $C_0$ is the sound speed at ambient pressure and temperature, and $s$ is the slope of the linear relation, both obtained experimentally.

Dividing both sides of (3.64) by $U_S$ yields

$$1 = \frac{C_0}{U_S} + s\,\frac{u_P}{U_S} \quad \text{.....(3.65)}$$

From (3.61), the volumetric strain can be expressed as

$$\frac{u_P}{U_S} = 1 - \frac{\rho_0}{\rho} = \frac{V_0 - V}{V_0} = \Delta \quad \text{.....(3.66)}$$

Substituting (3.66) into (3.65) yields

$$U_S = \frac{C_0}{1 - s\,\Delta} \quad \text{.....(3.67)}$$

From (3.66),

$$u_P = U_S\,\Delta = \frac{C_0\,\Delta}{1 - s\,\Delta} \quad \text{.....(3.68)}$$

Let

$$\mu = \frac{\rho}{\rho_0} - 1 = \frac{V_0}{V} - 1 \quad \text{.....(3.69)}$$

Substitute (3.66) into (3.69),

$$\Delta = \frac{\mu}{1 + \mu} \quad \text{.....(3.70)}$$

Substituting (3.67), (3.68) into (3.62) yields

$$P_H = \rho_0 \left(\frac{C_0}{1 - s\,\Delta}\right)\left(\frac{C_0\,\Delta}{1 - s\,\Delta}\right) = \frac{\rho_0\,C_0^2\,\Delta}{(1 - s\,\Delta)^2} \quad \text{.....(3.71)}$$

Substituting (3.70) into (3.71) yields

$$P_H = \frac{\rho_0 C_0^2 \left(\frac{\mu}{1+\mu}\right)}{\left(1 - s\frac{\mu}{1+\mu}\right)^2} \quad \text{.....(3.72)}$$

Plate impact experiments have been conducted by many researchers to provide Hugoniot data for various materials. Jones and Gupta (2000) conducted shock wave experiments to determine the refractive index and shock velocity of quartz. Braithwaite et al. (2006) obtained the shock Hugoniot properties of quartz feldspathic gneiss by plate impact experiments. The relationship between shock velocity $U_S$ and particle velocity $u_P$ of solid can be obtained from FIG. 3-10.

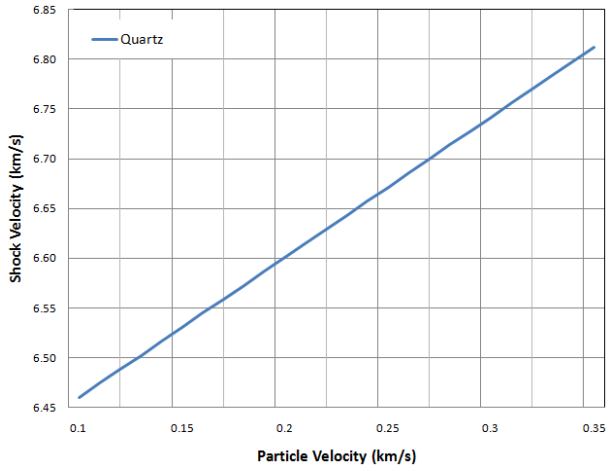


FIG. 3- 10 Shock-velocity dependence on particle-velocity for quartz

$$U_S = 6.319 + 1.41u_P \quad \text{.....(3.73)}$$

Nagayama et al. (2002) obtained a linear relation between the shock velocity and particle velocity of water from high velocity impact tests, as presented in FIG. 3-11.

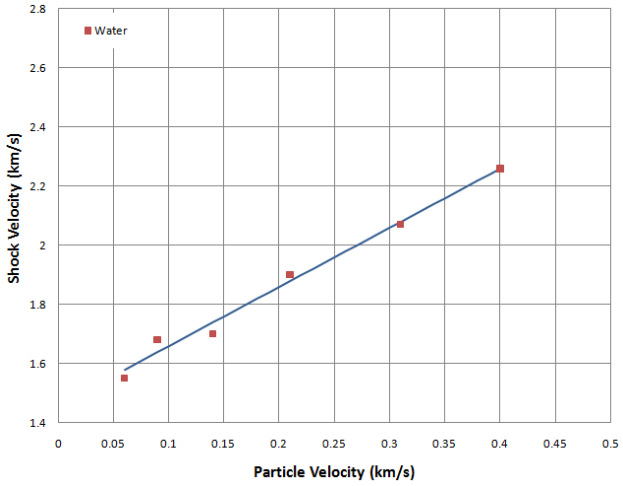


FIG. 3- 11 Shock-velocity dependence on particle-velocity for water

$$U_S = 1.460 + 2.0u_P \quad \text{.....(3.74)}$$

Kim et al. (1991) investigated the Hugoniot data of dry air and derived an expression for adiabatic exponent for shock compressed dry air in FIG. 3-12.

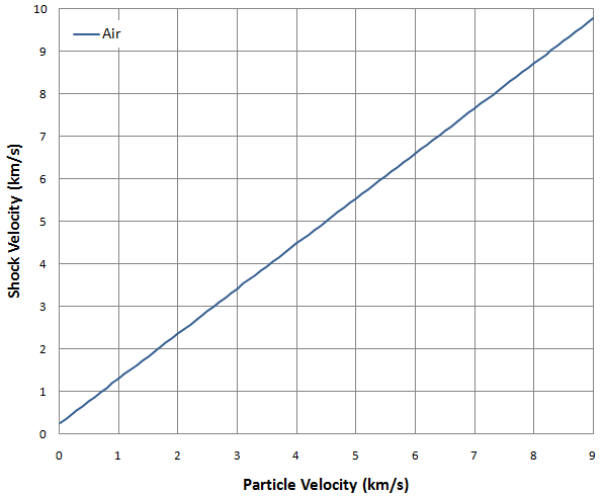


FIG. 3- 12 Shock-velocity dependence on particle-velocity for air

$$U_S = 0.241 + 1.06u_P \quad \text{.....(3.75)}$$

These Hugoniot data for quartz sand, water and air are used in the equations of state and are summarized in Table 3-3.

Table 3- 3 Equation of state parameters for soil

| | ***A*** | **ρ** (kg/m$^3$) | $C_o$ (km/s) | ***s*** | **k** | $\gamma_0$ |
|---|---|---|---|---|---|---|
| Solid | 0.7($A_s$) | 2650($\rho_s$) | 6.319 | 1.41 | 3 ($k_s$) | 1.0 |
| Water | 0.2($A_w$) | 1000($\rho_w$) | 1.460 | 2.00 | 7 ($k_w$) | 0.6 |
| Air | 0.1($A_a$) | 1.2($\rho_a$) | 0.241 | 1.06 | 1.4 ($k_a$) | 0.0 |
| Dry soil | 1.0 | 1430 | 0.530 | 1.64 | --- | 0.11 |
| Saturated soil | 1.0 | 1840 | 0.320 | 4.92 | --- | 0.11 |

An equation of state for states more general than the uniaxial strain condition in the plate impact experiments can be expressed as (Zukas 1990):

$$P = \rho\gamma(V)E = \frac{\gamma(V)}{V}E \quad \text{.....(3.76)}$$

where $\gamma(V)$ is the Gruneisen parameter, and $E$ is internal energy per unit mass. If shock pressure $P_H$ and internal energy $E_H$ are associated with a specific volume $V$ from a Hugoniot curve, the shock pressure is expressed as

$$P_H = \rho\gamma(V)E_H = \frac{\gamma(V)}{V}E_H \quad \text{.....(3.77)}$$

If the Hugoniot is the reference state, the equation of state can be expressed as

$$P - P_H = \frac{\gamma(V)}{V}(E - E_H) \quad \text{.....(3.78)}$$

Substituting (3.63) into (3.78) yields the equation:

$$P = P_H + \frac{\gamma}{V}(E - E_0) - \frac{\gamma}{V}\frac{P_H}{2}(V_0 - V) = P_H\left(1 - \frac{\gamma}{2}\mu\right) + \frac{\gamma}{V}(E - E_0) \quad \text{.....(3.79)}$$

Let

$$\gamma = \alpha + (\gamma_0 - \alpha)\frac{V}{V_0} \quad \text{.....(3.80)}$$

or

$$\frac{\gamma - \alpha}{V} = \frac{\gamma_0 - \alpha}{V_0} \quad \text{.....(3.81)}$$

Substituting (3.69) into (3.80) yields

$$\gamma = \frac{V}{V_0}(\gamma_0 + \alpha\mu) = \frac{1}{1+\mu}(\gamma_0 + \alpha\mu) \quad \text{.....(3.82)}$$

The internal energy per unit initial volume is:

$$E^{\nu} = \frac{E}{V_0} \quad \text{.....(3.83)}$$

Substituting (3.72), (3.82) and (3.83) into (3.79) yields

$$P = \frac{\rho_0\, C_0^2\, \mu\left[1 + \left(1 - \frac{\gamma_0}{2}\right)\mu - \frac{\alpha}{2}\mu^2\right]}{(1 + \mu - s\,\mu)^2} + (\gamma_0 + \alpha\,\mu)E^{\nu} \quad \text{.....(3.84)}$$

where the initial internal energy $E_0$ in (3.79) corresponds to the mechanical work done by the hydrostatic pressure in soil due to gravity. Using the parameters given in Table 3-3, Equation (3.84) can be used to calculate the pressures in the three phases of the soil.

For solid, the equation of state can be expressed as,

$$P = \frac{(2650)(6.319)^2\,\mu\,(1 + 0.5\mu)}{(1 - 0.41\mu)^2} + (1.0)E^{\nu} \quad \text{.....(3.85)}$$

For water, the equation of state can be expressed as,

$$P = \frac{(1000)(1.460)^2 \mu (1+0.7\mu)}{(1-\mu)^2} + (0.6)E^{\nu} \quad \text{.....(3.86)}$$

For air, the equation of state can be expressed as,

$$P = \frac{(1.2)(0.241)^2 \mu (1+\mu)}{(1-0.06\mu)^2} \quad \text{.....(3.87)}$$

The bulk modulus of the soil can be calculated as,

$$K = \frac{\rho_o C_o^2 \left[1+\left(1-\frac{\gamma_o}{2}\right)\mu - \frac{\alpha}{2}\mu^2\right]\left[1+\frac{2\mu(s-1)}{1+\mu-s\mu} + \frac{\mu(\gamma_o+\alpha\mu)}{(1+\mu)^2}\right] + \rho_o C_o^2 \mu\left(1-\frac{\gamma_o}{2}-\alpha\mu\right)}{(1+\mu-s\mu)^2}$$

$$+\left(\frac{(\gamma_o+\alpha\mu)^2}{(1+\mu)^2}+\alpha\right)E^{\nu} \quad \text{.....(3.88)}$$

As the compressibility of one phase of soil is different from another under the pressure, the volume of a particular soil phase cannot be explicitly determined. For a multi-phase soil medium under pressure, either a volume fraction or a weight fraction with respect to the original soil volume may be used to determine the content of each phase. If the initial volume fractions of the air, water and solid phases of soil are respectively $A_a$, $A_w$, and $A_s$, and $A_a^*$, $A_w^*$, and $A_s^*$ under the pressure, and $\rho_a$, $\rho_w$, and $\rho_s$ are the initial densities of the corresponding phases, the following equations can be obtained (Qian and Wang 1993):

$$A_a + A_w + A_s = 1 \quad \text{.....(3.89)}$$

$$\rho_o = A_s \rho_s + A_w \rho_w + A_a \rho_a \quad \text{.....(3.90)}$$

$$A_a^* = A_a \left( \frac{P_a}{P_0} \right)^{-k_a^{-1}} \quad \text{.....(3.91)}$$

$$A_w^* = A_w \left( \frac{k_w (P_w - P_0)}{\rho_w C_w^2} + 1 \right)^{-k_w^{-1}} \quad \text{.....(3.92)}$$

$$A_s^* = A_s \left( \frac{k_s (P_s - P_0)}{\rho_s C_s^2} + 1 \right)^{-k_s^{-1}} \quad \text{.....(3.93)}$$

where $\rho_0$ is the initial density of the soil, $P_0$ are the initial pressures, $k_s$, $k_w$, and $k_a$ are the respective exponents of the specific entropy of the solid, water and air phases, $C_w$ and $C_s$ are the sound speeds in water and solid, and $P_a$ , $P_w$ and $P_s$ are calculated using (3.84). The soil density under pressure $\rho$ can be expressed as

$$\rho = \rho_0 (A_s^* + A_w^* + A_a^*)^{-1}. \quad \text{.....(3.94)}$$

If the initial weight fractions of the air, water and solid phases of soil are respectively $R_a$, $R_w$, and $R_s$, it can be shown that

$$R_a + R_w + R_s = \frac{\rho_a A_a + \rho_w A_w + \rho_s A_s}{\rho_0} = \frac{\rho_0}{\rho_0} = 1 \quad \text{.....(3.95)}$$

The specific energy $E$ and the specific volume $V$ of the soil under pressure can be expressed in terms of the weight fractions of the three constituent phases as follows (Lovetskii et al. 1979):

$$E = R_a E_a + R_w E_w + R_s E_s \quad \text{.....(3.96)}$$

$$V = R_a V_a + R_w V_w + R_s V_s \quad \text{.....(3.97)}$$

The values of the EOS parameters for saturated soil are given in Table 3-3. These values are also valid for the dry soil, for example $A_s = 0.68$, $A_w = 0$, and $A_a = 0.32$.

# CHAPTER FOUR NUMERICAL ANALYSIS AND COMPARISON WITH TEST DATA

## 4.1 INTRODUCTION

Since shock wave propagation in soils including interaction between fluid (air) and solid (soil or structures), numerical simulation of explosion in soils is complex. Differences in characteristics were observed from detonation in two differing soil types: dry sand and saturated sand (Chapman et al. 2006, Gupta 1999). How to deal with soil properties in the simulation of explosion is important to obtain reasonably good simulation results. Therefore, there are two most important factors need to be considered for getting a good simulation. Two parameters are key in dealing with soil properties in explosion simulation and equation of state used.

Since the air and water are trapped within soil voids and deformed with the soil skeleton under blast loading, relative movement between the skeleton and the water and air can be neglected. Therefore, a stress tensor may be decomposed into a deviatoric stress component and a hydrostatic pressure:

$$\sigma_{ij} = \sigma_{ij}^{'} - P\delta_{ij} \quad \text{.....(4.1)}$$

where $\sigma_{ij}$ is the total stress, $P$ is hydrostatic pressure, positive in compression, and $\delta_{ij}$ is Kronecker delta. Deviatoric stress can be derived from soil material model and hydrostatic pressure can be determined from an equation of state.

Two methods are currently used to consider the soil properties in explosion simulation, the empirical method and the soil-model method.

In the empirical method, an equivalent input load is directly applied on concerned structures while the interaction between soil and explosive/structures is neglected. For example, when analyzing a plate subjected to the explosion detonated from a shallow-buried landmine, an empirical relationship of a specific impulse (Westine et al 1985) may be directly applied on the plate; this is known as US Army TACOM impulse model. The main advantage of this method is its ease in application. Validation of this method on some simple geometrical structures was done with carefully calibrated parameters in the impulse model (Williams et al 2002).

For the sake of simplification, the conventional way is to apply an equivalent input loads based on empirical functions which includes soil properties without equation of state. For example, *LOAD-BLAST boundary condition was implemented into LS-DYNA finite element code based on CONWEP air-blast functions (Randers-Pehrson and Bannister 1997) to simulate surface detonations. This input load cannot consider the effects on different soil types. A more accurate empirical relationship, called US Army TACOM impulse model, was developed by Westine et al. (1985) at Southwest Research Institute to predict the impulse applied by a buried mine to a plate at a given offset from the mine. The relationship is expressed as

$$i_n = f\left(r, d, D_{\min e}, s, \rho_{soil}, m_{\min e}, \beta, \theta\right) \quad (4.2)$$

where the soil density, $\rho_{\text{soil}}$, is considered. Other variables are defined in FIG. 4-1.

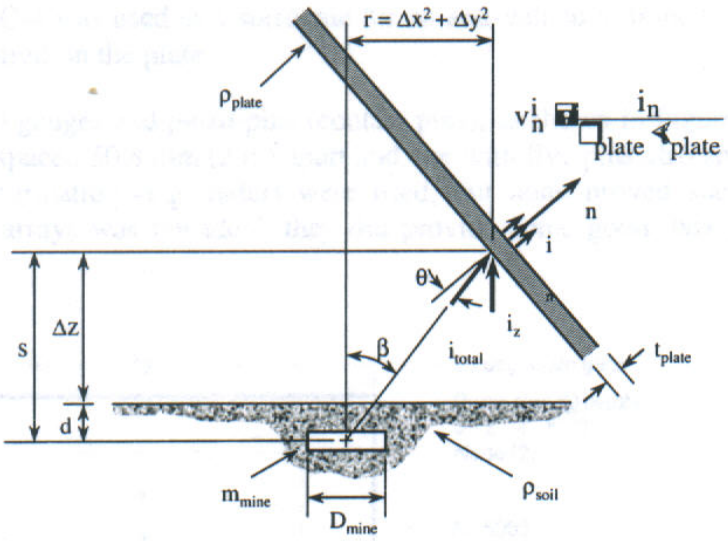


FIG. 4- 1 Definition of variables in US Army TACOM impulse model (Westine et al. 1985)

If the model parameters are carefully calibrated (Williams et al 2002), this empirical model can predict the effect mine blast on simple geometries reasonable well.

This method is obviously not capable of capturing the complex transient interactions between the soil and detonation products, which may substantially affect the estimated blast loads and the resultant structure. Soil and debris could not be implemented directly into the soil finite element model.

In order to compensate this limitation, in the soil-model method proposed herein the constitutive models are invoked to simulate the soil behavior in explosion (Gupta 1999, Wang 2001).

The soil and foam material model was applied by Wang (2001) in LS-DYNA (*MAT5) to simulate a series of explosions in air and soil. The simulation results were

compared reasonably well with experimental results. The soil and foam model may be considered as a special kind of cap model, but the cap is a plane cap in principal stress space (Krieg 1972). Although this model is highly efficient, it has the following disadvantages: lack of associative flow plasticity, instability in unconfined states, and no consideration of strain rate effect.

To date the equations of state that can be used in numerical simulation of explosion in soils limited. Sedgwick (1974) applied for Tillotson equation of state in the two-dimensional HELP computer code to solve the interaction between buried explosive charges. Dynamic material properties experiments were performed to provide the necessary soil equation of state parameters which are required as input to the numerical model. The equation of state for the solid component and the substance in the pores (gas or liquid) were taken in the Mie-gruneisen form by Lovetskill, Maslennikov and Fetisov (1979). The gaseous component was assumed to be an ideal gas and the temperature of all the components was assumed to be identical. A particular form of the Mie-gruneisen equation of state was applied by Grujicic et al (2008) to calculate pressure dependence on mass density and internal-energy density. Qian (1993) and Wang (2004) both applied Kandaur conceptual equation of state based on the three-phase soil structure in the soil model for blast loading.

In this chapter, viscoplastic cap soil model and equation of state model are integrated into LS-DYNA finite element code (PC version) as user-defined material and EOS model respectively. A series of landmine explosion tests in dry sand and saturated sand conducted by Materials Sciences Corporation (2007) are simulated using the user-

defined soil model and EOS model. The simulation results are evaluated through comparison against experimental data.

## 4.2 PROPERTIES OF SOIL USED IN EXPLOSIVE TESTS

The soil subjected to the plate impact tests by Chapman et al. (2006) was quartz sand provided by the Concrete Structure Section (CSS), Department of Civil and Environmental Engineering, Imperial College, UK. The sand had average particle size of 230 μm and dry soil density of 1520 ± 50 kg $m^{-3}$. Since the density of quartz is 2650 kg $m^{-3}$, the porosity of the sand was about 43%. If all the voids were filled with water, the theoretical maximum water content and density would be 22% and 1950 kg $m^{-3}$, respectively.

A sandy soil was provided by the Army Research Laboratory (ARL), Aberdeen, MD, for the explosive tests conducted by Materials Sciences Corporation (2006). Table 4-1 provides a comparison of the soil properties. Since the properties of the ARL soil are very comparable to those of the CSS quartz sand, the EOS models based on the CSS quartz sand test data were used in the numerical simulations of the explosive tests.

Table 4- 1 Properties of soil specimens

| Soil | Provided by | Density (kg $m^{-3}$) | Volume ratio of water | Porosity |
|---|---|---|---|---|
| Dry Sand | CSS | 1520 | 0% | 43% |
| | ARL | 1871 | 0% | 31.23% |
| Saturated Sand | CSS | 1950 | 22% | 43% |
| | ARL | 2072 | 20.12% | 31.23% |

## 4.3 DESCRIPTION OF EXPLOSION TEST

To verify the validity of the revised soil model under blast loading, the EOS models along with the viscoplastic cap model are incorporated into the software LS-DYNA (LSTC 2003) as user-defined subroutines for numerical simulations.

Explosive tests at a 3-cm depth of burial (DOB) for dry (3 tests) and saturated (3 tests) sandy soil were conducted by the Materials Sciences Corporation (2006). Tests data were provided by ARL. As shown in FIG. 4-2, a 70-cm high cylindrical tank, made of a 1.2-cm thick steel pipe with a 60-cm inner diameter, was filled with the test soil. A 100-gram C4 explosive charge with 6.4-cm diameter and 2-cm thickness was placed at a 3-cm depth in the soil at the center of the tank. Nine "pencil" pressure transducers were placed above the soil mass to measure air pressure from the explosive gas bubble expansion. Transducers #1 through #5 were placed at the same standoff distance of 30 cm and pointing toward the center of C4 at 0, ±22.5, and $\pm 45^{o}$ angles, #6 through #8 were placed at 70 cm and at 0 and $\pm 30^{o}$ angles, and #9 at 113 cm and at $0^{o}$ angle. Transducers #1, #6 and #9, respectively located at 30 cm, 70 cm and 110 cm directly above the soil, are selected for comparisons between the numerical results and measured air pressure due to buried explosions. The scheme of the explosive tests set-up is shown in FIG. 4-3. FIG. 4-4 and FIG. 4-5 are explosive tests photos taken by high speed video for saturated soil and dry soil, respectively.

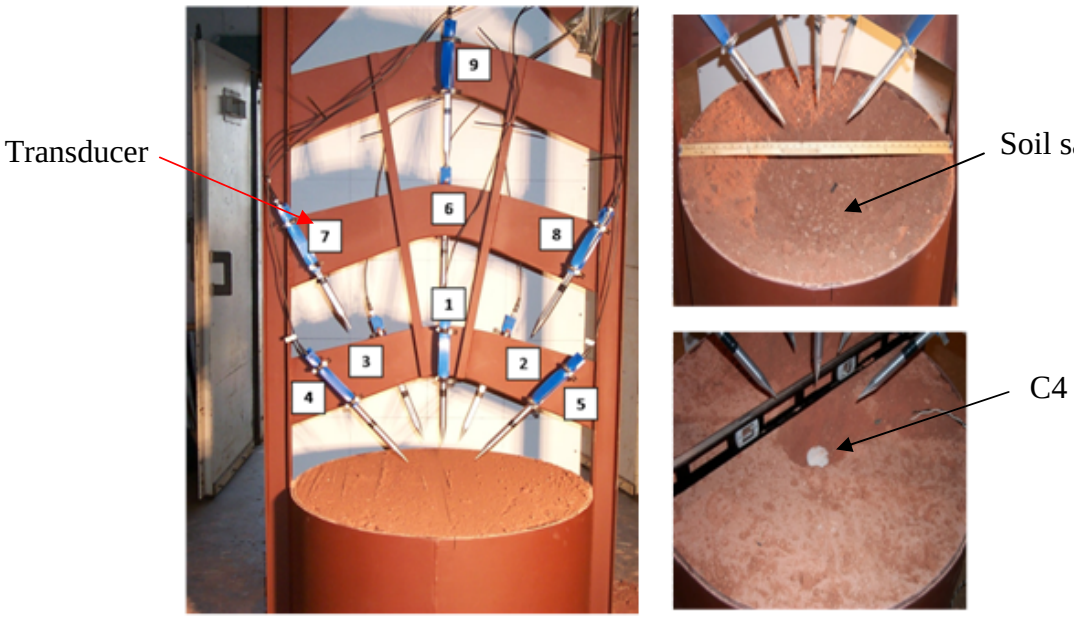


FIG. 4- 2 Explosive test set-up

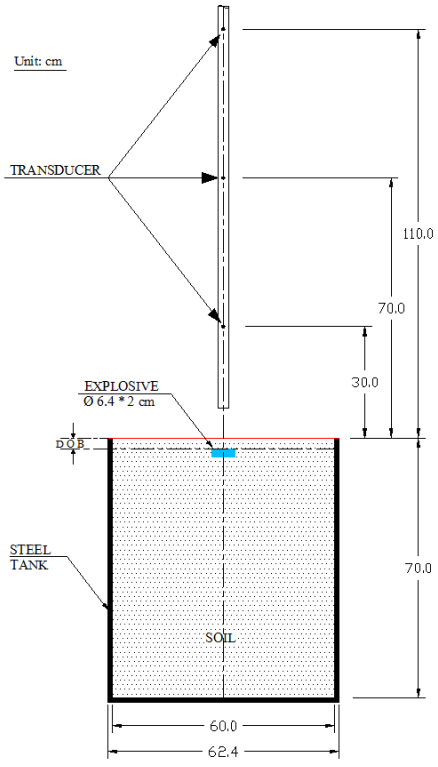


FIG. 4- 3 Schematic explosive test set-up

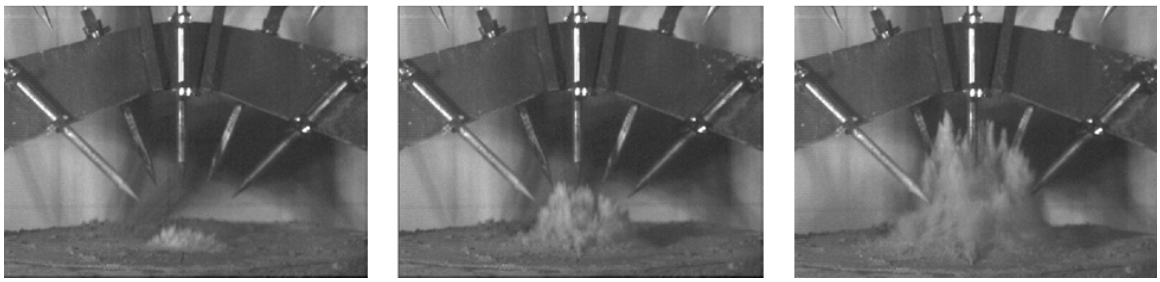

40μsec 417μsec 833μsec

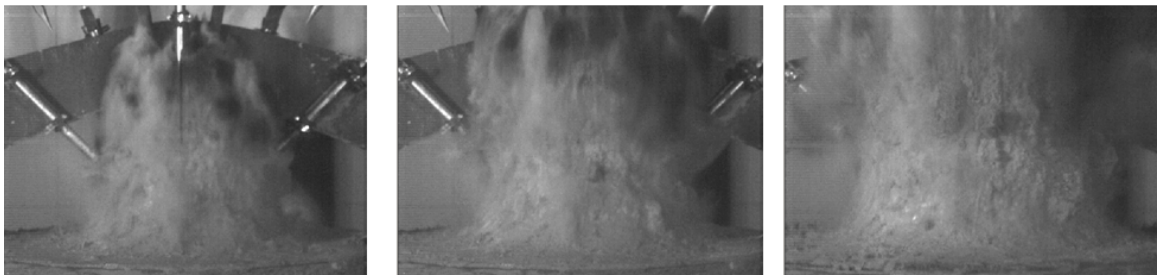

1042μsec 1202μsec 1455μsec

FIG. 4- 4 Explosive test for saturated soil with DOB=3 cm by high speed video

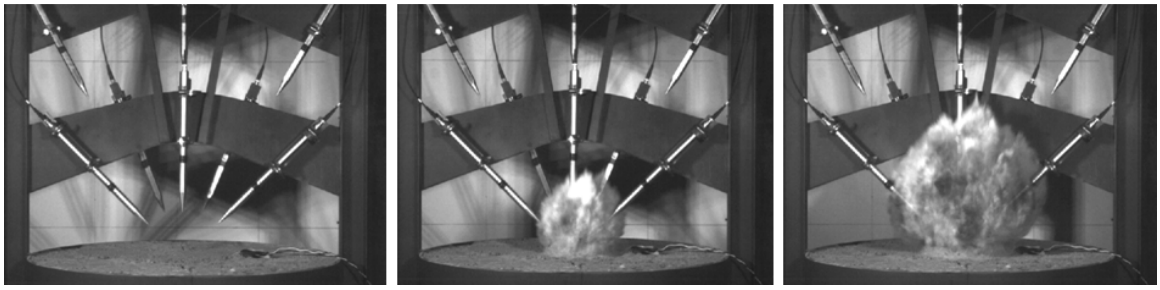

4μsec 212μsec 420μsec

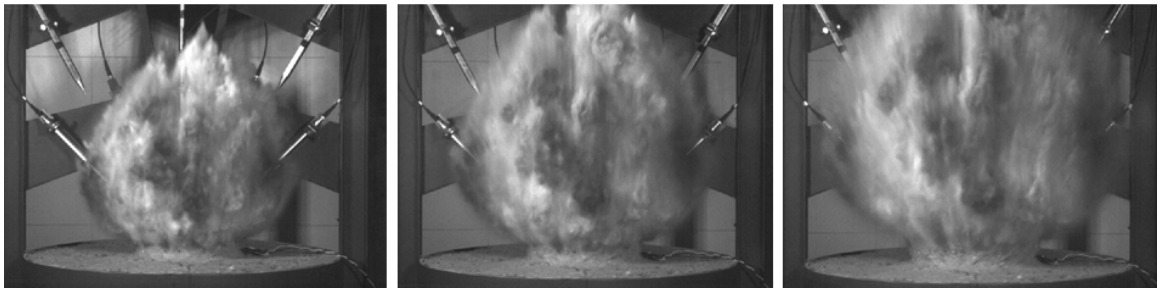

614μsec 836μsec 1044μsec

FIG. 4- 5 Explosive test for dry soil with DOB=3 cm by high speed video

## 4.4 FINITE ELEMENT MODEL

Taking advantage of symmetry, only a quarter of the test setup was modeled. The finite element model is shown in FIG. 4-6 containing a 110-cm air volume above and a 70-cm soil volume below the soil surface, meshed with 6,400 8-node solid ALE elements. Fine mesh was generated for the explosive and for the air and soil volumes surrounding the C4 where high strain gradients are anticipated. The fine mesh of soil elements extended 3 cm above and below, and 4.8 cm outward in the radial direction beyond the circumference of the C4 explosive. The fine mesh of air elements extended 8 cm above the soil surface and 8 cm in the radial direction. Coarser mesh was used in the region further away from the explosive to reduce computation time. The materials used in finite element model and their equation of states are shown in FIG. 4-7.

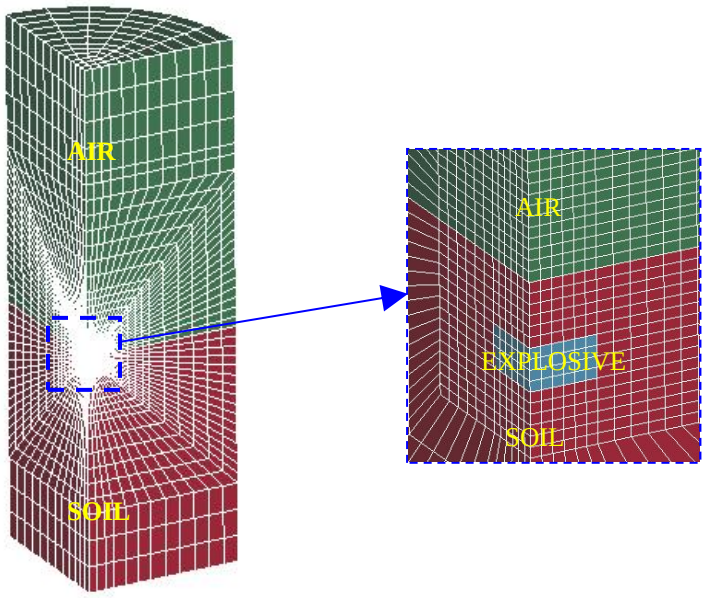


FIG. 4- 6 Finite element mesh

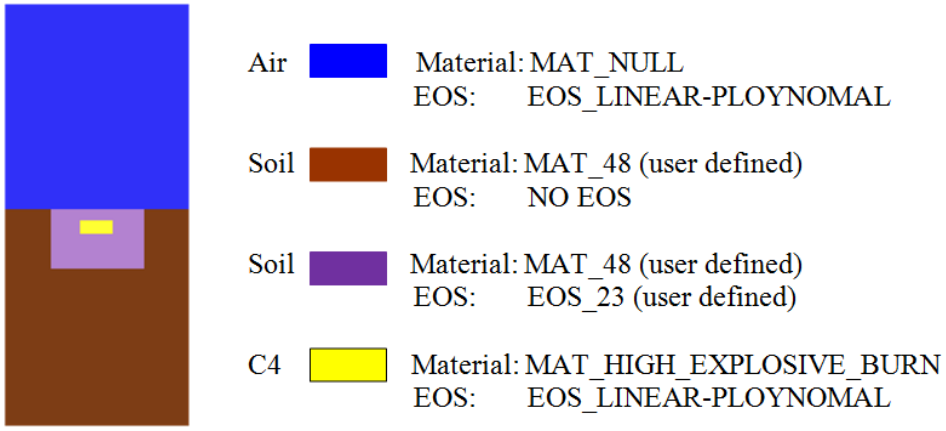


FIG. 4- 7 Material and EOS model

The steel tank was treated as a fixed boundary of the soil. All the exterior boundary of the air was also fixed. The height of the air in the finite element model was set 110cm, which was sufficient for investigating pressure vs. time history at the positions of the transducers. The nodes on the interfaces between the air, soil and explosive were merged, which was the most reliable and economic way to simulate contact.

To avoid large distortions in the elements by the explosion, automatic rezoning was achieved by using the Arbitrary Lagrangian-Eulerian (ALE) technique ("LS-DYNA" 1998). Set as multiple materials, explosive, soil and air were allowed within the same mesh so that the explosive product (i.e., the fire ball) would be able to expand into initial soil and air meshes and the soil could be ejected into the air mesh.

There are a total of 12 material parameters in the viscoplastic cap model: $\eta$, $N$, $f_0$ in the viscous flow rule; $W$, $D$, $R$, $X_0$ in the cap surface; $\alpha$, $\beta$, $\gamma$, $\theta$ in the failure surface;

and $T$ in the tension cutoff surface. In addition, the bulk modulus $K$ and the shear modulus $G$ are needed for the elastic soil response. These parameters are determined from various static soil tests. Values of the model parameters for a sandy soil are given in Table 4-2.

Table 4- 2 Viscoplastic cap model parameters for sandy soil

| **Sand** | **K** (MPa) | **G** (MPa) | **A** (MPa) | **B** ($MPa^{-1}$) | **Γ** (MPa) | **θ** | **R** |
|---|---|---|---|---|---|---|---|
| **Dry** | 106.4 | 63.85 | 0.0642 | 0.34283 | 0.00589 | 0.18257 | 5.00 |
| **Saturated** | 1000 | 20.00 | 0.0625 | 0.36430 | 0.00320 | 0.24900 | 5.32 |
| **Sand** | **W** | **D** ($MPa^{-1}$) | $\mathbf{X_0}$(MPa) | **T** (MPa) | **H** ($\mu sec^{-1}$) | $\mathbf{f_0}$ (MPa) | **N** |
| **Dry** | 0.2142 | 0.00952 | 0.01 | 0.0069 | $2\times10^{-4}$ | $1.0\times10^{5}$ | 1.0 |
| **Saturated** | 0.2250 | 0.00884 | 0.01 | 0.0072 | $1\times10^{-4}$ | $1.2\times10^{5}$ | 1.0 |

The explosion product of C4 is modeled with the JWL equation of state (Dobratz and Crawford 1985). It can be written in the form

$$P = A\left(1-\frac{\omega}{R_1V}\right)e^{-R_1V} + B\left(1-\frac{\omega}{R_2V}\right)e^{-R_2V} + \frac{\omega E}{V} \quad \text{.....(4.3)}$$

where $A$, $B$, $R_1$, $R_2$ and $\omega$ are constants determined from the experiments, $V$ is the relative volume, $E$ is the internal energy. The EOS parameters for C4 are listed in Table 4-3.

Table 4- 3 JWL equation of state parameters for C4

| A (MPa) | B (MPa) | $R_1$ | $R_2$ | ω | $E_0$ (MPa) | $V_0$ |
|---|---|---|---|---|---|---|
| 609970 | 12950 | 4.5 | 1.4 | 0.25 | 9000 | 1 |

The air above the soil is modeled with the LINEAR-POLYNOMIAL equation of state ("LS-DYNA" 1998). It can be written in the form

$$P = C_0 + C_1\mu + C_2\mu^2 + C_3\mu^3 + \left(C_4 + C_5\mu + C_6\mu^2\right)E \quad \text{.....(4.4)}$$

where $C_0$, $C_1$, $C_2$, $C_3$, $C_5$ and $C_6$ are polynomial equation coefficient. $\mu = \frac{\rho}{\rho_0} - 1$, and $\frac{\rho}{\rho_0}$ is the ratio of current density to reference density. $E$ is the internal energy, $V$ is the relative volume. The EOS parameters for air are listed in Table 4-4.

Table 4- 4 LINEAR-POLYNOMIAL equation of state parameters for air

| $C_0$ | $C_1$ | $C_2$ | $C_3$ | $C_4$ | $C_5$ | $C_6$ | $E_0$ (MPa) | $V_0$ |
|---|---|---|---|---|---|---|---|---|
| -1.0e-6 | 0.0 | 0.0 | 0.0 | 0.4 | 0.4 | 0.0 | 0.25 | 1 |

As illustrated in FIG. 4-8, at detonation (time t = 0), energy prescribed by Eq. (4.3) is released from the center of the C4 elements. This pressure is transferred to the soil elements surrounding the C4, which are within the fine mesh of the model. The EOS models developed are used to account for thermodynamic equilibrium for the air, water and solid phases of these soil elements. The shock front pressure decays exponentially with distance from the point of detonation, and pressure level is much lower when the shock front reaches the fine mesh boundary. Thus, EOS models are not used for soil elements in the coarse mesh. This process is illustrated in FIG. 4-9, simply.

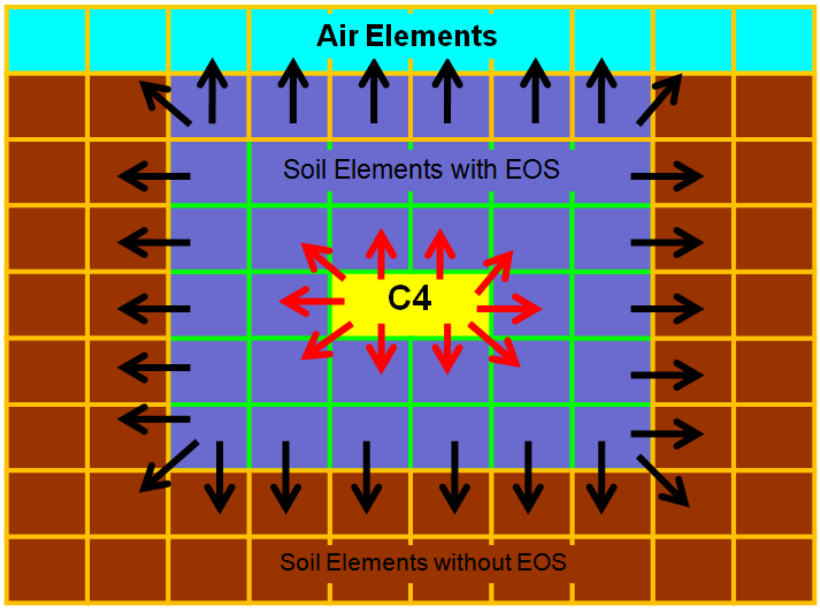


FIG. 4- 8 Material and EOS models used for the FE mesh

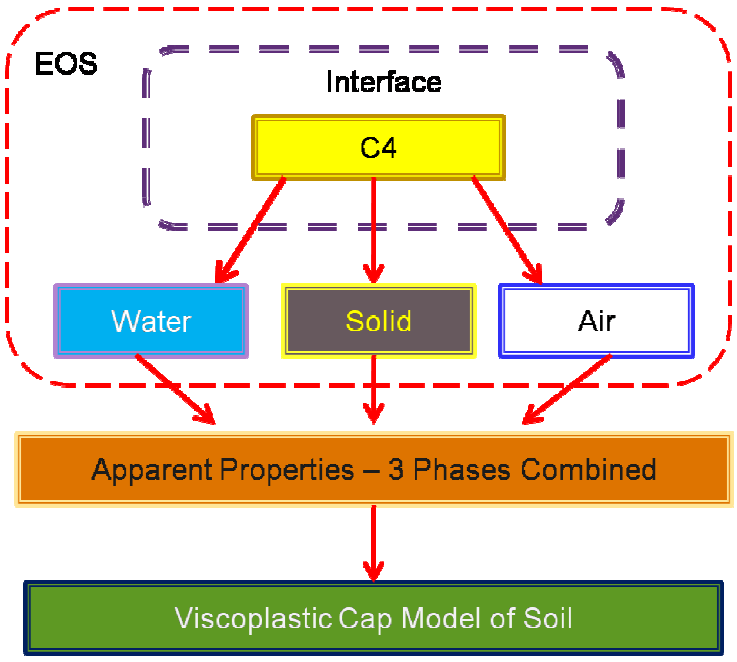


FIG. 4- 9 Energy transmission chart

The flowchart in FIG. 4-10 illustrates the implementation of the algorithm using an incremental time-step approach. The model is subjected to gravity load to provide the initial pressure and energy of the soil. The change in volume over a time step is calculated for each soil element after detonating the C4. The changes in volume of the three phases are calculated by Eq. (3.91), (3.92) and (3.93). During each time step, the internal energy consisting of the deviatoric strain energy and the mechanical work done by the hydrostatic pressure is updated. The new work done by the pressure on the change in volume from each phase is added to the internal energy of the soil element by Eq. (3.96). The soil bulk modulus is updated using Eq. (3.88) for subsequent soil stress and strain calculations in the viscoplastic cap model. The instructions for the implementation of a user-defined EOS are given in the Appendix B of the LS-DYNA user's manual (LSTC 2003).

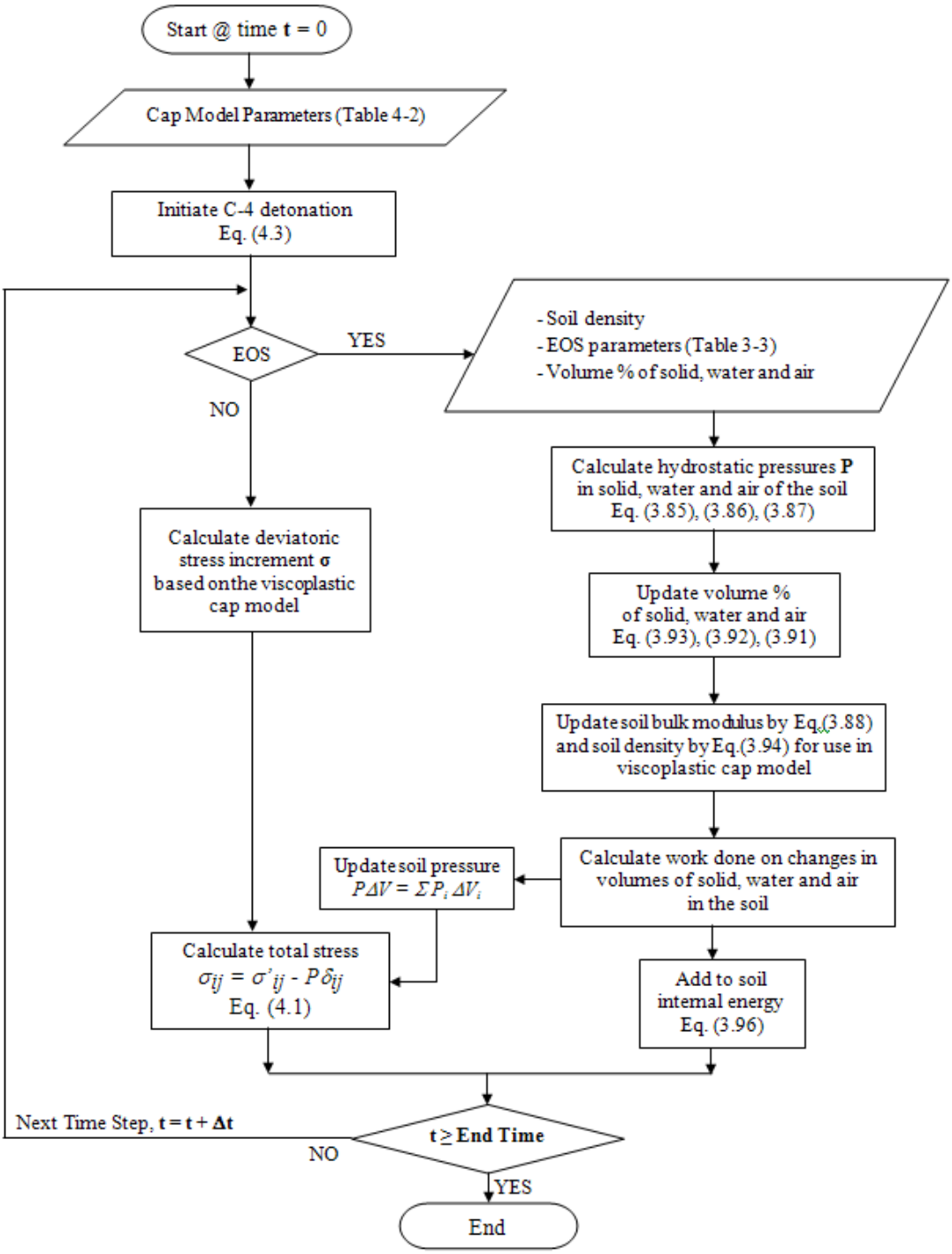


FIG. 4- 10 Flowchart showing the solution algorithm for use in LS-DYNA

## 4.5 SIMULATION FOR SATURATED SOIL

### 4.5.1 SIMULATION CASES AT DIFFERENT ELEMENT

**Case 1 (under the C4):**

A soil element (#654), shown in FIG. 4-11, whose center is located at 3 cm to the right and 2.75 cm down from the center of C4, is selected from a saturated soil test to illustrate the numerical procedure. Before the shock wave arrives at t =20μsec, its soil density is 2055 kg/m$^3$, bulk modulus is 1000MPa, and the volume fractions of solid, water and air are respectively 70%, 20% and 10%. When the shock arrives at time step t =20+5=25μsec, hydrostatic pressures in the solid, water and air phases are calculated to be 5.02MPa, 0.0874MPa and 0.000215MPa, respectively, by Eq. (3.85), (3.86) and (3.87). The volume fractions in soil are updated using Eq. (3.91), (3.92) and (3.93), to be 70.15%, 20.10% and 9.1%. Using Eq. (3.88) and (3.94) to update the soil bulk modulus and density are 1142.12MPa and 2063 kg m$^{-3}$. The soil volume increment can be obtained from LS-DYNA, total volume increment is -1.7076 E-05 (μ=7.601E-05), solid volume increment $\Delta V_s$ is -8.201E-06 (μ=4.743E-05), water volume increment $\Delta V_w$ is -1.353E-06 (μ=4.10E-05) and air volume increment $\Delta V_a$ is -7.522E-6 (μ=3.0852E-03). The soil pressure is 2.43MPa. It can be passed to deviatoric stress to calculate total stress by Eq. (4.1). The soil internal energy is 0.0000417MPa by Eq. (3.96). By now, all parameters of viscoplastic cap model and EOS are known. The next time step can be run. At t= 40μsec, soil bulk modulus arrives peak value 2000MPa. The volume fractions in soil are 72.92%, 20.51% and 8.75%, respectively. The increments of volume fractions in soil are 2.92%,

0.51% and -1.25%, respectively. The procedure of volume fractions change is shown in FIG. 4-12.

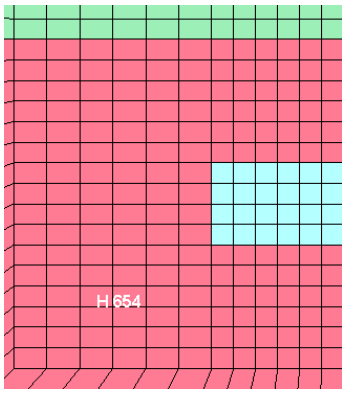


FIG. 4- 11 Element #654

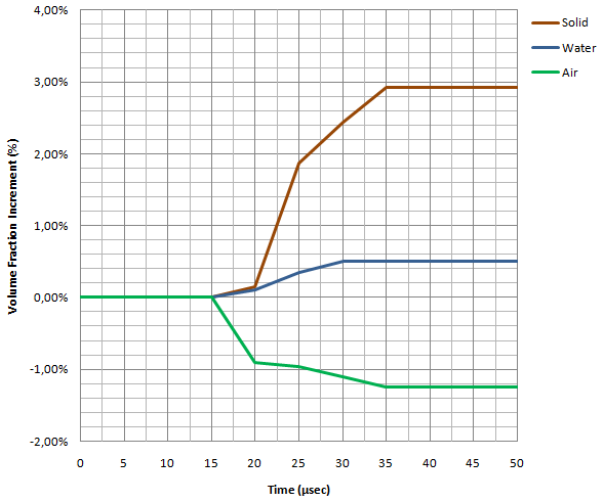


FIG. 4- 12 Saturated soil increments of volume fractions in element #654

**Case 2 (flush with the C4):**

A soil element (#748), shown in FIG. 4-13, whose center is located at 3 cm to the right from the center of C4 and flush with the center of C4, is selected from a saturated

soil test to illustrate the numerical procedure. Before the shock wave arrives at t =20μsec, its soil density is 2055 kg/m$^3$, bulk modulus is 1000MPa, and the volume fractions of solid, water and air are respectively 70%, 20% and 10%. When the shock arrives at time step t =20+5=25μsec, hydrostatic pressures in the solid, water and air phases are calculated to be 3.48MPa, 0.0615MPa and 0.0002MPa, respectively, by Eq. (3.85), (3.86) and (3.87). The volume fractions in soil are updated using Eq. (3.91), (3.92) and (3.93), to be 70.13%, 20.10% and 9.08%. Using Eq. (3.88) and (3.94) to update the soil bulk modulus and density are 1133.23MPa and 2060 kg m$^{-3}$. The soil volume increment can be obtained from LS-DYNA, total volume increment is -1.662 E-05 (μ=7.711E-05), solid volume increment $\Delta V_s$ is -8.175E-06 (μ=4.743E-05), water volume increment $\Delta V_w$ is -1.212E-06 (μ=4.10E-05) and air volume increment $\Delta V_a$ is -7.233E-6 (μ=3.0852E-03). The soil pressure is 2.15MPa. It can be passed to deviatoric stress to calculate total stress by Eq. (4.1). The soil internal energy is 0.0000417MPa by Eq. (3.96). By now, all parameters of viscoplastic cap model and EOS are known. The next time step can be run. At t= 40μsec, soil bulk modulus arrives peak value 2000MPa. The volume fractions in soil are 72.31%, 20.51% and 8.84%, respectively. The increments of volume fractions in soil are 2.31%, 0.51% and -1.26%, respectively. The procedure of volume fractions change is shown in FIG. 4-14.

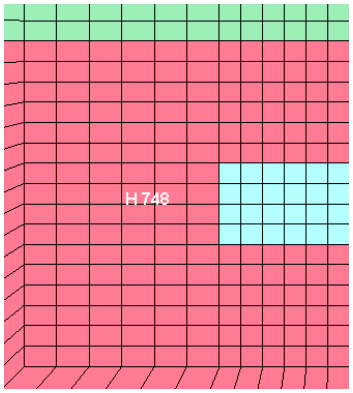


FIG. 4- 13 Element #748

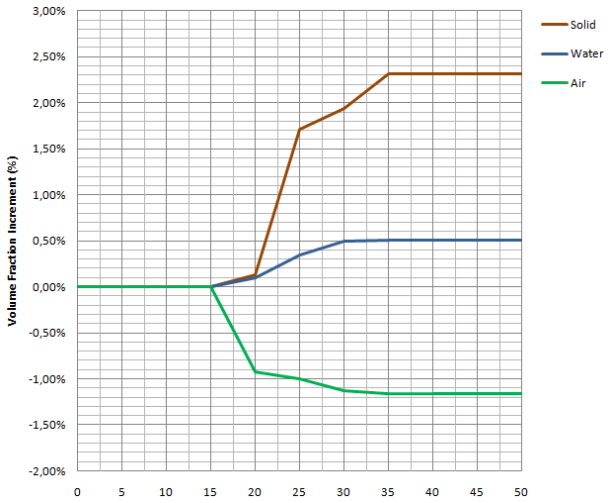


FIG. 4- 14 Saturated soil increments of volume fractions in element #748

**Case 3 (above the C4):**

A soil element (#852), shown in FIG. 4-15, whose center is located at 3 cm to the right and 2.75 cm above from the center of C4, is selected from a saturated soil test to illustrate the numerical procedure. Before the shock wave arrives at t =20μsec, its soil density is 2055 kg/m$^3$, bulk modulus is 1000MPa, and the volume fractions of solid, water and air are respectively 70%, 20% and 10%.

There is a little difference between the elements above C4 and the elements under the C4. The equation to calculate hydrostatic pressure can be expressed as:

$$p = \rho_0 C^2 \mu + \gamma_0 E^v \quad \text{.....(4.5)}$$

For solid, this equation can be expressed as:

$$p = (2650)(6.319)^2 \mu + (1.0) E^v \quad \text{.....(4.6)}$$

For water, this equation can be expressed as:

$$p = (1000)(1.460)^2 \mu + (0.6) E^v \quad \text{.....(4.7)}$$

For air, this equation can be expressed as:

$$p = (1.2)(0.241)^2 \mu \quad \text{.....(4.8)}$$

When the shock arrives at time step t =20+5=25μsec, hydrostatic pressures in the solid, water and air phases are calculated to be -4.21MPa, -2.011MPa and -0.832MPa, respectively, by Eq. (4.6), (4.7) and (4.8). The volume fractions in soil are updated using Eq. (3.91), (3.92) and (3.93), to be 68.99%, 19.44% and 6.99%. Using Eq. (3.88) and (3.94) to update the soil bulk modulus and density are 923.23MPa and 2032 kg $m^{-3}$. The soil volume increment can be obtained from LS-DYNA, total volume increment is 4.233 E-05 (μ=-9.348E-05), solid volume increment $\Delta V_s$ is 0.875E-05 (μ=-3.691E-05), water volume increment $\Delta V_w$ is 1.226E-05 (μ=-5.421E-05) and air volume increment $\Delta V_a$ is 2.122E-05 (μ=-7.188E-03). The soil pressure is -5.786MPa. It can be passed to deviatoric stress to calculate total stress by Eq. (4.1). The soil internal energy is 0.0000417MPa by

Eq. (3.96). By now, all parameters of viscoplastic cap model and EOS are known. The next time step can be run. At t= 35μsec, since shock wave arrives, soil above C4 is blown by the force of the explosion. The volume fractions in soil are 0.0%, 0.0% and 0.0%, respectively. The increments of volume fractions in soil are -70.0%, -20.0% and –10.0%, respectively. The procedure of volume fractions change is shown in FIG. 4-16.

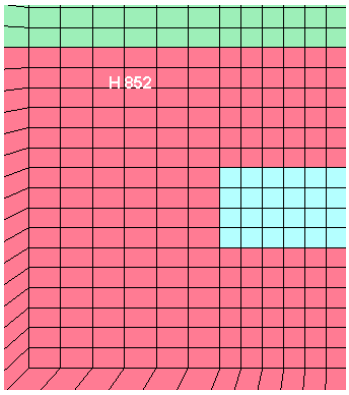


FIG. 4- 15 Element #852

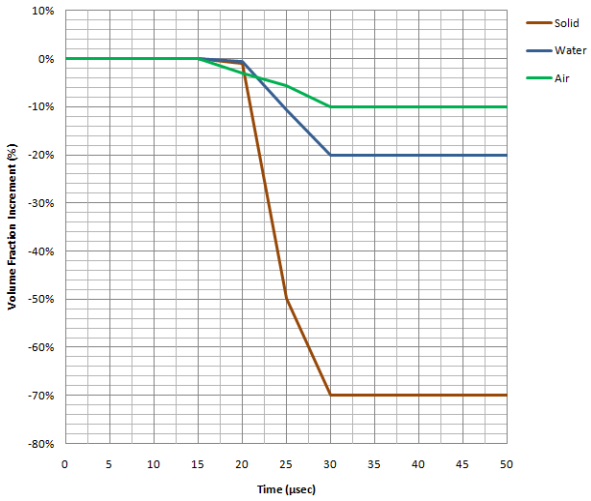


FIG. 4- 16 Saturated soil increments of volume fractions in element #852

**Case 4 (Air element above the C4):**

An air element (#4498), shown in FIG. 4-17, whose center is located at 30 cm above from the center of C4, is selected from a saturated soil test to illustrate the numerical procedure. Initially, this element is defined by material model of air. Since the ALE (Arbitrary Lagrangian-Eulerian) calculation is selected by this study, the primary advantage of ALE is the number and types of materials present in an element can change dynamically when elements with more than one material. Under blasting loading, a part of volume of the element 4498 is occupied by soil debris following an explosion, shown in FIG. 4-18. The soil volume fraction arrive peak value 17.1% at 300μsec.

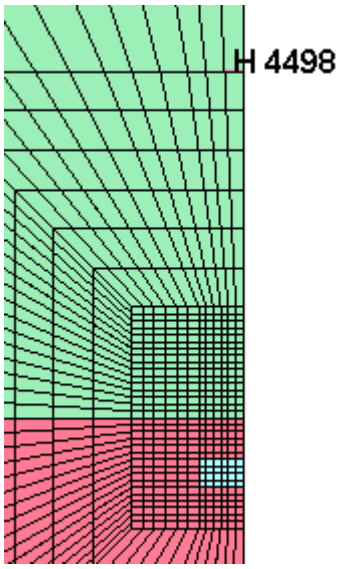


FIG. 4- 17 Air element #4498

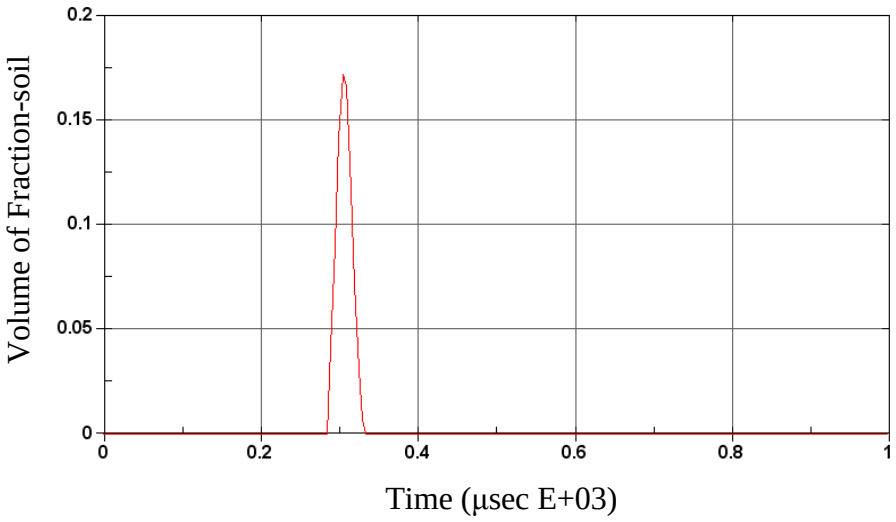


FIG. 4- 18 Volume fraction of saturated soil in air element #4498

### 4.5.2 COMPARISON OF SIMULATION WITH TEST RESULTS

From FIG. 4-19 to FIG. 4-27 present the air pressure time-histories at three tests respectively, which were recorded by the pencil gages (see Fig. 8) after a C4 charge was detonated in saturated sand at a DOB = 3 cm (Materials Sciences Corporation 2006). A comparison between the predicted shock front air pressure and the experimental data obtained at distances of 30 cm, 70 cm, and 110 cm directly above the soil is shown in FIG. 4-28. The difference between the numerical results and the average test data at 30, 70 and 110-cm standoff distances are 4.5%, 12.5% and 7.2%, respectively.

Density and bulk modulus are the most sensitive parameters in simulation model. A comparison among simulation results with the density decreased to 90% of initial density and with the bulk modulus decreased to 90% of initial bulk modulus and density and bulk modulus keep the initial value is shown in FIG. 4-29.

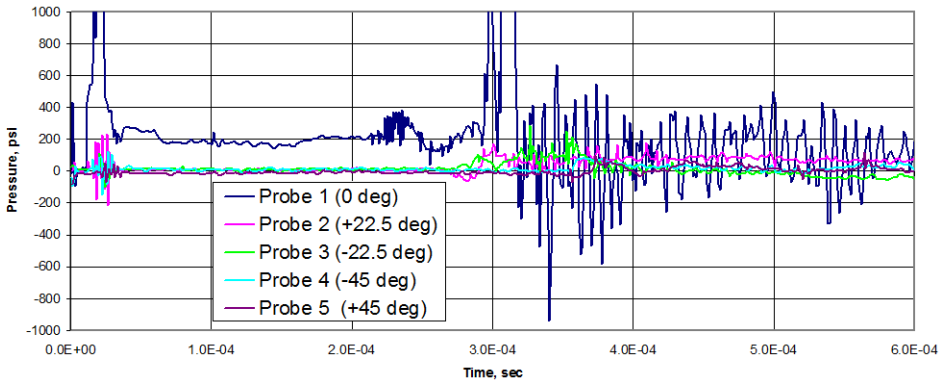


FIG. 4- 19 Saturated sand air pressure time-histories, 30 cm standoff distance #1

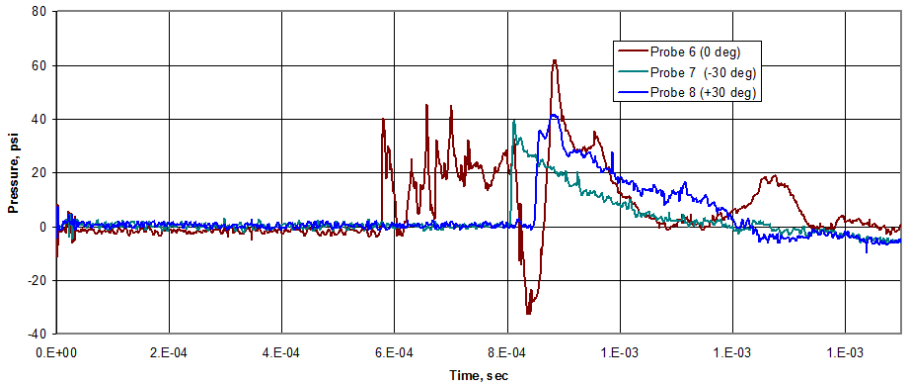


FIG. 4- 20 Saturated sand air pressure time-histories, 70 cm standoff distance #1

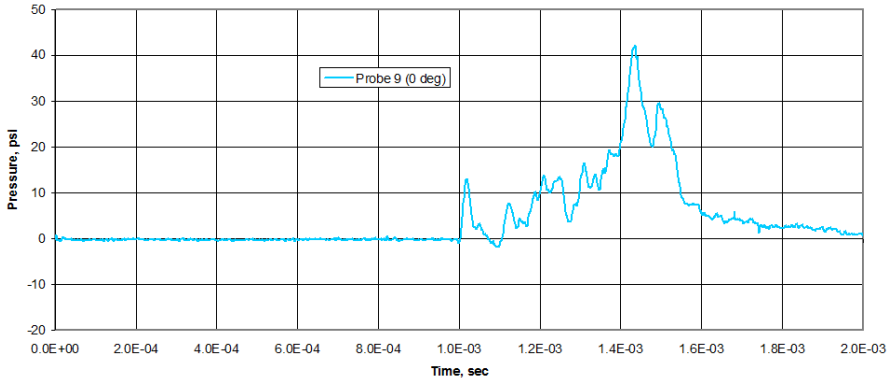


FIG. 4- 21 Saturated sand air pressure time-histories, 110 cm standoff distance #1

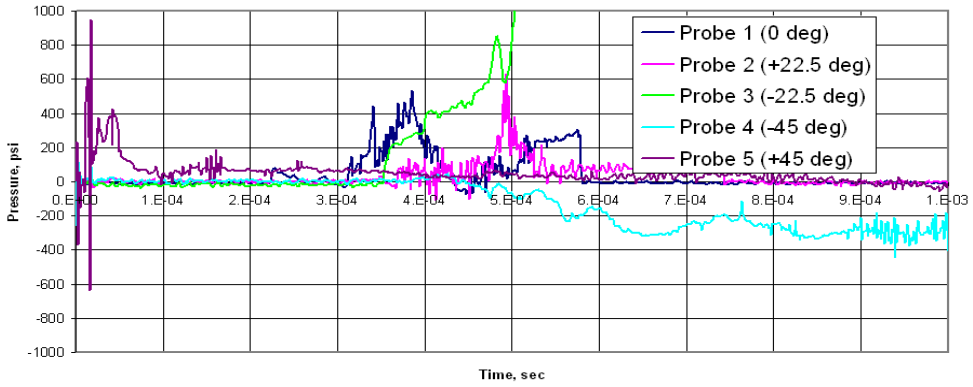


FIG. 4- 22 Saturated sand air pressure time-histories, 30 cm standoff distance #2

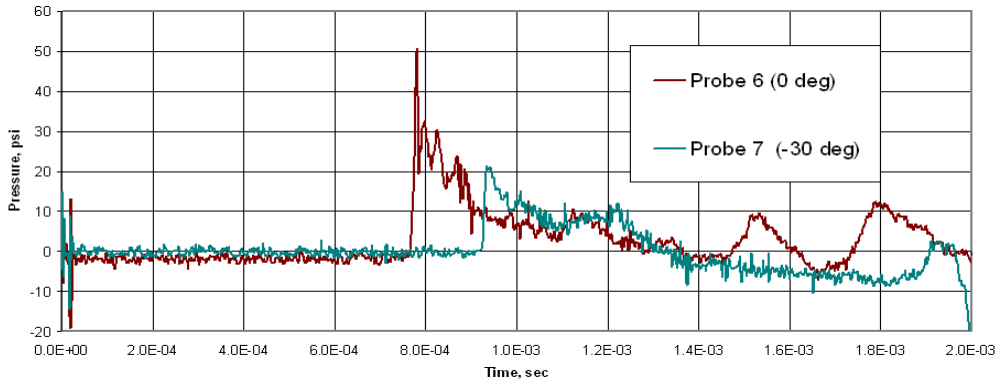


FIG. 4- 23 Saturated sand air pressure time-histories, 70 cm standoff distance #2

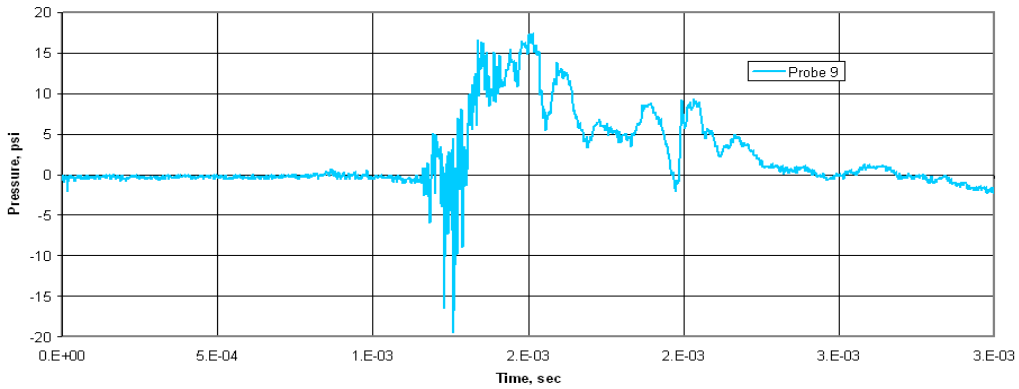


FIG. 4- 24 Saturated sand air pressure time-histories, 110 cm standoff distance #2

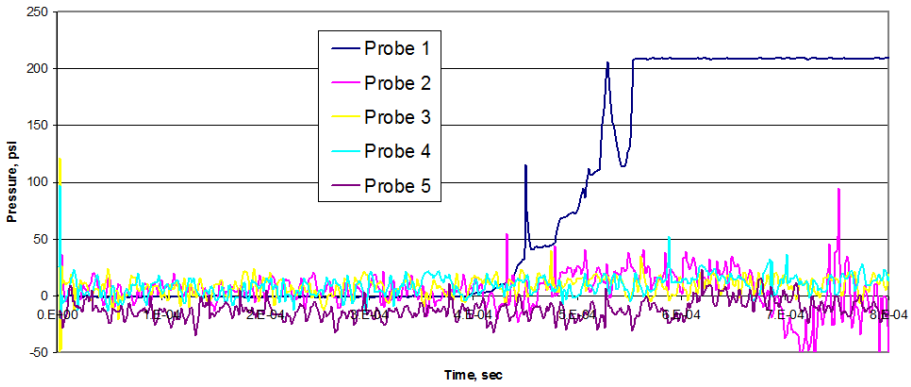


FIG. 4- 25 Saturated sand air pressure time-histories, 30 cm standoff distance #3

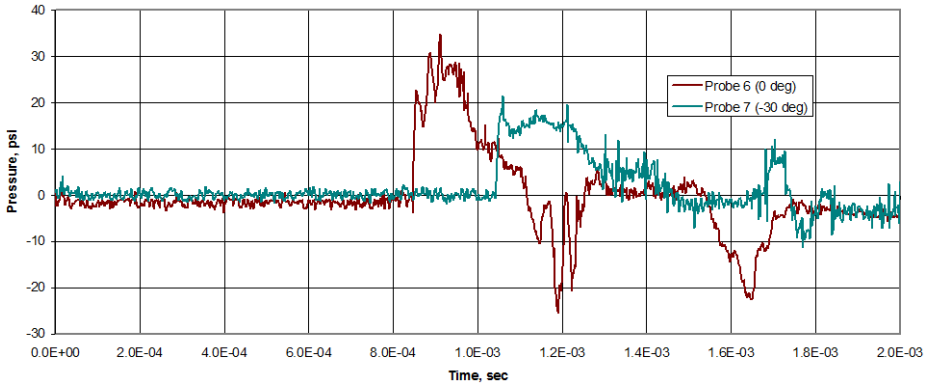


FIG. 4- 26 Saturated sand air pressure time-histories, 70 cm standoff distance #3

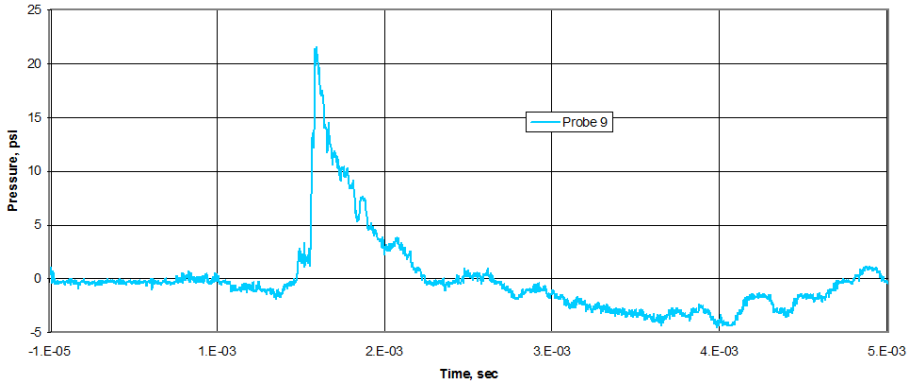


FIG. 4- 27 Saturated sand air pressure time-histories, 110 cm standoff distance #3

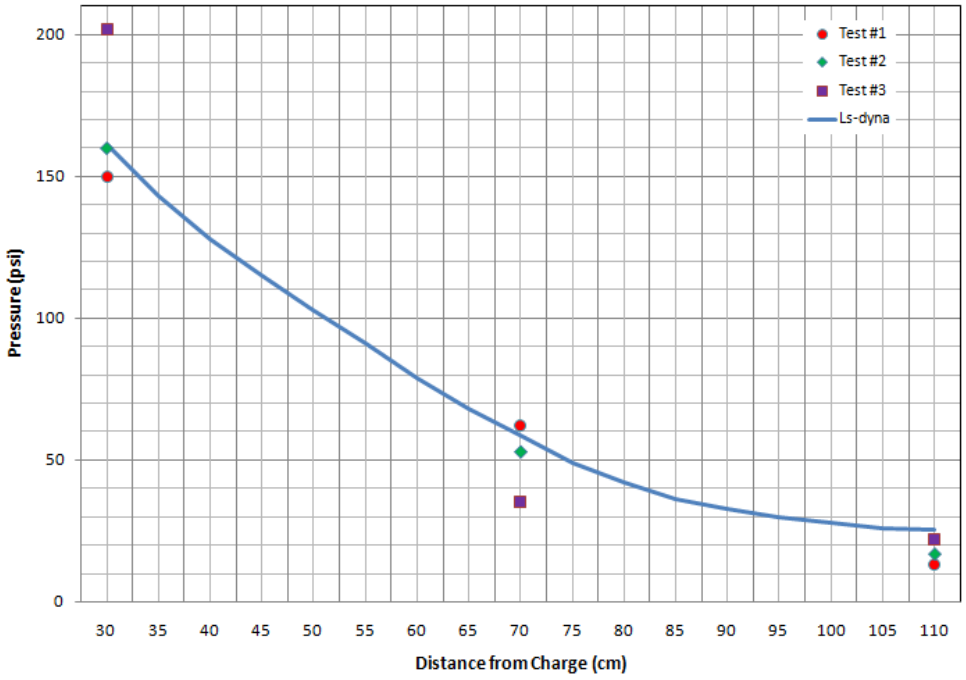


FIG. 4- 28 Comparison between numerically predicted and experimental values for saturated sand (Shock front pressure in air VS. Transducer distance)

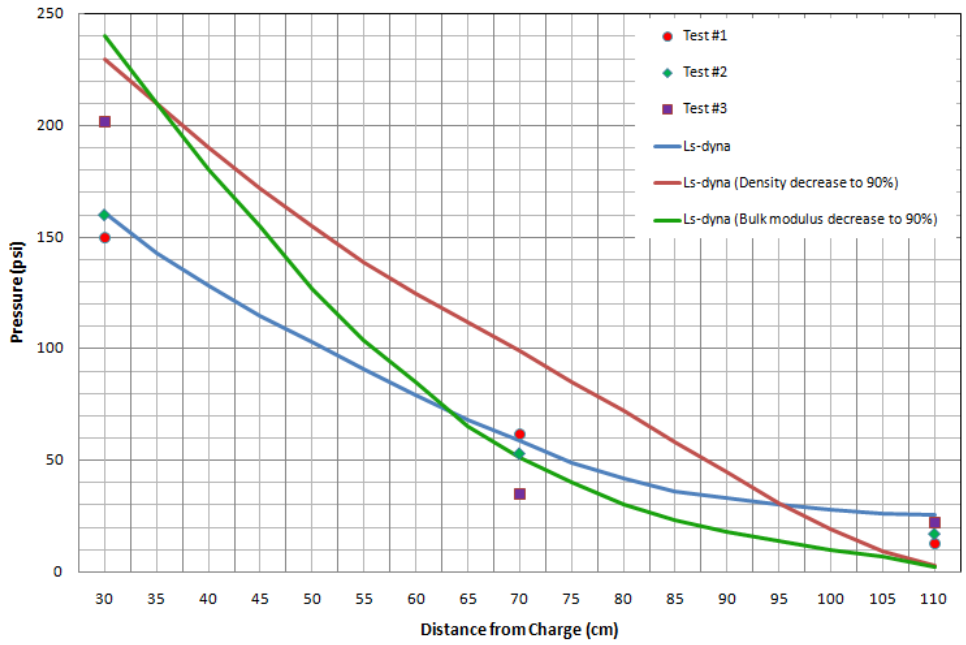


FIG. 4- 29 Comparison of simulation results due to parameters change for saturated soil

The saturated soil volume fractions of three phases in a part of finite element mash before the shack wave arriving is shown in FIG. 4-30. The saturated soil volume fractions of three phases in a part of finite element mash at the 180μsec is shown in And FIG. 4-31.

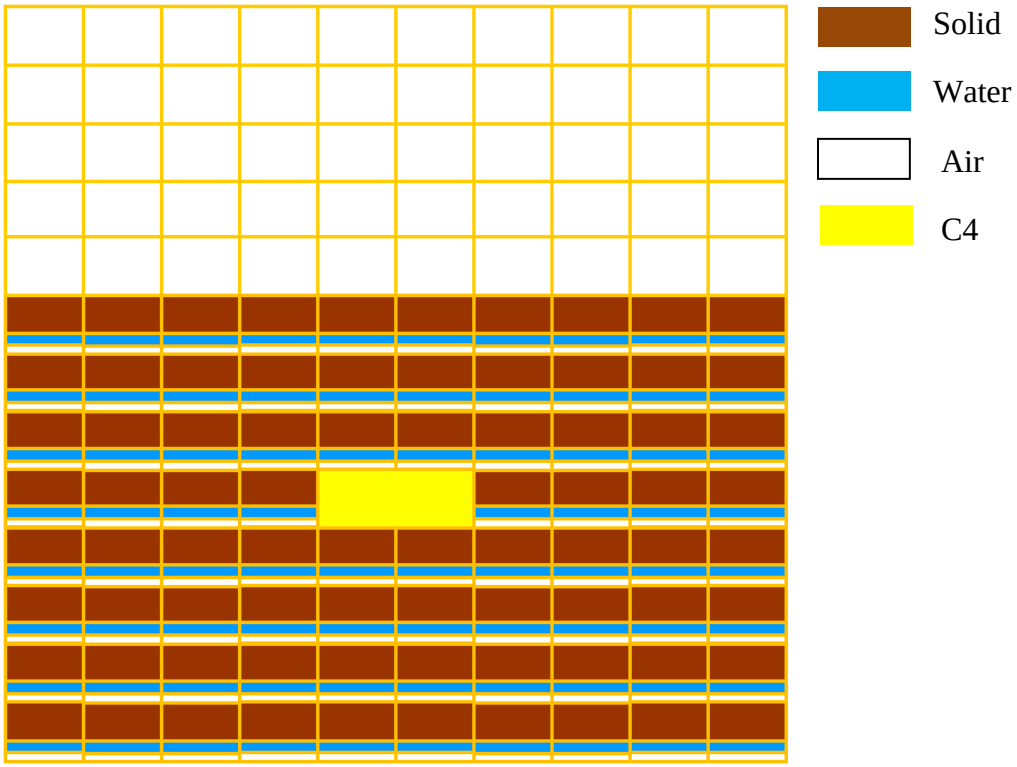


FIG. 4- 30 Saturated soil volume fractions of three phases before the shack wave arrives

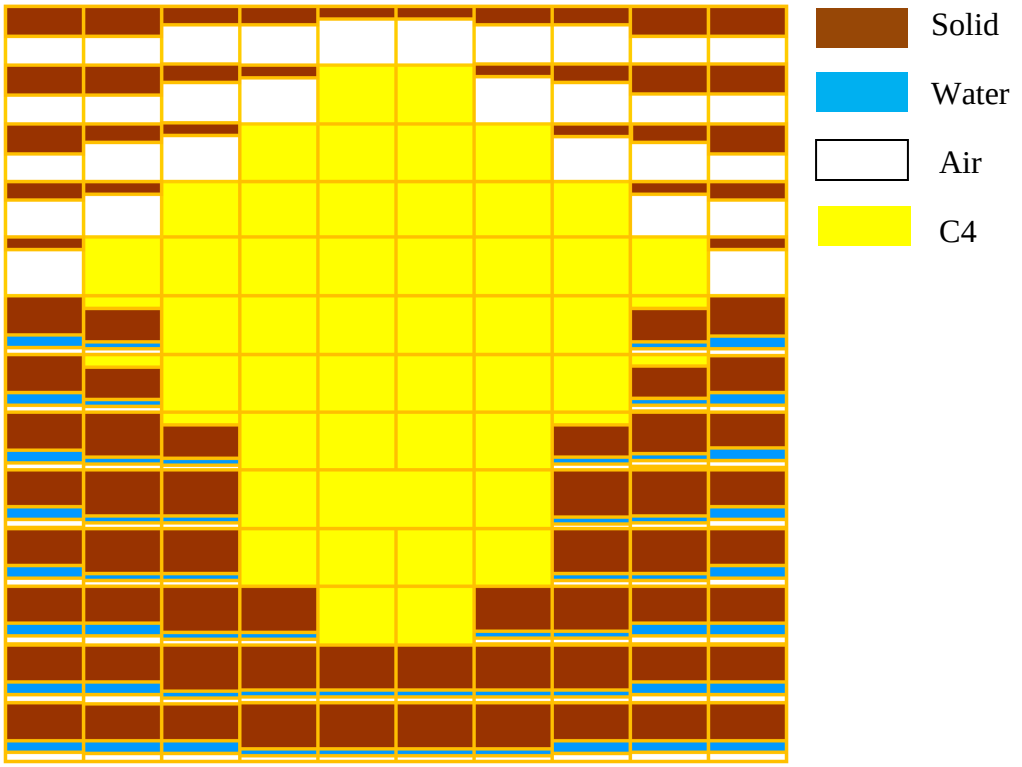


FIG. 4- 31 Saturated soil volume fractions of three phases at 180μsec

## 4.6 SIMULATION FOR DRY SOIL

### 4.6.1 SIMULATION CASES AT DIFFERENT ELEMENT

**Case 1 (under the C4):**

A soil element (#654), shown in FIG. 4-11, whose center is located at 3 cm to the right and 2.75 cm down from the center of C4, is selected from a dry soil test to illustrate the numerical procedure. Before the shock wave arrives at t =20μsec, its soil density is 1802 kg/m$^3$, bulk modulus is 106.4MPa, and the volume fractions of solid, water and air are respectively 68%, 0.0% and 32%. When the shock arrives at time step t

=20+5=25μsec, hydrostatic pressures in the solid, water and air phases are calculated to be 2.13MPa, 0.0MPa and 0.000215MPa, respectively, by Eq. (3.85), (3.86) and (3.87). The volume fractions in soil are updated using Eq. (3.91), (3.92) and (3.93), to be 70.04%, 0.0% and 29.97%. Using Eq. (3.88) and (3.94) to update the soil bulk modulus and density are 117.16MPa and 1811 kg $m^{-3}$. The soil volume increment can be obtained from LS-DYNA, total volume increment is -2.387E-05 (μ=4.481E-06), solid volume increment $\Delta V_s$ is -7.879E-06 (μ=4.743E-05), water volume increment $\Delta V_w$ is 0.0 and air volume increment $\Delta V_a$ is -1.599E-05 (μ=6.163E-03). The soil pressure is 1.62MPa. It can be passed to deviatoric stress to calculate total stress by Eq. (4.1). The soil internal energy is 0.0000175MPa by Eq. (3.96). By now, all parameters of viscoplastic cap model and EOS are known. The next time step can be run. At t= 40μsec, soil bulk modulus arrives peak value 513MPa. The volume fractions in soil are 82.68%, 0.0% and 17.4%, respectively. The increments of volume fractions in soil are 14.68%, 0.0% and –14.6%, respectively. The procedure of volume fractions change is shown in FIG. 4-32.

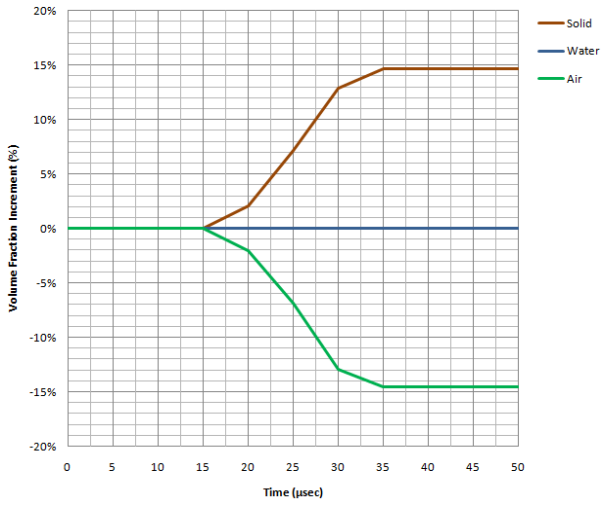


FIG. 4- 32 Dry soil volume fraction in element #654

**Case 2 (flush with the C4):**

A soil element (#748), shown in FIG. 4-13, whose center is located at 3 cm to the right from the center of C4 and flush with the center of C4, is selected from a dry soil test to illustrate the numerical procedure. Before the shock wave arrives at t =20μsec, its soil density is 1802 kg/m$^3$, bulk modulus is 106.4MPa, and the volume fractions of solid, water and air are respectively 68%, 0.0% and 32%. When the shock arrives at time step t =20+5=25μsec, hydrostatic pressures in the solid, water and air phases are calculated to be 3.72MPa, 0.0MPa and 0.000201MPa, respectively, by Eq. (3.85), (3.86) and (3.87). The volume fractions in soil are updated using Eq. (3.91), (3.92) and (3.93), to be 70.02%, 0.0% and 30.0%. Using Eq. (3.88) and (3.94) to update the soil bulk modulus and density are 112.34MPa and 1808 kg m$^{-3}$. The soil volume increment can be obtained from LS-DYNA, total volume increment is -1.933 E-05 (μ=6.412E-05), solid volume increment $\Delta V_s$ is -8.119E-06 (μ=4.919E-05), water volume increment $\Delta V_w$ is 0.0 and air volume increment $\Delta V_a$ is -1.1131E-05 (μ=7.075E-03). The soil pressure is 1.33MPa. It can be passed to deviatoric stress to calculate total stress by Eq. (4.1). The soil internal energy is 0.0000175MPa by Eq. (3.96). By now, all parameters of viscoplastic cap model and EOS are known. The next time step can be run. At t= 40μsec, soil bulk modulus arrives peak value 513MPa. The volume fractions in soil are 81.33%, 0.0% and 18.4%, respectively. The increments of volume fractions in soil are 13.33%, 0.0% and –13.6%, respectively. The procedure of volume fractions change is shown in FIG. 4-33.

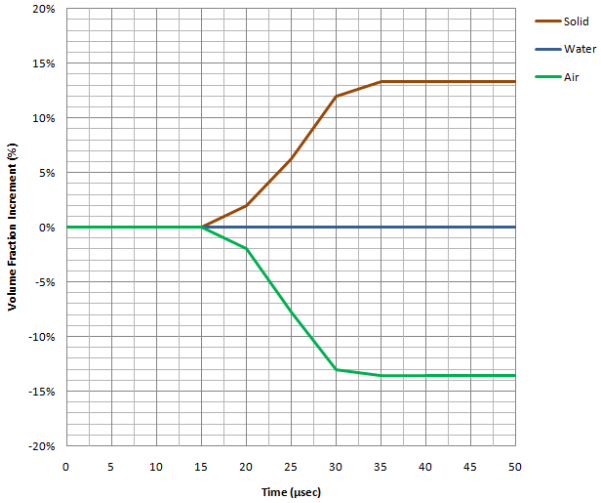


FIG. 4- 33 Dry soil volume fraction in element #748

**Case 3 (above the C4):**

A soil element (#852), shown in FIG. 4-15, whose center is located at 3 cm to the right and 2.75 cm above from the center of C4, is selected from a dry soil test to illustrate the numerical procedure. Before the shock wave arrives at t =20μsec, its soil density is 1802 kg/m$^3$, bulk modulus is 106.4MPa, and the volume fractions of solid, water and air are respectively 68%, 0.0% and 32%. When the shock arrives at time step t =20+5=25μsec, hydrostatic pressures in the solid, water and air phases are calculated to be -3.62MPa, 0.0MPa and 0.0313MPa, respectively, by Eq. (4.6), (4.7) and (4.8). The volume fractions in soil are updated using Eq. (3.91), (3.92) and (3.93), to be 65.03%, 0.0% and 30.10%. Using Eq. (3.88) and (3.94) to update the soil bulk modulus and density are 103.02MPa and 1800 kg m$^{-3}$. The soil volume increment can be obtained from LS-DYNA, total volume increment is 5.119 E-05 (μ=-7.762E-05), solid volume increment $\Delta V_s$ is 1.496E-05 (μ=-4.743E-05), water volume increment $\Delta V_w$ is 0.0 and air volume

increment $\Delta V_a$ is 3.623E-05 (μ=-4.0852E-03). The soil pressure is -0.94MPa. It can be passed to deviatoric stress to calculate total stress by Eq. (4.1). The soil internal energy is 0.0000175MPa by Eq. (3.96). By now, all parameters of viscoplastic cap model and EOS are known. The next time step can be run. At t= 35μsec, since shock wave arrives, soil above C4 is blown by the force of the explosion. The volume fractions in soil are 0.0%, 0.0% and 0.0%, respectively. The increments of volume fractions in soil are -68.0%, 0.0% and –32.0%, respectively. The procedure of volume fractions change is shown in FIG. 4-34.

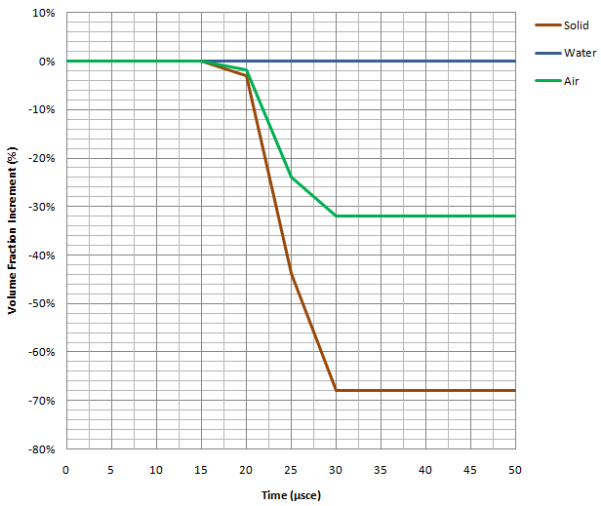


FIG. 4- 34 Dry soil volume fraction in element #852

**Case 4 (Air element above the C4):**

An air element (#4498), shown in FIG. 4-17, whose center is located at 30 cm above from the center of C4, is selected from a dry soil test to illustrate the numerical procedure. Under blasting loading, a part of volume of the element 4498 is occupied by

soil debris following an explosion, shown in FIG. 4-35. The soil volume fraction arrive peak value 2.17% at 250μsec.

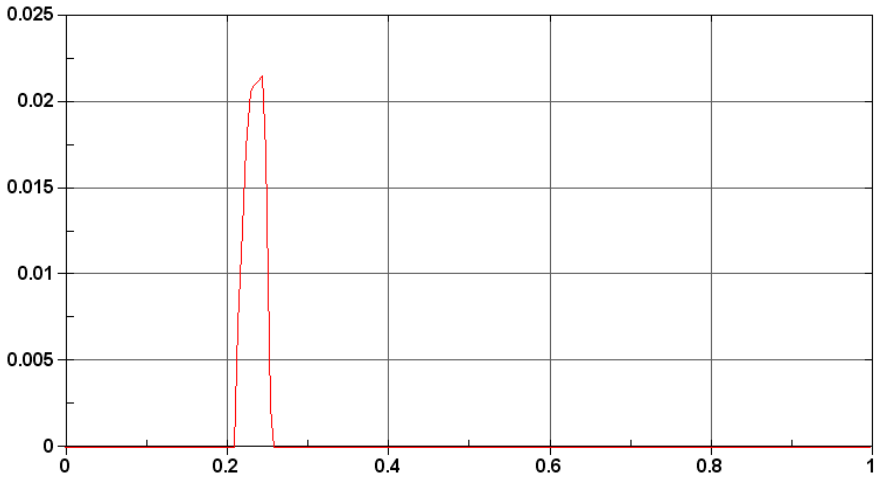


FIG. 4- 35 Volume fraction of dry soil in air element #4498

### 4.6.2 COMPARISON OF SIMULATION WITH TEST RESULTS

From FIG. 4-36 to FIG. 4-44 present the air pressure time-histories, which were recorded by the pencil gages (see Fig. 8) after a C4 charge was detonated in dry sand at a DOB = 3 cm (Materials Sciences Corporation 2006).

The predicted shock front arrival times in the air directly above the explosion are compared against those read from the data traces recorded by transducers #1, #6 and #9 in FIG. 4-45. The difference between the predicted shock front arrival time and the average test data at 0, 22.5 and $45^{o}$ offset angles are 1.8%, 4.4%, and 9.7%, respectively.

A comparison between the predicted shock front air pressure and the experimental data obtained at distances of 30 cm, 70 cm, and 110 cm directly above the soil is shown in FIG. 4-46. The difference between the numerical results and the average test data at 30, 70 and 110-cm standoff distances are 2.2%, 20% and 64%, respectively. A comparison among simulation results when the density is decreased to 90% of initial density, when the bulk modulus is decreased to 90% of initial bulk modulus and density and bulk modulus keep the initial value is shown in FIG. 4-47.

The dry soil volume fractions of three phases in a part of finite element mash before the shack wave arriving is shown in FIG. 4-48. The dry soil volume fractions of three phases in a part of finite element mash at the 120μsec are shown in FIG. 4-49.

The soil ejecta heights between high speed video and numerical simulation at time = 420, 830 and 1040 μs since detonation for tests in dry sand and in saturated sand are compared in FIG. 4-50, 4-51 and 4-52, respectively. The maximum difference between the predicted and measured ejecta heights is 24% for explosive tests in dry sand and 9.6% in saturated sand.

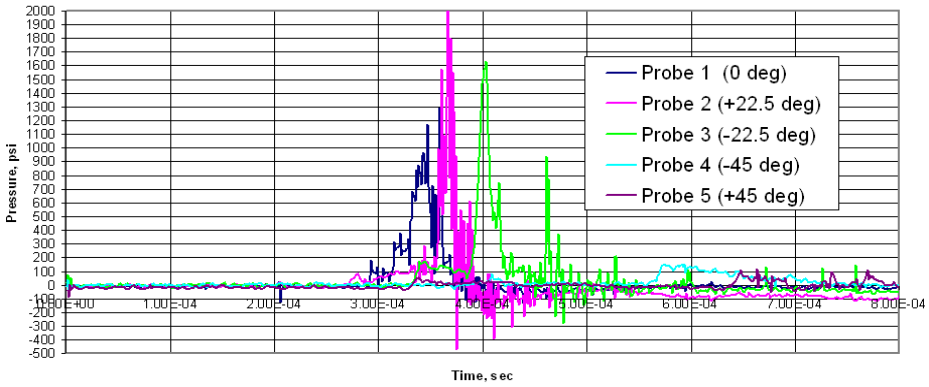


FIG. 4- 36 Dry sand air pressure time-histories, 30 cm standoff distance #1

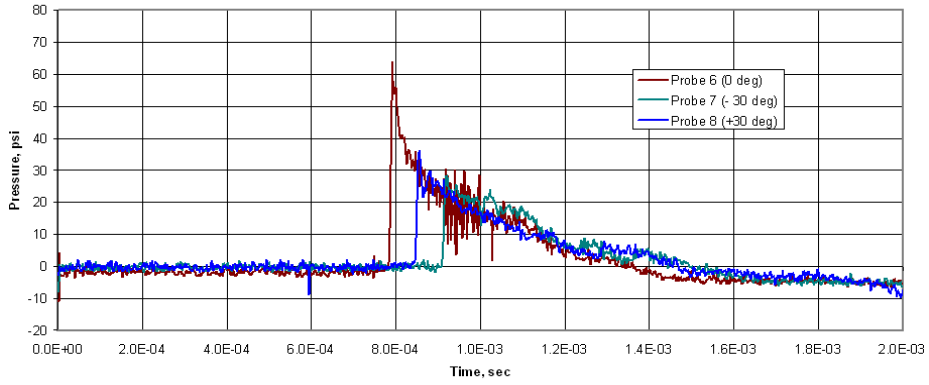


FIG. 4- 37 Dry sand air pressure time-histories, 70 cm standoff distance #1

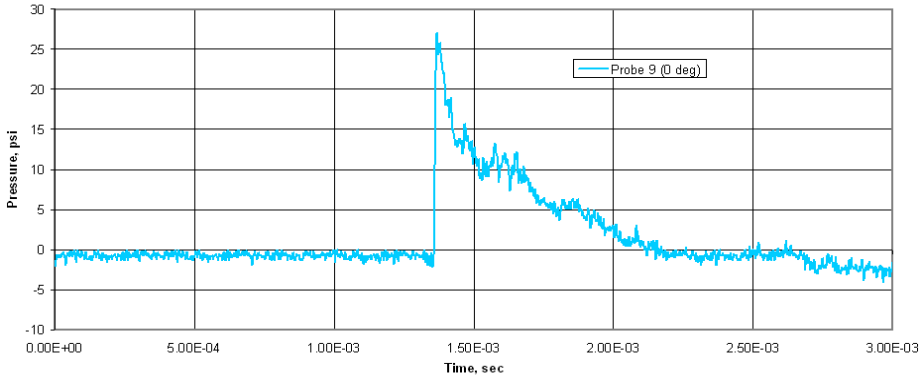


FIG. 4- 38 Dry sand air pressure time-histories, 110 cm standoff distance #1

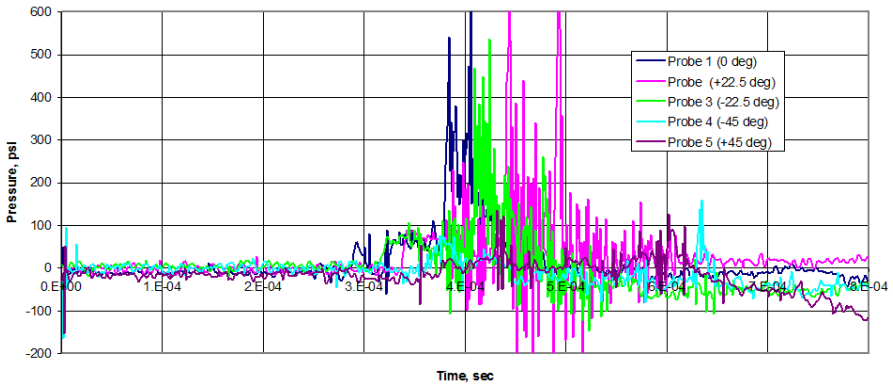


FIG. 4- 39 Dry sand air pressure time-histories, 30 cm standoff distance #2

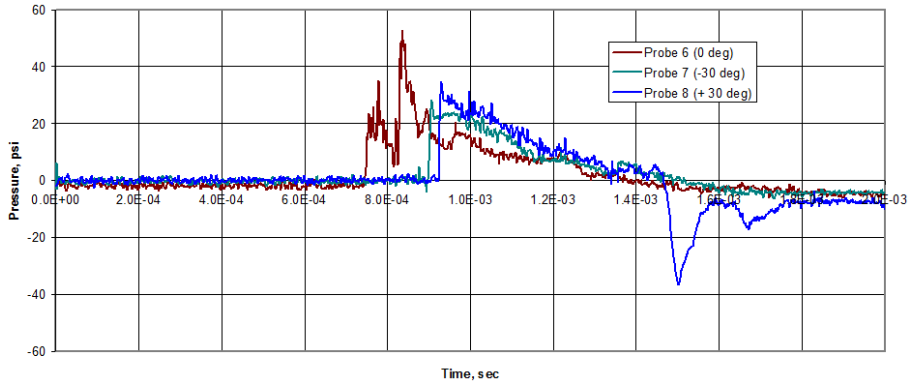


FIG. 4- 40 Dry sand air pressure time-histories, 70 cm standoff distance #2

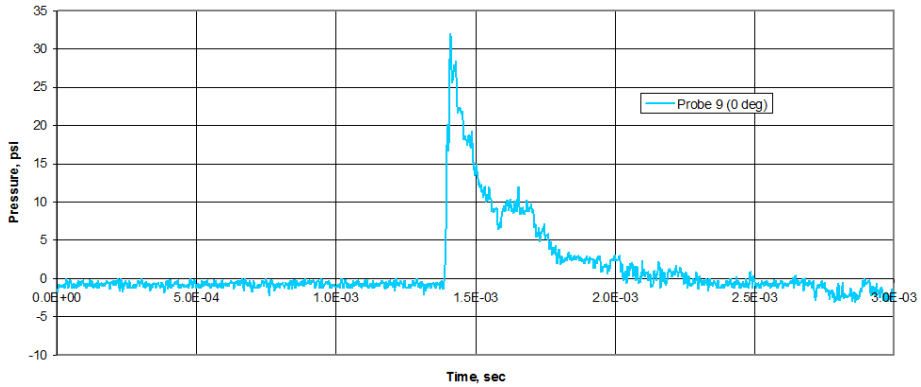


FIG. 4- 41 Dry sand air pressure time-histories, 110 cm standoff distance #2

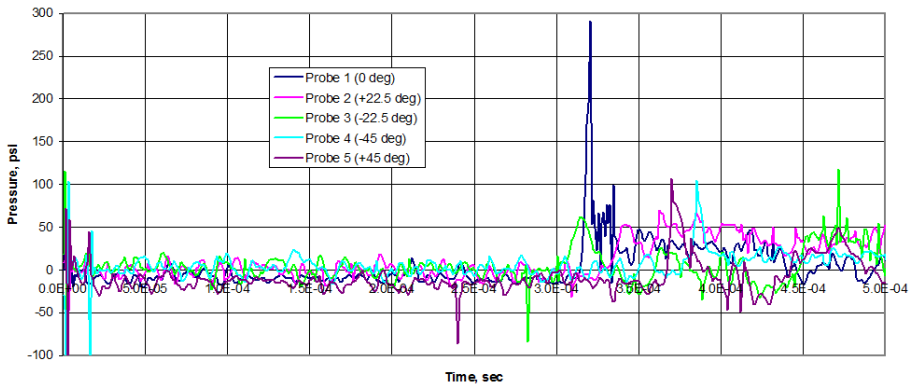


FIG. 4- 42 Dry sand air pressure time-histories, 30 cm standoff distance #3

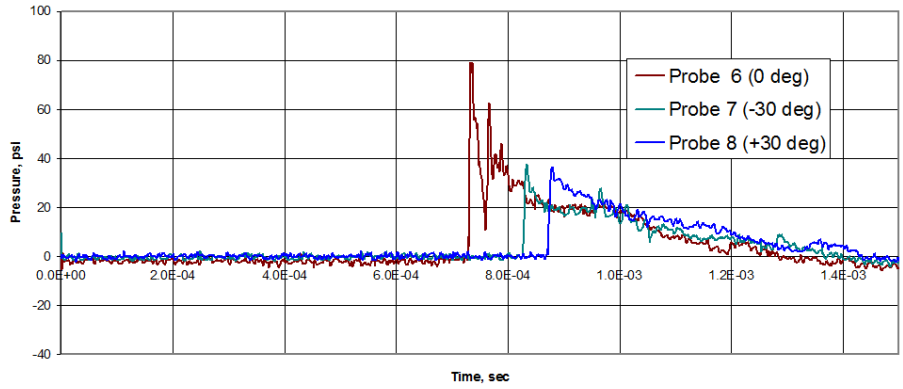


FIG. 4- 43 Dry sand air pressure time-histories, 70 cm standoff distance #3

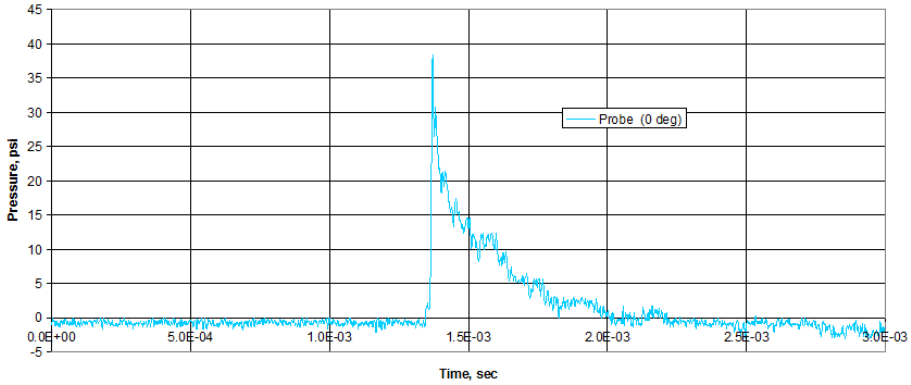


FIG. 4- 44 Dry sand air pressure time-histories, 110 cm standoff distance #3

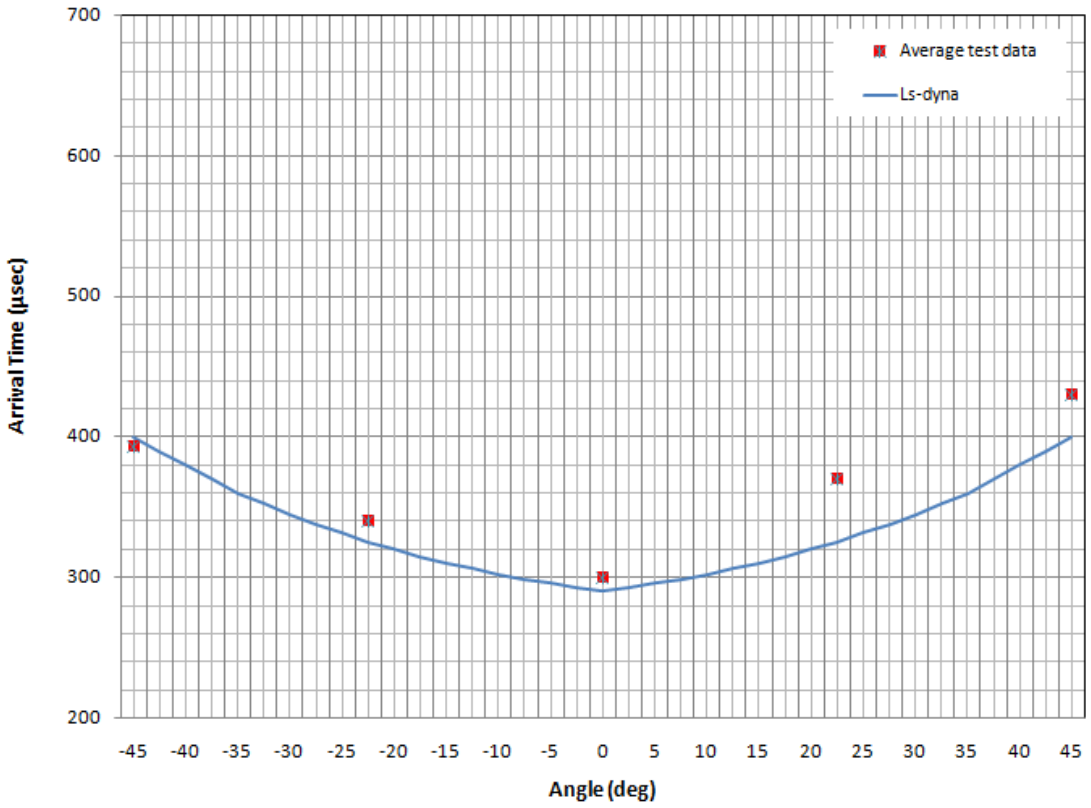


FIG. 4- 45 Comparison between numerically predicted and experimental values for dry sand (Blast wave arrival time VS. Transducer offset angle)

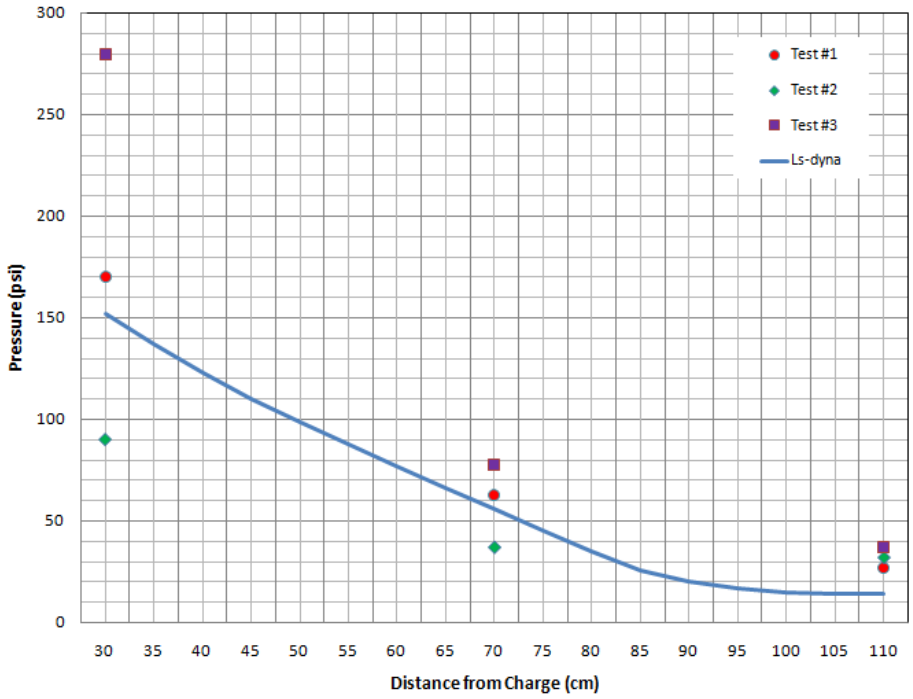


FIG. 4- 46 Comparison between numerically predicted and experimental values for dry sand (Shock front pressure in air VS. Transducer distance)

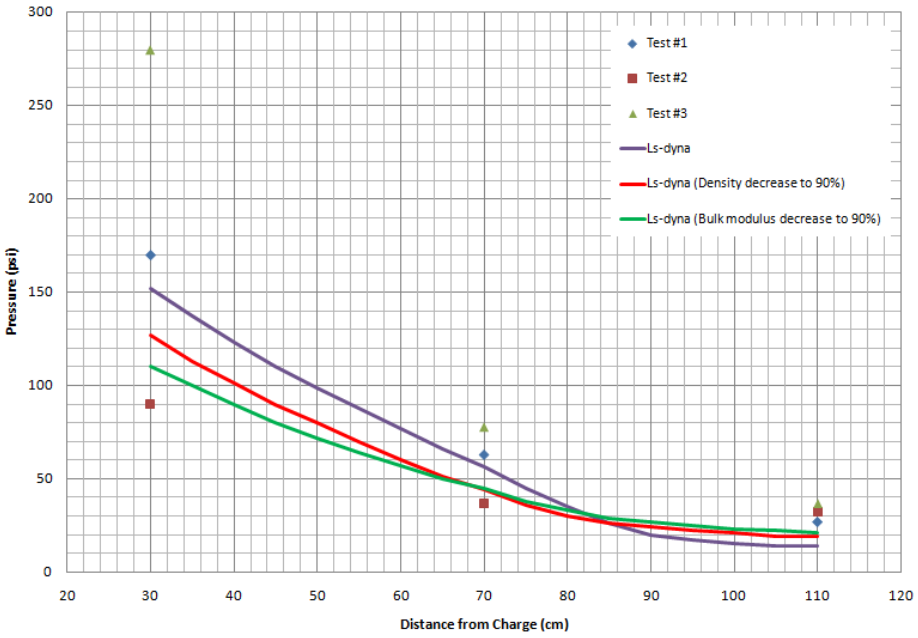


FIG. 4- 47 Comparison of simulation results due to parameters change for dry soil

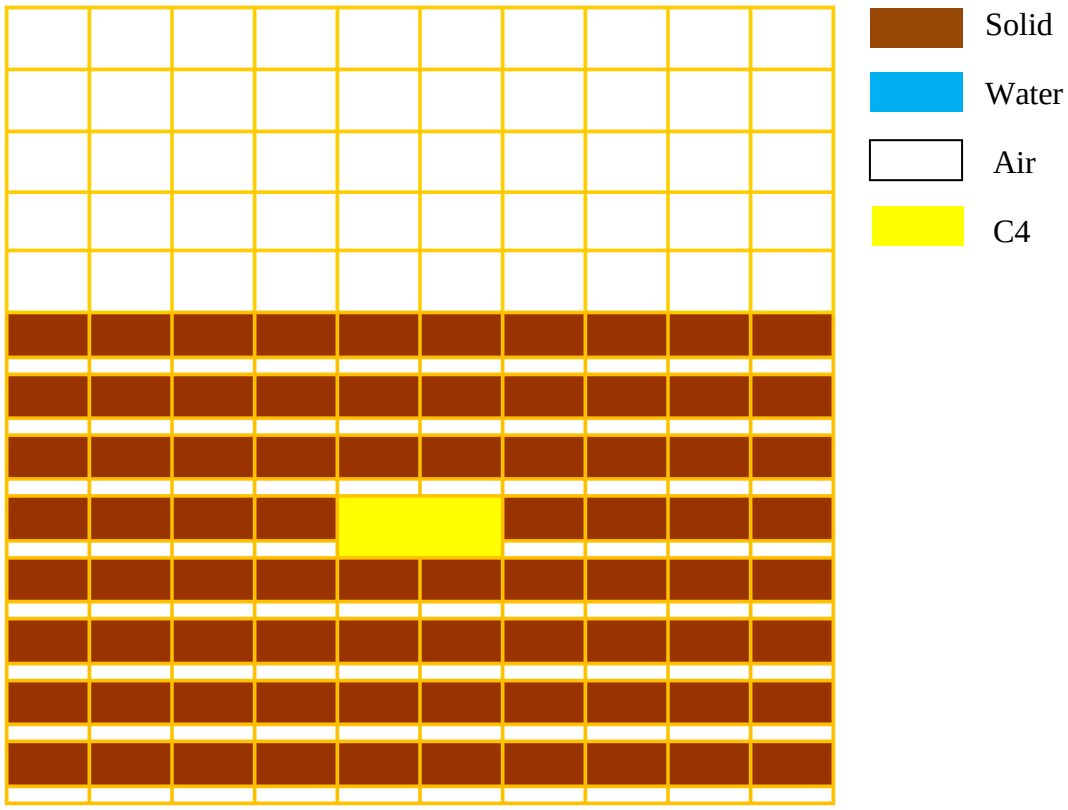


FIG. 4- 48 Dry soil volume fractions of three phases before the shack wave arrives

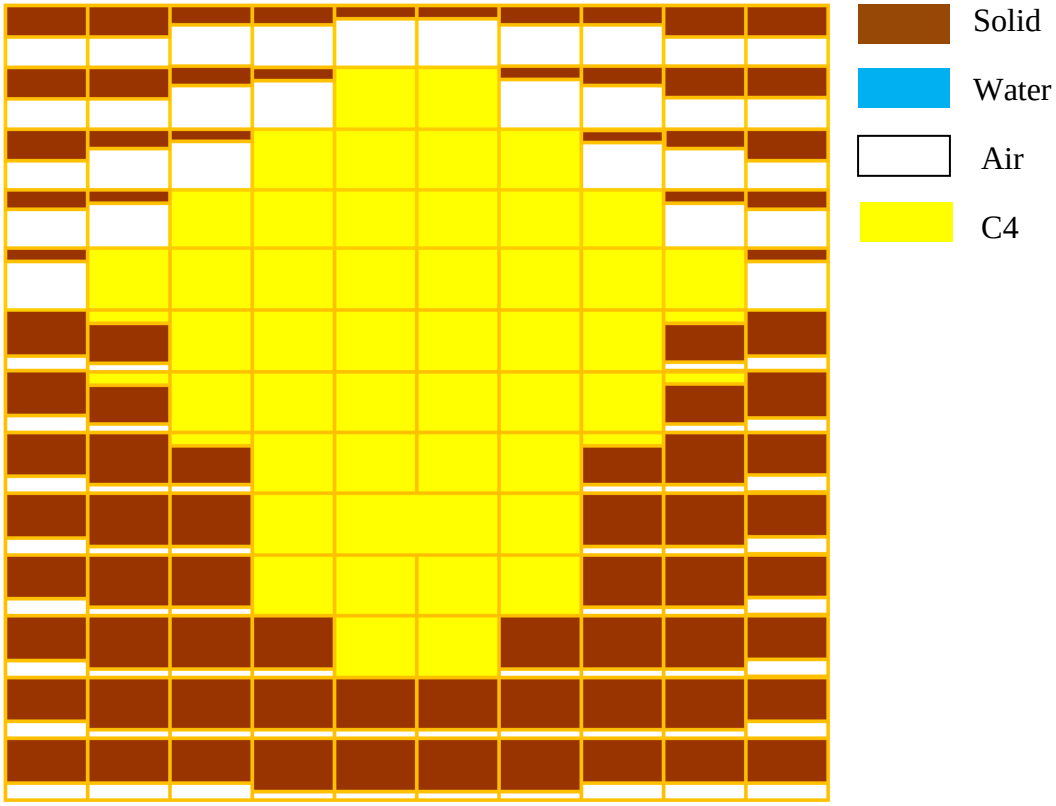


FIG. 4- 49 Dry soil volume fractions of three phases at 120μsec

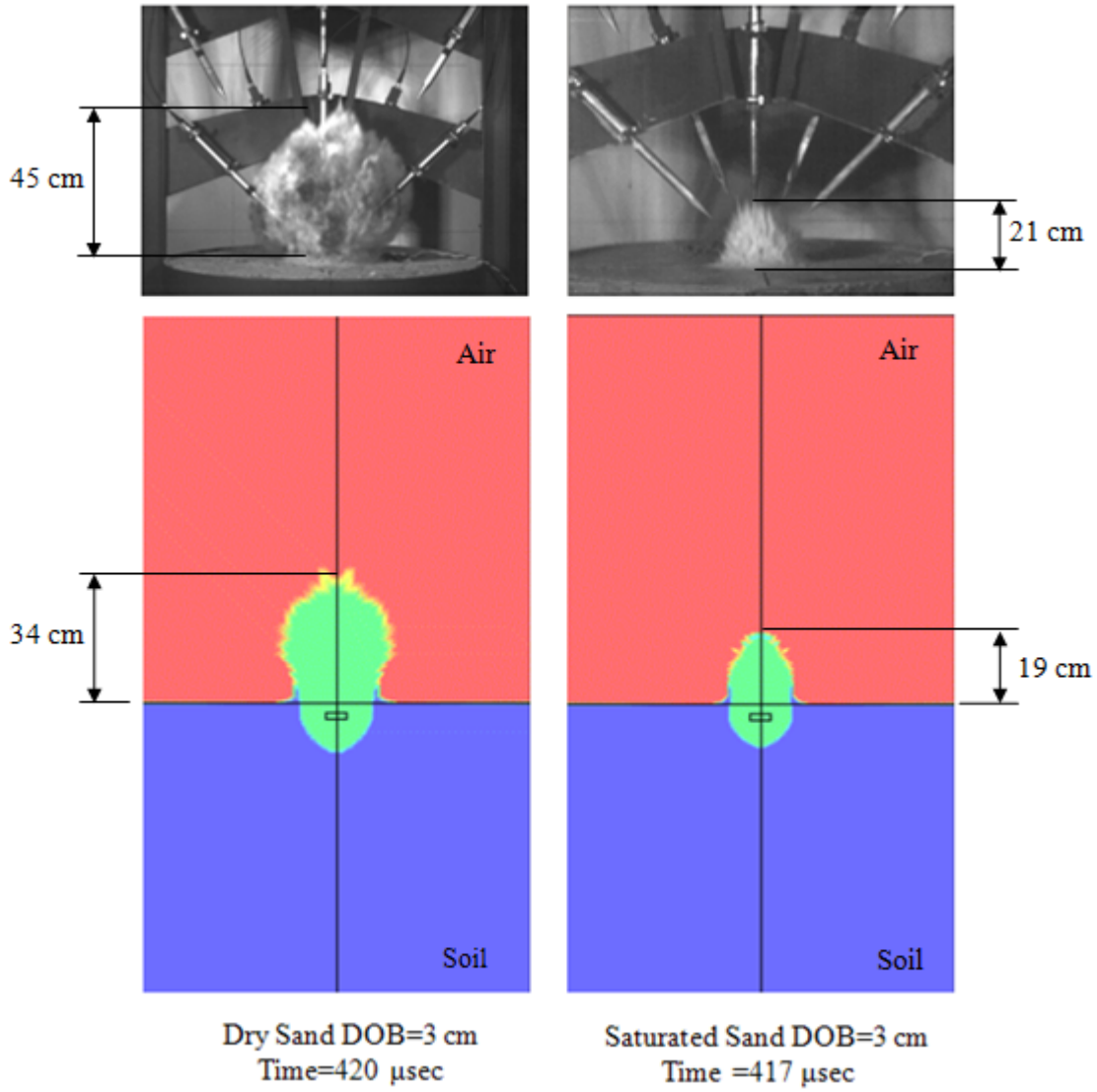


FIG. 4- 50 Comparison of soil ejecta heights: High speed video vs. Simulation at time = 420 µsec

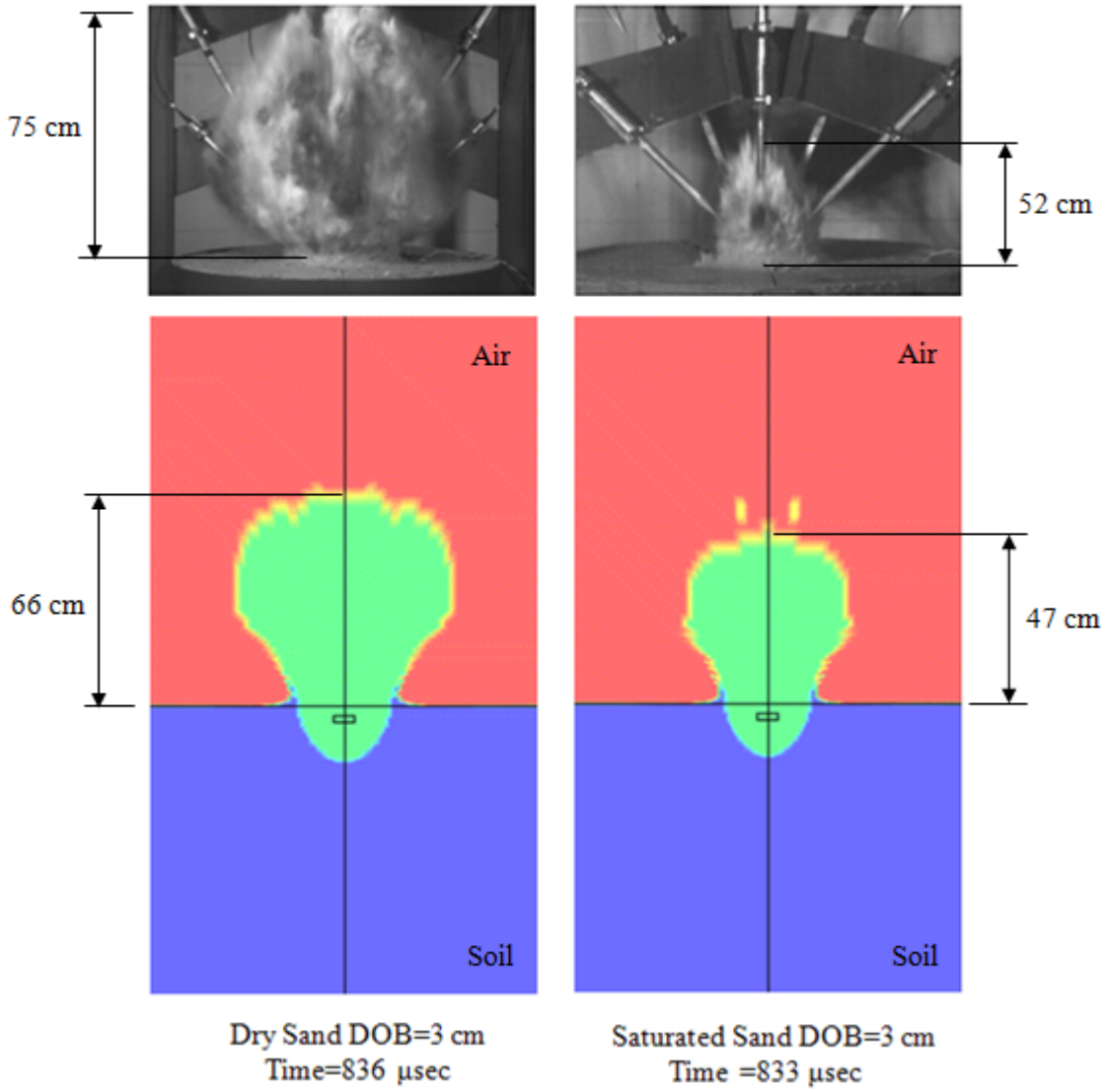


FIG. 4- 51 Comparison of soil ejecta heights: High speed video vs. Simulation at time = 830 µsec

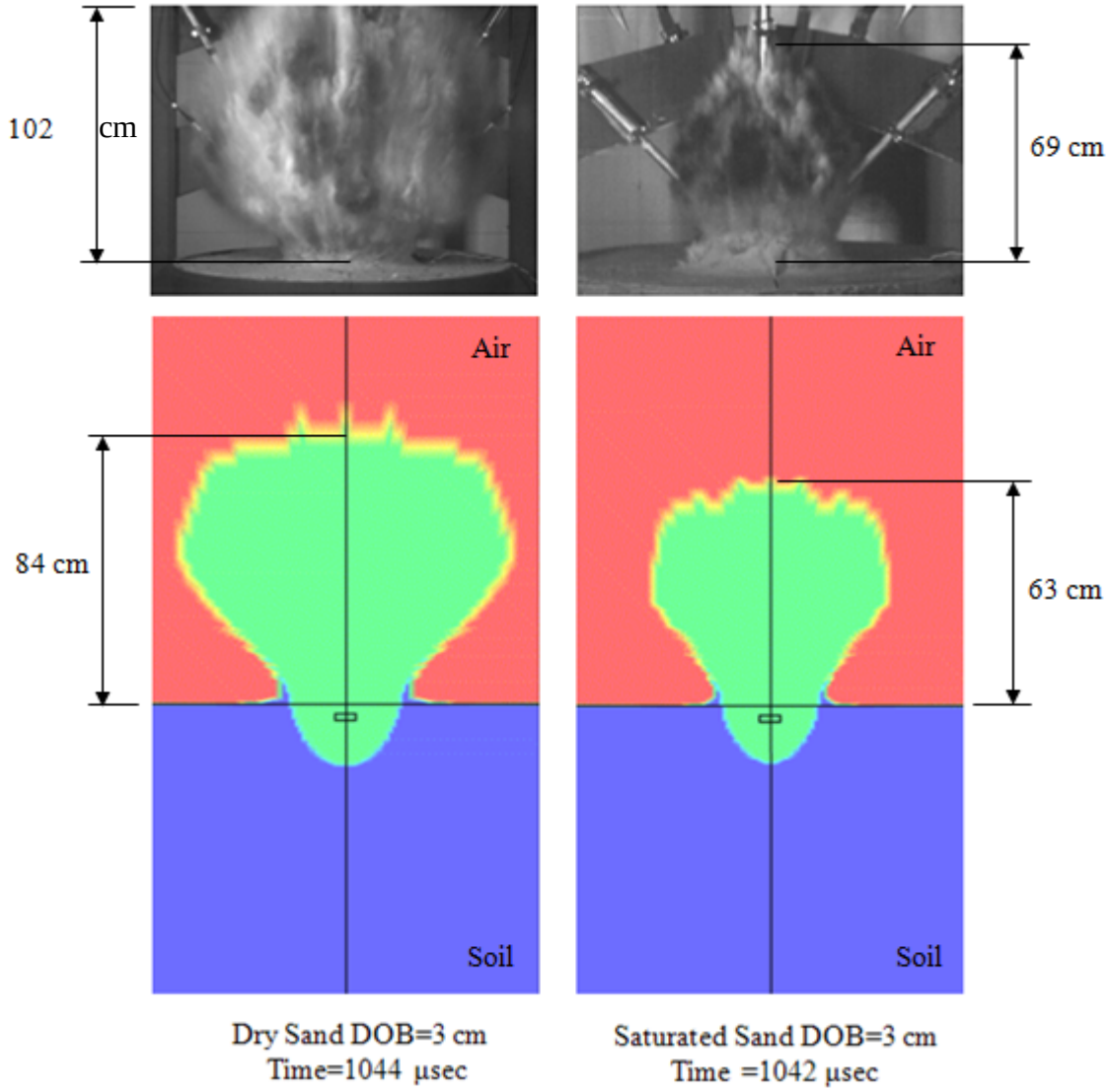


FIG. 4- 52 Comparison of soil ejecta heights: High speed video vs. Simulation at time = 1040 µsec

## 4.7 CONCLUSIONS

By means of comparison against experimental data, predictions of the viscoplastic cap model demonstrate better agreement than those of the inviscid cap model, more accurate 7% than inviscid cap model, since the viscoplastic model can capture the high strain-rate (with durations in milliseconds) effects on explosion simulation. The high strain effects are manifested by an apparent increase of shock wave propagation speed, peak overpressure and impulse. Although the effects on certain variables are not apparent, such as the air blast shock wave propagation and the explosion characteristics, the high strain rate effects are generally significant (Jackson et al, 1980) and cannot be neglected in explosion simulation.

A fine mesh (about $0.14cm^3$ per element) needs to be used in order to improve the simulation accuracy. Besides, the high strain-rate effects need to be studied through explosion tests in clayey soils in order to draw a general conclusion.

# CHAPTER FIVE CONCLUSIONS AND RECOMMENDATIONS

## 5.1 CONCLUSIONS

This thesis investigates and proposes soil models, implements the models in LS-DYNA finite element code, and evaluates the performance of viscoplastic cap material model with equation of states through comparison against available explosion test data. The soil behavior under blast loading, the phenomena due to explosion, are particularly studied.

Two viscoplastic cap models are based on Perzyna's theory and Duvant-Lions' theory studied. By comparing with the solutions to a hypothetical loading test, the two viscoplastic models produce virtually identical responses when the viscous parameters are judiciously selected for each model. However, differences between the Perzyna's and the Duvant-Lions' model were observed when simulating the experiment tests conducted under rapid loading. The prediction of the Perzyna's model appears to agree better (about 4%) with experimental data than that of the Duvant-Lions' model, and the Perzyna's model is more flexible for data fitting, more accurate about 6.6% than Duvant-Lions' model. Therefore, the Perzyna's viscoplastic cap model is implemented into LS-DYNA to represent the soil model with consideration of strain-rate effect.

To improve the accuracy of simulation results, three phases equation of states are developed based on Mie-Gruneison equation of state. For soil mass surrounding the source of energy release, equation of state models for the three phases of soil are developed as each of the three phases responds differently to shock loading. Finally,

these three phase equation of states have been integrated with the viscoplastic cap model and incorporated into the LS-DYNA software as user-supplied subroutines for numerical simulations of explosive tests in dry soil as well as in wet soil.

By means of comparison against experimental data, the predicted time of arrival and the overpressure in air directly above buried explosions agree well with the experimental data. There was noticeable improvement using the revised cap model with EOS for the prediction of wet soil behavior under blast loading than dry soil. It is concluded that the revised cap model with EOS is adequate for blast loading behavior simulations for soil with different degrees of water contents.

## 5.2 RECOMMENDATIONS

Refinements of viscoplastic cap models would include a more realistic treatment for tension cutoff for the Perzyna type and a more elaborate formulation for the Duvant-Lions type. The former is very important to the simulation of underground explosion. The latter is to improve the flexibility of the Duvant-Lions' model.

A series of explosion tests needs to be conducted in clayey soil with different degrees of water contents. As evidenced by the previous experimental studies, the clayey soils are more sensitive to the loading rate than the sandy soil. If these tests are being conducted, the comprehensive static tests for the same soil should also be conducted to calibrate soil model parameters and EOS parameters. More simulations can be run with equation of state for soils with various degrees of saturation. This step is essential for ensuring the accuracy of the numerical simulations.

## REFERENCE

Aboil, C.A and Roth W.H. (1982), "Bounding surface plasticity applied to cyclic loading of sand." *In Proceedings of the International Symposium on Numerical Models*, Zurick: 65-72.

Adachi, T., Mimura, M. and Oka, F. (1985), "Descriptive accuracy of several existing constitutive models for normally consolidated clays." *Proc. 5th Int. Conf. Numer. Meth. Geomech., Nagoya*., 1: 259-266.

Alonso, E. E., Gens, A. and Josa, A. (1990), "A constitutive model for partially saturated soils." *Geotechnique*, 46(2): 405-430.

Bardet, J.P. (1985), "Application of bounding surface plasticity to cyclic sand behavior." *In Proceedings of the 2nd International Conference on Soil Dynamics and Earthquake Engineering*, Springler and Verlag, 1985(2): 3-16.

Bishop, A.W. (1959). "The principle of effective stress," *Teknisk Ukeblad*., 106(39): 859-863.

Bishop, AW. and Blight GE. (1963), "Some aspects of effective stress in saturated and partly saturated soils." *Geotechnique*., 12(2):125-144.

Blight, G.E. (1965), *In moisture equilibria and moisture changes in soils beneath covered areas: a symposium in print.* Edited by G.D. Aitchison. Butterworth, Sydney, Australia, 259-269.

Bolzon, G., Schrefler, B.A. and Zienkiewicz, O.C. (1996), "Elasto-plastic soil constitutive laws generalized to partially saturated states." *Geotechnique*, 46(2): 279-289.

Borja, R. I. and Kavazanjian, E. Jr (1985), "A constitutive model for the stress-strain-time behavior of wet clays." *Geotechnique*., 35(3): 283-298.

Bragov, A.M., Lomunov, A.K., Sergeichev, I.V., Proud, W., Tsembelis, K., and Church, P. (2005). "A method for determining the main mechanics properties of soft soils at high strain rates ($10^3$-$10^5 s^{-1}$) and load amplitudes up to several gigapascals," *Technical Physics letters*., 31(6):530-531.

Braithwaite, C.H., Proud, W.G. and Field, J.E. (2006), "The shock hugoniot properties of quartz feldspathic gneiss and amphibolites." *Shock Compression of Condensed Matter*., 2006: 1435-1438.

Brinkgreve, R.B.J. (2005), "Selection of soil models and parameters for geotechnical engineering application." In: *soil constitutive models: Evaluation, selection and calibration*, Geo-frontier Conference of ASCE, Austin, Texas: 69-98.

Budhu, M. (2007). *Soil Mechanics and Foundations*, John Wiley & Sons Canada, Ltd.

Burland, JB. (1965), "Some aspects of the mechanical behavior of partly saturated soils." *Proceedings of the Symposium on Moisture Equilibrium and Moisture Changes in the Soils beneath Covered Areas.* Butterworths: Sydney, Australia, 1965: 270-278.

Chapman, D.J., Tsembelis, K., and Proud, W.G. (2006). "The behavior of water saturated sand under shock-loading," *Proc. SEM Ann. Conf. and Exposition on Experimental and Applied Mechanics*, St. Louis, Missouri, 400-406.

Chen, W.F. and Baladi, G.Y. (1985), *Soil plasticity: Theory and Implementation*, Elsevier, Amsterdam, The Netherlands.

Cui, Y.J. and Delage, P. (1996). "Yielding and plastic behavior of an unsaturated compacted silt." *Geotechnique*., 46(2): 291-311.

Dafalias, Y. F. (1982), "Bounding surface elastoplasticity viscoplasticity for particulate cohesive media." *IUTAM Symp. on Deformation and Failure of Granular Materials*: 97-107

Dafalias, Y. F. and Herrmann, L.R. (1982), "Bounding surface formulation of soil and cyclic loads." *Soil Mechanics-Transient and Cyclic Loads*, John Wiley & Sons London, Ltd.

Dafalias, Y.F. and Popov, E. (1976), "Plastic internal variables formalism of cyclic plasticity." *Journal of Applied Mechanics*, 98(4): 645-651

Das, Braja M. (1983), *Advanced soil mechanics*, 1st ED., Hemisphere Publishing Corporation., Washington, New York, London.

Dangla, P., Malinsky, L. and Coussy, O. (1997), "Plasticity and imbibitions-drainge curves for unsaturated soils." *In Proceedings of the 6th International Symposium on Numerical Models in Geomechanics*., 1997, Montreal, Que: 141-146.

DiMaggio, F.L. and Sandler, I.S. (1971), "Material model for granular soils." *J. Engrg. Mech. Div*. ASCE, 97(EM3): 935-950.

Drake, J.L. and Little, C.D. (1983), "Ground shock from penetrating conventional weapons, proceedings: symposium on the interaction of non-nuclear munitions with structures." *US Air Force Academy, Colorado Springs, CO, Part I, 10-13 May*: 1-6

Drucker, D.C., Gibson, R.E. and Henkel, D.J.(1957), "Soil mechanics and work hardening theories of plasticity." *Trans.*, ASCE, 122: 338-346.

Fredlund, D.G. and Rahardjo, H. (1993), *Soil mechanics for unsaturated soils*, John Wiley and Sons, Inc., New York.

Fredlund, D.G. and Morgenstern, N.R. (1977), "Stress state variables and unsaturated soils." *Journal of the Geotechnical Engineering*., Division, ASCE, 103(GT5): 447-466.

Gallipoli, D., Gens, A., Sharma, R., and Vaunat, J. (2003), "An elastoplastic model for unsaturated soil incorporating the effects of suction and degree of saturation on mechanical behavior." *Geotechnique*., 53(1): 123-135.

Gens, A. (1996), "Constitutive modeling: Application to compacted soils." *In Proceedings of the 1st International Conference on Unsaturated Soils*, Paris, French: 1179-1200.

Gens, A., Danchez, M. and Sheng, D. (2006), "On constitutive modeling of unsaturated soils." *Acta Geotechnica*, 1(3): 137-147.

Goldscheider, M. (1984), "True triaxial tests on dense sands." In: *Constitutive relations for soils* (eds. Gudehus, G., Darve, F., and Vardoulakis, L.). Balkema, Rotterdam.

Grujicic, M., Pandurangan, B., Cheeseman, B.A., Roy, W.N., and Skaggs, R.R. (2008), "Parameterization of the porous material model for sand with different levels of water saturation," *Soil Dynamics and Earthquake Engineering*., 28: 20-35.

Gupta, D.A. (1999), "Estimation of vehicle floor plate loading and response due to detonation of a mine shallow-buried in dry sand and wet tuff." US Army Ground Vehicle Survivability Symposium, Apr. 29~May 1, Monterey, CA.

Hashiguchi, K. and Ueno, M. (1977), "Elasto-plastic constitutive laws of granular materials." *In Proceedings of the 9$^{th}$ International Conference on Soil Mechanics and Foundation Engineering*, Tokyo, Japan: 73-82.

Henrych, J. (1979), *The dynamics of explosion and its use*, Elsevier, New York.

Jackson, J.G., Ehrgott, J.Q. and Rohani, B. (1980), "Loading rate effects on compressibility of sand." *J. Geotech. Engrg. div.* ASCE, 106(8): 839-852.

Jennings, JEB and Burland, JB. (1962), "Limitations to the use of effective stress in unsaturated soils." *Geotechnique*., 12(2):125-144.

Jommi, C. (2000), "Remarks on the constitutive modeling of unsaturated soils." *In Proceedings of the International Workshop on Unsaturated Soil*, 2000, Trento, Italy: 139-153.

Jones, S.C. and Gupta, Y.M. (2000), "Refractive index and elastic properties of z-cut quartz shocked to 60 kbar." *Journal of Applied Physics*., 88(10): 5671-5679

Kaliakin, V. N. (1985), *Bounding surface elastoplasticity viscoplasticity for clays.* PhD dissertation, University of California.

Katona, M.G. (1984), "Verification of viscoplastic cap model." *J. Geotech. Engrg*., 110(8): 1106-1125.

Kim, I.H., Hong, S.H., Jhung, K.S., Oh, K.H. and Yoon, Y.K. (1991), "Relationship among shock-wave velocity, particle velocity, and adiabatic exponent for dry air." *Journal of Applied Physics*., 70(2): 1048-1050

Kohgo, Y., Nakano, M. and Miyazaki, T. (1993), "Theoretical aspects of constitutive modeling for unsaturated soils." *Soils and Foundations*., 33(4): 49-63.

Krieg, R. D. (1972), A simple constitutive description fro cellular concrete, Report SC-DR-72-0883, Livermore Software Technology Corporation, Livermore, CA.

Lade, P.V. (2005), "Overview of constitutive models for soils." In: *soil constitutive models: Evaluation, selection and calibration*, Geo-frontier Conference of ASCE, Austin, Texas: 1-34.

Livermore Software Technology Corporation (1998), LS-DYNA theoretical manual. Livermore, California.

Livermore Software Technology Corporation (2003), *LS-DYNA Keyword user's manual*. Version 970. Livermore, California.

Loret, B. and Khalili, N. (2000), "A three-phase model for unsaturated soils." *Int.l J. Numer. Anal. Meth. Geomech*., 24:893-927.

Loret, B. and Khalili, N. (2002), "An effective stress elastic-plastic model for unsaturated porous media." *Mechanics of Materials*., 34: 97-116.

Lovetskill, E. E., Maslennikov, A. M. and Fetisov, V. S. (1979), "Dissipation of the energy of an explosion in a porous elastoplastic medium." *J. Applied Mechanics and Technical Physics*., 20(6): 766-770.

Lu, N., Wu, B. and Tan, C.P. (2007), "Tensile strength characteristics of unsaturated sands." *J. Geotech. Geoenviron. Eng*., 133(2): 144-154.

Lu, N and Likos, W. J. (2006), "suction stress characteristic curve for unsaturated soils." *J. Geotech. Geoenviron. Eng*., 132(2): 131-142.

Materials Sciences Corporation (2006). *Methodology for improved characterization of land mine explosions.* Presentation at the Technical Interchange Meeting of SBIR Phase II Plus Program, Contract DAAD17-01-C-0111, Horsham, Pennsylvania.

Matsui, T. and Abe, N. (1985), "Elasto-viscoplastic constitutive equation of normally consolidated clays based on flow surface theory." *Proc. 5th Int. Conf. Numer. Meth. Geomech., Nagoya* 1: 407-413.

Maugin, Gerard A. (1992), *The thermomechanics of plasticity and fracture*, 1st ED., Press Syndicate of University of Cambridge Hemisphere Publishing Corporation., Cambridge, New York, Victoria.

McVay, M. and Taesiri, Y. (1985), "Cyclic behavior of pavement base materials." *Journal of Geotechnical Engineering Div.* ASCE, 111(1): 399-416.

Morgenstern, N.R. (1979), "Properties of compacted clays." *In Contribution to Panel Discussion, Session IV, Proceedings of the 6th Panamerican Conference on Soil Mechanics and Foundation Engineering*, Lima, Peru 3: 349-354.

Murayama, S. and Shibata, T. (1964), "Flow and stress relaxation of clays (theoretical studies on the rheological properties of clay, part I)." *IUTAM Symp. Rheology and Soil Mechanics, Grenoble*, 99-129. *Conf. Soil Mech., San Francisco* 2: 423-426.

Murray, E.J. (2002), "An equation of state for unsaturated soils." *Can. Journal of Geotechnical*., 39: 125-140.

Nagayama, K., Mori, Y., Shimada, K. and Nakahara, M. (2002). "Shock Hugoniot compression curve for water up to 1 GPa by using a compressed gas gun," *Journal of Applied Physics*, 91(1): 476-482.

Perzyna, P. (1966), "Fundamental problems in viscoplasticity." *Adv. Appl. Math*., 9: 243-377.

Prévost, J.H. and Popescu, R. (1996), "Constitutive Relations for Soil Materials." *Electronic Journal of Geotechnical Engineering.* ASCE.

Proud, W.G., Chapman, D.J., Williamson, D.M., Tsembelis, K., Addiss, J., Bragov, A., Lomunov, A., Cullis, I.G., Church, P.D., Gould, P., Porter, D., Cogar, J.R. and Borg, J.

(2007), "The dynamic compaction of sand and related porous systems." *Shock Compression of Condensed Matter*., 2007: 1403-1408.

Qian, Q. H. and Wang, M. Y. (1993), "FEM in saturated soil under explosive loading." *In Proceedings of the 6th International Symposium on Interaction of Nonnuclear Munitions with Structures.* Panama City Beach: Florida, U.S., 1993: 282-288.

Randers-Pehrson, G. and Bannister, K. (1997), *Airblast loading model for DYNA2D and DYNA3D*, ARL-TR-1310, Army Research Laboratory, Aberdeen Proving Ground, MD

Richardson, A. M. and Whitman, R. V. (1963), "Effect of strain rate upon undrained shear resistance of a saturated remoulded fat clay." *Geotechnique*., 13: 310-324.

Roscoe, K.H., Schofield, A.N. and Thurairjah, A. (1963), "Yielding of clays in state wetter than critical." *Geotechnique*., 13(3): 211-240.

Rubin, M. (1991), "Simple, convenient isotropic failure surface." *J. Engineering Mechanics. Div.* ASCE, 117: 348-369.

Russell, A.R. and Khalili, N.A. (2005), "A unified bounding surface plasticity model for unsaturated soils." *International Journal for Numerical and Analytical Methods in Geomechanics*., 30(3): 181-212.

Sandler, I.S., DiMaggio, F.L. and Baladi, G.Y.(1976), "Generalized cap model for geological materials." *J. Geotechnical Engineering. Div.* ASCE, 102(GT7): 683-699.

Sandler, I.S. and Rubin, D. (1979), "An algorithm and a modular subroutine for the cap model." *Int. J. Numer. Analy. Meth. Geomech*., 3: 173-186.

Santagiuliana, R. and Schrefler, B.A. (2006), "Enhancing the Bolzon-Schrefler-Zienkiewicz constitutive model for partially saturated soil." *Transport in Porous Media.*, 65(1): 1-30.

Schwer, L.E. and Murray, Y.D. (1994), "A three-invariant smooth cap model with mixed hardening," *Inter. J. Numer. Analy. Meth. Geomech*., 18: 657-688.

Sedgwick, R. T., Gaffeny, E. S., Wilkins, D. E. and Walsh, L. J. (1974), A combined numerical and experimental investigate of the effect of buried explosive charges, Report DAAK-02-73-C-0103, U.S. Mobility Equipment of Research and Development Center, Ft. Belvoir, VA.

Sheng, D., Fredlund, D.G. and Gens, A. (2008), "A new modeling approach for unsaturated soils using independent stress variables." *Canadian Geotechnical Journal*., 45: 511-534.

Sheng, D., Sloan, S.W. and Gens, A. (2004), "A constitutive model for unsaturated soils: thermomechanical and computational aspects." *Computational Mechanics*., 33(6): 453-465.

Simo, J.C., Ju, J.W., Pister, K.S. and Taylor, R.L. (1988), "Assessment of cap model: consistent return algorithms and rate-dependent extension." *J. Engrg. Mech*., ASCE, 114(2): 191-218.

Singh, After A. and Mitchell, J. K. (1968), "General stress-strain-time function for soils, cture." *J. Soil Mech. Found Div.* ASCE, vol.94, no.SMI, 1968.

Sun, D.A., Sheng, D. and Sloan, S.W. (2007), "Elastoplastic modeling of hydraulic and stress-strain behavior of unsaturated soil." *Mechanics of Materials*., 39(3): 212-221.

Swift, R. S. (1975), "Examination of the mechanical properties for a Kayenta sandstone form the mixed company site." *Technical report DNA3683F*. Washington: Defense Nuclear Agency.

Terzaghi, K. (1936), "The shearing resistance of saturated soils." *In Proceedings of the 1st Internatinoal Conference on Soil Mechanics and Foundation Engineering*, Cambridge, Mass., 1: 54-56.

Tillotson, J.H. (1962), "Metallic Equations of State for Hypervelocity Impact." *General Atomic.* Rep. GA-3216, 137p.

Toll, D.G. (1990), "A framework for unsaturated soil behavior." *Geotechnique*., 40(1): 31-44.

Tong, X.L. (2005), "Finite element simulation of soil behaviors under high strain rate loading." Master thesis, The University of Nebraska-Lincoln, U.S.A.

Tong, X., and Tuan, C.Y. (2007), "Viscoplastic cap model for soils under high strain rate loading." *J. Geotechnical and Geoenvironmental Engineering*., 133: 206-214.

Vaunat, J., Romero, E. and Jommi, C. (2000), "An elastoplastic hy-dromechanical model for unsaturated soils." International Workshop on Unsaturated Soils, 2000, Trento, Italy: 121-138.

Veyera, G.E, Charlie, W.A. and Ross C. A. (1993), "Strain-rate effects in unsaturated soils." *Proceeding of the sixth international symposium on interaction of nonnuclear munitions with structures*. Panama City Beach, Florida: 300-304.

Wang, J. (2001), *Simulation of landmine explosion using LS-DYNA3D software: Benchmark work of simulation of explosion in soil and air*, Report DSTO-TR-1168, Aeronautical and Maritime Research Laboratory, Australia.

Wang, Z., Hao, H., and Lu, Y. (2004). "A three-phase soil model for simulating stress wave propagation due to blast loading," *Int. J. Numer. Anal. Meth. Geomech*., 28: 33-56.

Wang, Z., and Lu, Y. (2003). "Numerical analysis on dynamic deformation mechanism of soils under blast loading," *Soil Dynamics and Earthquake Engineering*: 705-714.

Westine, P.S., Morris, B.L., Cox, P.A. and Polch, E.Z. (1985), *Development of computer program fro floor plate response from land mine explosions*, Technical Report No. 13045, US Army Tank-Automotive Command, Warren, MI.

Wheeler, S.J. (1996), "Inclusion of specific water volume within an elastio-plastic model for unsaturated soil." *Canadian Geotechnical Journal*., 33(1): 42-57.

Wheeler, S.J. and Sivakumar, V. (1995), "An elasto-plastic critical state framework for unsaturated soil." *Geotechnique*., 45(1): 35-53.

Wheeler, S.J., Sharma, R.S. and Buisso, M.S.R. (2003), "Coupling of hydraulic hysteresis and stress-strain behavior in unsaturated soils." *Geotechnique*., 53(1): 41-54.

Whitlow, R. (1995), *Basic soil mechanics*, 3rd Ed., John Wiley & Sons Inc., New York.

Whitman, R.V. (1957), *Testing soils with transient loads*, Philadelphia: American Society for Testing and Materials. STP 232: 242-254.

Willams, K., McClennan, S., Durocher, R. St-Jean, B. and Tremblay, J. (2002), "Validation of a loading model for simulating blast mine effects on armoured vehicles." *In Proceedings of the 7th International LS-DYNA users conference*, Dearborn, MI. 6: 35-44.

Wong, H., Morvan, M. and Branque, D. (2009), "A 13-parameter model for unsaturated soil based on bounding surface plasticity." *Journal of Rock Mechanics and Geotechnical Engineering*., 2(2): 135-142.

Zukas, J.A. (1990). *High Velocity Impact Dynamics*, John Wiley & Sons, New York.

# APPENDIX A

## SUBROUTINE OF USER DEFINED MATERIAL MODEL

```
subroutine umat48(cm,eps,sig,epsp,hsv,dt1,capa,etype,tt,temper,failel,crv)
c     Perzyna's Viscoplastic Cap Model for Soil :
c     cm(1) = young's modulus
c     cm(2) = possion's ratio
c     cm(3) = buckling modulus
c     cm(4) = shear modulus
c     cm(5) = alfa   in Faliure Surface
c     cm(6) = beta   ...
c     cm(7) = gama   ...
c     cm(8) = theta  ...
c     cm(9) = r      cap surface axis ratio
c     cm(10)= d      hardening law exponent
c     cm(11)= w      hardeng law coefficient (limit plastic strain)
c     cm(12)= x0     initial hardening pressure
c     cm(13)= tcut   tension cut off (tcut<=0)
c     cm(14)= conv   convegent factor (default value = 0.001)
c     cm(15)= itmat  maximum iteration number (default value = 1000)
c     hsv(1)=total z-component strain
c     hsv(2)=hardening parameter, kn
c     hsv(3)=volumetric plastic strain, evpn
c     hsv(4)=first stress invariant, J1
c     hsv(5)=second deviatoric stress invariant, SJ2
c     hsv(6)=response mode number, mode

      include 'iounits.inc'
      character*(*) etype
      dimension cm(*),eps(*),sig(*),hsv(*),crv(101,2,*)
      dimension cmat(6,6),dmat(6,6),hr(6,6),hh(6,6),dfds(6),ddfdds(6,6)
      dimension ddfdsl(6),dfaids(6),ab(6),sig1(6),se(6)
      real*4 kn,kn1,ln,ln1,kn10,k0
      logical faille

c     Input the user defined material parameters
      bulk=cm(1)
      gshr=cm(2)
      alfa=cm(3)
      beta=cm(4)
      gama=cm(5)
      theta=cm(6)
```

```
      r=cm(7)
      d=cm(8)
      w=cm(9)
      x0=cm(10)
      tcut=cm(11)
      conv=cm(12)
      itmax=cm(13)
      yita=cm(14)
      fai0=cm(15)
      expon=cm(16)
c     Calculate the initial hardening parameter k0 or input kn
      if (hsv(2).eq.0) then
            if (x0.ge.10000.0) then
              kn=x0
            else
              call capi(x0,r,alfa,beta,gama,theta,k0,ieer)
              if (ieer.eq.10) then
                k0=x0
              endif
              kn=k0
            endif
      else
            kn=hsv(2)
      endif

c     Form the elastic material matrix [cmat] and its reverse matrix [dmat]
      cmatii=bulk+4.0/3.0*gshr
      cmatij=bulk-2.0/3.0*gshr
      cmatjj=gshr
      do 140 i=1,6
      do 140 j=1,6
140   cmat(i,j)=0.0
      do 160 i=1,6
            if (i.le.3) then
              cmat(i,i)=cmatii
              do 150 j=1,3
                if (i.ne.j) cmat(i,j)=cmatij
150           continue
            else
              cmat(i,i)=cmatjj
            endif
160   continue
      call mrevs(6,cmat,dmat)

c     Calculate the elastic trial strss {sig1} = {sig0} + [cmat]:{eps}
```

```
          do 180 i=1,6
            aa=0.0
            do 170 j=1,6
              aa=aa+cmat(i,j)*eps(j)
 170      continue
            sig1(i)=-(sig(i)+aa)
 180   continue

c    Given other initial values
      if (kn.ge.10000.0) then
            xn=x0
          else
        xn=kn+r*(alfa-gama*exp(-beta*kn)+theta*kn)
          endif
          evpn0=w*(1-exp(-d*(xn-x0)))
          dlamd=0.0
          dk=0.0
          kn1=kn
c    Deal with tension cutoff
      sj1e=sig1(1)+sig1(2)+sig1(3)
      if (sj1e.gt.(-tcut)) goto 450
      sj1n1=-tcut
      ppe=sj1e/3.0
          ppt=sj1n1/3.0
          dse=0.0
      do 190 i=1,6
            if (i.le.3) then
          se(i)=sig1(i)-ppe
              fmu=1.0
            else
              se(i)=sig1(i)
              fmu=2.0
            endif
            dse=dse+fmu*se(i)*se(i)
 190   continue
     sj2e=sqrt(0.5*dse)
          sj2n1=sj2e
          sj2t=alfa-gama*exp(-beta*(-tcut))+theta*(-tcut)
          if (sj2e.gt.sj2t) sj2n1=sj2t
     ratio=0.0
          if (sj2e.ne.0.0) ratio=sj2n1/sj2e
          do 200 i=1,6
            if (i.le.3) then
              sig1(i)=se(i)*ratio+ppt
            else
```

```
            sig1(i)=se(i)*ratio
          endif
200   continue
      goto 800

c     Check other status of the elastic trial stress
450   continue
          call differ(sig1,kn1,fai,dfds,ddfdds,ddfdsl,dfaids,dfaidl,hsk
     $     ,mode,alfa,beta,gama,theta,r,d,w,x0,tcut,yita,fai0,expon)
          if (mode.eq.0) goto 800
          residi=fai-dlamd/yita/dt1

c *** local iteration to fulfill: residi = fai - dlamd/yita/dt => convergence
          itt=0
500   itt=itt+1
c     2.1: [hh] = | [cmat] + dlamd*[ddfdds] |-1
      do 510 i=1,6
          do 510 j=1,6
510   hr(i,j)=dmat(i,j)+dlamd*ddfdds(i,j)
      call mrevs(6,hr,hh)
c     2.2: divd = {dfaids}:[hh]:{dlamd*{ddfdsl}+{dfds}} + 1/yita/tt - dfaidl
      divd=0.0
          do 520 i=1,6
          ab(i)=0.0
          do 520 j=1,6
          ab(i)=ab(i)+hh(i,j)*(dlamd*ddfdsl(j)+dfds(j))
520   continue
      do 530 i=1,6
          divd=divd+ab(i)*dfaids(i)
530   continue
      divd=divd+1.0/yita/dt1-dfaidl
c     2.3: dlamd = dlamd + residi/divd ;
      dlamd=dlamd+residi/divd
c     2.4: {sig1} = {sig} + [cmat]*{{eps}-dlamd*{dfds}}
      devpn=0.0
      do 550 i=1,6
            ac=0.0
            do 540 j=1,6
            ac=ac+cmat(i,j)*(-eps(j)-dlamd*dfds(j))
540       continue
        sig1(i)=-sig(i)+ac
            if (i.le.3) devpn=devpn+dlamd*dfds(i)
550   continue

          if (kn.ge.10000.0) then
```

```
            kn1=kn
          else
            evpn1=evpn0+devpn
            if (evpn1.ge.w) evpn1=0.9*w
        xn1=-1.0/d*log(1.0-evpn1/w)+x0
        kn10=kn1
            itk=0
 570    continue
        itk=itk+1
        ff=kn10+r*(alfa-gama*exp(-beta*kn10)+theta*kn10)-xn1
            if (abs(ff).lt.abs(conv*kn10)) goto 580
            dfekn=gama*beta*exp(-beta*kn10)+theta
            kn1=kn10-ff/(1.0+r*dfekn)
            kn10=kn1
            if (itk.ge.itmax) then
c             write(6,*)'not convergence for kn1-kn-ff',kn1,kn,ff
              goto 580
        endif
            goto 570
 580    continue
      endif
c 2.5: residi(new) = fai - dlamd/yita/dt
      call differ(sig1,kn1,fai,dfds,ddfdds,ddfdsl,dfaids,dfaidl,hsk
     $    ,mode,alfa,beta,gama,theta,r,d,w,x0,tcut,yita,fai0,expon)
          residi=fai-dlamd/yita/dt1
c 2.6: check if the convergence condition is satisfied
          if (abs(residi).lt.abs(conv)) goto 800
          if (itt.ge.itmax) then
            write(6,*) 'NOT CONVERGE',itt,residi
          else
            goto 500
          endif
c *** local iteration end
 800  continue
c Output the variables
      do 820 i=1,6
 820    sig(i)=-sig1(i)

          hsv(1)=hsv(1)+eps(3)
          hsv(2)=kn1
c         write(6,*)'output',mode,kn1,kn
          xn1=kn1+r*(alfa-gama*exp(-beta*kn1)+theta*kn1)
          hsv(3)=hsv(3)+w*(1.0-exp(-d*(xn1-x0)))
          pn1=(sig(1)+sig(2)+sig(3))/3.0
          hsv(4)=pn1*3.0
```

```
      dsig11=sig(1)-pn1
      dsig22=sig(2)-pn1
      dsig33=sig(3)-pn1
      dsa=dsig11*dsig11+dsig22*dsig22+dsig33*dsig33
      dse=sig(4)**2+sig(5)**2+sig(6)**2

      hsv(5)=sqrt(0.5*dsa+dse)
      hsv(6)=float(mode)
      return
      end

c determine the initial hardening parameter k0 according to x0
c
    subroutine capi_dup(x0,r,alfa,beta,gama,theta,k0,ieer)
      real*4 kn,k0
      ieer=0
      cretia=1e-5*(alfa-gama)
      itc=0
      k0=0.0
 40   f0=alfa-gama*exp(-beta*k0)+theta*k0
      dfek0=gama*beta*exp(-beta*k0)+theta
      f=k0+r*f0-x0
      if (abs(f).lt.cretia) goto 60
      kn=k0-f/(1.0+r*dfek0)
      k0=kn
      itc=itc+1

      if (itc.gt.60) goto 50
      goto 40
 50   ieer=10
 60   return
      end

c
c calcuate the reverse matrix
c
    subroutine mrevs(ns,cmat,dmat)
      dimension cmat(ns,ns),dmat(ns,ns)
      do 100 i=1,ns
      do 100 j=1,ns
100   dmat(i,j)=cmat(i,j)
      do 200 n=1,ns
        diag=dmat(n,n)
        do 130 j=1,ns
130   dmat(n,j)=-dmat(n,j)/diag
```

```
      do 150 i=1,ns
        if (n.eq.i) goto 150
        do 140 j=1,ns
          if (n.eq.j) goto 140
          dmat(i,j)=dmat(i,j)+dmat(i,n)*dmat(n,j)
140     continue
150   dmat(i,n)=dmat(i,n)/diag
      dmat(n,n)=1.0/diag
200   continue
      return
      end

c   calcuate the flow vector of failure surface

      subroutine differ(ssn1,kn1,fai,dfds,ddfdds,ddfdsl,dfaids,dfaidl,
     $ hsk,mode,alfa,beta,gama,theta,r,d,w,x0,tcut,yita,fai0,expon)
      real*4 kn1,ln1
      dimension ssn1(6),dfds(6),ddfdds(6,6),ddfdsl(6),dfaids(6)
      dimension dj1ds(6),dj2ds(6),se(6),amat(6,6)
c   Get the basic flow vector : dj1ds = {dj1/ds}; dj2ds = {dj2/ds}
      sj1=ssn1(1)+ssn1(2)+ssn1(3)
      pp0=sj1/3.0
      toth=2.0/3.0
      aa=0.0
      do 120 i=1,6
        if (i.le.3) then
          dj1ds(i)=1.0
        else
        dj1ds(i)=0.0
        endif
        se(i)=ssn1(i)-dj1ds(i)*pp0
        if (i.le.3) then
          dj2ds(i)=se(i)
        else
          dj2ds(i)=2.0*se(i)
        endif
        aa=aa+se(i)*dj2ds(i)
        do 100 j=1,6
          amat(i,j)=0.0
          if (i.eq.j) then
            if (i.le.3) amat(i,j)=toth
            if (i.gt.3) amat(i,j)=2.0
          else
            if (i.le.3.and.j.le.3) amat(i,j)=-0.5*toth
          endif
```

```
 100     continue
 120  continue
      sj2=sqrt(0.5*aa)
c     Check the stress status: Mode = 0 -> elastic ; -1 -> tension;
c                              1 -> failure ;  2 -> cap
      mode=0
           fval=0.0
           dfj1=0.0
           dfj2=0.0
           ddfj1=0.0
           ddfj2=0.0
           ddfj12=0.0
           ddfj1k=0.0
           ddfj2k=0.0
           dkdl=0.0
           dfdk=0.0
           ln1=max(kn1,0.0)
c          if (sj1.le.-tcut) then
c            write(6,*)'differ-1',sj1,-tcut,ln1
c            fval=sj2-(-tcut)
c            dfj1=1.0
c            if (fval.gt.0.0) mode=-1
c          else if (sj1.gt.-tcut.and.sj1.le.ln1) then
           if (sj1.le.ln1) then
             fval=sj2-(alfa-gama*exp(-beta*sj1)+theta*sj1)
             dfj1=-gama*beta*exp(-beta*sj1)-theta
             dfj2=0.5/sj2
             ddfj1=gama*beta*beta*exp(-beta*sj1)
             ddfj2=-0.25/sj2/sj2/sj2
             if (fval.gt.0.0) mode=1
           else
             xn1=kn1+r*(alfa-gama*exp(-beta*kn1)+theta*kn1)
             a1=(sj1-ln1)/r
             a1r=a1/r
             a2=(xn1-ln1)/r
             aa=sqrt(a1*a1+sj2*sj2)
             a3=1.0/aa/aa/aa
             fval=aa-a2
             dfj1=a1/aa/r
             dfj2=0.5/aa
             ddfj1=-a1r*a1r*a3+1.0/aa/r/r
             ddfj2=-0.25*a3
             ddfj12=-0.5*a1r*a3
             dldk=0.0
             if (kn1.gt.0) dldk=1.0
```

```
            ddfj1k=-ddfj1*dldk
            ddfj2k=-ddfj12*dldk
            dfedl=gama*beta*exp(-beta*kn1)+theta
            dkdl=3.0*dfj1/(w*d*exp(-d*(xn1-x0)))/(1.0+r*dfedl)
            dfdk=-dfj1*dldk-dfedl*dldk
            if (fval.gt.0.0) mode=2
          endif
          if (fval.le.0.0) goto 800
c
c    MODE != 0 --> viscoplasticity
c     dfai=dfai/df ;  dfaidl=dfai/dlamd ; dfds=df/ds ; ddfdds=ddf/dds
c
          fai=(fval/fai0)**expon
          dfai=expon*(fval/fai0)**(expon-1.0)/fai0
          hsk=dkdl
          dfaidl=dfai*dfdk*dkdl
          do 140 i=1,6
            dfds(i)=dfj1*dj1ds(i)+dfj2*dj2ds(i)
            ddfdsl(i)=(ddfj1k*dj1ds(i)+ddfj2k*dj2ds(i))*dkdl
            dfaids(i)=dfai*dfds(i)
 140      continue
          do 160 i=1,6
          do 160 j=1,6
          ddfdds(i,j)=ddfj1*dj1ds(i)*dj1ds(j)+ddfj12*(dj1ds(i)*dj2ds(j)+
     $    dj1ds(j)*dj2ds(i))+ddfj2*dj2ds(i)*dj2ds(j)+dfj2*amat(i,j)
 160      continue
 800      return
          End
```

# APPENDIX B

## SUBROUTINE OF USER DEFINED EOS MODEL

```
      subroutine ueos23s(iflag,cb,pnew,hist,rho0,eosp,specen,
     & df,dvol,v0,pc,dt,tt,crv,first)

c***  variables
c         iflag ----- =0 calculate bulk modulus
c                     =1 update pressure and energy
c         cb -------- bulk modulus
c         pnew ------ new pressure
c         hist ------ history variables
c         rho0 ------ reference density
c         eosp ------ EOS constants
c         specen ---- energy/reference volume
c         df -------- volume ratio, v/v0 = rho0/rho
c         dvol ------ change in volume over time step
c         v0 -------- reference volume
c         pc -------- pressure cut-off
c         dt -------- time step size
c         tt -------- current time
c         crv ------- curve array
c         first ----- logical .true. for tt,crv,first time step
c                     (for initialization of the history variables)
c
      include 'nlqparm'
      logical first
      dimension hist(*),eosp(*),crv(101,2,*)
      real*4 As,Aw,Aa,dvols,dvolw,dvola

c     solid,water,air--precent
      As0 =eosp(1)
      Aw0 =eosp(2)
      Aa0 =eosp(3)

c     solid,water,air--density
      rs =eosp(4)
      rw =eosp(5)
      ra =eosp(6)

c     solid,water,air--ks,kw,ka
      sk =eosp(7)
```

```
      wk =eosp(8)
       ak =eosp(9)

c     input parameters--mixed soil
      c  =eosp(10)
      s1 =eosp(11)
      s2 =eosp(12)
      s3 =eosp(13)
      g0 =eosp(14)
      sa =eosp(15)
      s11=s1-1.
      s22=2.*s2
      s33=3.*s3
      s32=2.*s3
      sad2=.5*sa
      g0d2=1.-.5*g0
      roc2=rho0*c**2

c     input parameters--solid
      cs  =eosp(16)
      ss1 =eosp(17)
      ss2 =eosp(18)
      ss3 =eosp(19)
      gs0 =eosp(20)
      ssa =eosp(21)
      ss11=ss1-1.
      ss22=2.*ss2
      ss33=3.*ss3
      ss32=2.*ss3
      sads2=.5*ssa
      g0ds2=1.-.5*gs0
      rocs2=rs*cs**2

c     input parameters--water
      cw  =eosp(22)
      sw1 =eosp(23)
      sw2 =eosp(24)
      sw3 =eosp(25)
      gw0 =eosp(26)
      swa =eosp(27)
      sw11=sw1-1.
      sw22=2.*sw2
      sw33=3.*sw3
      sw32=2.*sw3
      sadw2=.5*swa
```

```
      g0dw2=1.-.5*gw0
      rocw2=rw*cw**2

c     input parameters--air
      ca  =eosp(28)
      sa1 =eosp(29)
      sa2 =eosp(30)
      sa3 =eosp(31)
      ga0 =eosp(32)
      saa =eosp(33)
      sa11=sa1-1.
      sa22=2.*sa2
      sa33=3.*sa3
      sa32=2.*sa3
      sada2=.5*saa
      g0da2=1.-.5*ga0
      roca2=ra*ca**2

      p0  =eosp(34)

          if (hist(1).eq.0) then
            hist(1)=As0
            hist(2)=Aw0
            hist(3)=Aa0
            hist(4)=0.0
            hist(5)=0.0
            hist(6)=0.0
            As=hist(1)
            Aw=hist(2)
            Aa=hist(3)
            dvols=hist(4)
            dvolw=hist(5)
            dvola=hist(6)
          else
            As=hist(1)
            Aw=hist(2)
            Aa=hist(3)
            dvols=hist(4)
            dvolw=hist(5)
            dvola=hist(6)
          endif

          RRs=As*rs/rho0
          RRw=Aw*rw/rho0
          RRa=Aa*ra/rho0
```

```
            specens=specen*RRs
            specenw=specen*RRw
            specena=specen*RRa

            Vsold=(df*v0-2.0*dvol)*As
            Vwold=(df*v0-2.0*dvol)*Aw
            Vaold=(df*v0-2.0*dvol)*Aa

c***  calculate the bulk modulus for the EOS contribution to the sound speed
      if (iflag.eq.0) then
c     from solid
      xmu=1.0/df-1.
      dfmu=df*xmu
      facp=.5*(1.+sign(1.,xmu))
      facn=1.-facp
      xnum=1.+xmu*(+g0d2-sad2*xmu)
      xdem=1.-xmu*(s11+dfmu*(s2+s3*dfmu))
      tmp=facp/(xdem*xdem)
      a=roc2*xmu*(facn+tmp*xnum)
      b=g0+sa*xmu
      pnum=roc2*(facn+facp*(xnum+xmu*(g0d2-sa*xmu)))
      pden=2.*xdem*(-s11 +dfmu*(-s22+dfmu*(s2-s33+s32*dfmu)))
      cb=pnum*(facn+tmp)-tmp*a*pden+sa*specen+
     &       b*df**2*max(pc,(a+b*specen))

      if (cb.lt.0.02) then
         cb=cb
      else
         cb=0.02
      endif

c***  update the pressure and internal energy
      else

c     from solid
      dfs=df*(As/As0)
      xmus=1.0/dfs-1.
      dfmus=dfs*xmus
      facps=.5*(1.+sign(1.,xmus))
      facns=1.-facps
      xnums=1.+xmus*(+g0ds2-sads2*xmus)
      xdems=1.-xmus*(ss11+dfmus*(ss2+ss3*dfmus))
      tmps=facps/(xdems*xdems)
      a=rocs2*xmus*(facns+tmps*xnums)
```

```
      b=gs0+ssa*xmus
      dvov0s=.5*(dvols)/(As0*v0)
      denoms=1.+b*dvov0s
      pnews=(a+specens*b)/max(1.e-6,denoms)
      pnews=max(pnews,pc)

      specens=specens-pnews*dvov0s


c     from water
      dfw=df*(Aw/Aw0)
      xmuw=1.0/dfw-1.
      dfmuw=dfw*xmuw
      facpw=.5*(1.+sign(1.,xmuw))
      facnw=1.-facpw
      xnumw=1.+xmuw*(+g0dw2-sadw2*xmuw)
      xdemw=1.-xmuw*(sw11+dfmuw*(sw2+sw3*dfmuw))
      tmpw=facpw/(xdemw*xdemw)
      a=rocw2*xmuw*(facnw+tmpw*xnumw)
      b=gw0+swa*xmuw
      dvov0w=.5*(dvolw)/(Aw0*v0)
      denomw=1.+b*dvov0w
      pneww=(a+specenw*b)/max(1.e-6,denomw)
      pneww=max(pneww,pc)

      specenw=specenw-pneww*dvov0w

c     from air
      dfa=df*(Aa/Aa0)
      xmua=1.0/dfa-1.
      dfmua=dfa*xmua
      facpa=.5*(1.+sign(1.,xmua))
      facna=1.-facpa
      xnuma=1.+xmua*(+g0da2-sada2*xmua)
      xdema=1.-xmua*(sa11+dfmua*(sa2+sa3*dfmua))
      tmpa=facpa/(xdema*xdema)
      a=roca2*xmua*(facna+tmpa*xnuma)
      b=ga0+saa*xmua
      dvov0a=.5*(dvola)/(Aa0*v0)
      denoma=1.+b*dvov0a
      pnewa=(a+specena*b)/max(1.e-6,denoma)
      pnewa=max(pnewa,pc)

      specena=specena-pnewa*dvov0a
```

```
 if (pnews/=0.0.AND.pneww/=0.0.AND.pnewa/=0.0.AND.dvol/=0.0) then
    pnew=(pnews*dvols+pneww*dvolw+pnewa*dvola)/dvol
 else
     pnew=pnews+pneww+pnewa
 endif

      specen=specens+specenw+specena

      As=As*(sk*(pnews-p0)/(rs*cs**2)+1)**(-(sk)**(-1))
      Aw=Aw*(wk*(pneww-p0)/(rw*cw**2)+1)**(-(wk)**(-1))
      Aa=Aa*(pnewa/p0)**(-(ak)**(-1))

      hist(1)=As
      hist(2)=Aw
      hist(3)=Aa

      dvols=df*v0*As-Vsold
      dvolw=df*v0*Aw-Vwold
      dvola=df*v0*Aa-Vaold

      hist(4)=dvols
      hist(5)=dvolw
      hist(6)=dvola


endif
return
end
```

# APPENDIX C

## LS-DYNA INPUT DECK

```
$---+----1----+----2----+----3----+----4----+----5----+----6----+----7----+----8
$  LS-DYNA(971) DECK WRITTEN BY : eta/FEMB-PC version 28.0
$  ENGINEER :
$  PROJECT :
$  UNITS : MM, TON, SEC,  N
$  TIME : 03:01:01 PM
$  DATE : FRIDAY, Aug 20, 2010
$---+----1----+----2----+----3----+----4----+----5----+----6----+----7----+----8
*KEYWORD
$---+----1----+----2----+----3----+----4----+----5----+----6----+----7----+----8
*TITLE
dob32.dyn (explosive)
$---+----1----+----2----+----3----+----4----+----5----+----6----+----7----+----
$---+----1----+----2----+----3----+----4----+----5----+----6----+----7----+----8
$                                                                              $
$                                CONTROL CARD                                  $
$                                                                              $
$---+----1----+----2----+----3----+----4----+----5----+----6----+----7----+----8
*CONTROL_ACCURACY
$      OSU       INN    PIDOSU
         1         3
*CONTROL_ALE
$      DCT      NADV      METH      AFAC      BFAC      CFAC      DFAC      EFAC
         2         1         2      -1.0       0.0       0.0       0.0       0.0
$    START       END     AAFAC     VFACT      PRIT       EBC      PREF   NSIDEBC
       0.0       0.0       0.0       0.0       0.0         0       0.0
*CONTROL_ENERGY
$     HGEN      RWEN    SLNTEN     RYLEN
         2         2         1         1
*CONTROL_HOURGLASS
$      IHQ        QH
         4       0.1
*CONTROL_CONTACT
$   SLSFAC    RWPNAL    ISLCHK    SHLTHK    PENOPT    THKCHG     ORIEN    ENMASS
         1       0.0         1         0         1         0         1         0
$   USRSTR    USRFRC     NSBCS    INTERM     XPENE     SSTHK      ECDT   TIEDPRJ
         0         0        10         0       4.0         0         0         0
*CONTROL_OUTPUT
$    NPOPT    NEECHO    NREFUP    IACCOP     OPIFS    IPNINT    IKEDIT    IFLUSH
         0         0         0         0       0.0
$    IPRTF
         0
*CONTROL_TIMESTEP
$   DTINIT    TSSFAC      ISDO    TSLIMT     DT2MS      LCTM     ERODE      MS1ST
   1.0e-04       0.2         0       0.0       0.0         0         1         0
$   DT2MSF
       0.0
*CONTROL_TERMINATION
$   ENDTIM    ENDCYC     DTMIN    ENDENG    ENDMAS
    1000.0         0       1.0       0.0       0.0


$---+----1----+----2----+----3----+----4----+----5----+----6----+----7----+----8
```

```
$                                                                             $
$                        DATABASE CONTROL FOR BINARY                          $
$                                                                             $
$---+----1----+----2----+----3----+----4----+----5----+----6----+----7----+----8
*DATABASE_BINARY_D3PLOT
$  DT/CYCL      LCDT      BEAM     NPLTC
       5.0
*DATABASE_BINARY_D3THDT
$  DT/CYCL      LCDT
       5.0

$---+----1----+----2----+----3----+----4----+----5----+----6----+----7----+----8
$                                                                             $
$                             DATABASE EXTENT CARDS                           $
$                                                                             $
$---+----1----+----2----+----3----+----4----+----5----+----6----+----7----+----8
*DATABASE_EXTENT_BINARY
$^
$    NEIPH     NEIPS    MAXINT    STRFLG    SIGFLG    EPSFLG    RLTFLG    ENGFLG
        15                             1
$   CMPFLG    IEVERP    BEAMIP     DCOMP      SHGE     STSSZ    N3THDT   IALEMAT
                  0
$  NINTSLD
$         1
$---+----1----+----2----+----3----+----4----+----5----+----6----+----7----+----8
$                                                                             $
$                                  PART CARDS                                 $
$                                                                             $
$---+----1----+----2----+----3----+----4----+----5----+----6----+----7----+----8
*PART
$HEADING
SOIL
$      PID     SECID       MID     EOSID      HGID      GRAV    ADPOPT      TMID
         1         1        12         6
*PART
$HEADING
C4
$      PID     SECID       MID     EOSID      HGID      GRAV    ADPOPT      TMID
         2         2         2         2
*PART
$HEADING
AIR
$      PID     SECID       MID     EOSID      HGID      GRAV    ADPOPT      TMID
         3         3         3         1
$---+----1----+----2----+----3----+----4----+----5----+----6----+----7----+----8
$                                                                             $
$                                SECTION CARDS                                $
$                                                                             $
$---+----1----+----2----+----3----+----4----+----5----+----6----+----7----+----8
*SECTION_SOLID_ALE
$    SECID    ELFORM       AET
         1        11
$     AFAC      BFAC      CFAC      DFAC     START       END     AAFAC
       0.0       0.0       0.0       0.0       0.0       0.0       0.0
*SECTION_SOLID_ALE
$    SECID    ELFORM       AET
         2        11
$     AFAC      BFAC      CFAC      DFAC     START       END     AAFAC
       0.0       0.0       0.0       0.0       0.0       0.0       0.0
*SECTION_SOLID_ALE
$    SECID    ELFORM       AET
```

```
         3        11
$     AFAC      BFAC      CFAC      DFAC     START       END     AAFAC
       0.0       0.0       0.0       0.0       0.0       0.0       0.0
$---+----1----+----2----+----3----+----4----+----5----+----6----+----7----+----8
$                                                                        $
$                                MATERIAL CARDS                          $
$                                                                        $
$---+----1----+----2----+----3----+----4----+----5----+----6----+----7----+----8
*MAT_SOIL_AND_FOAM
$^M-1
$      MID        RO         G      BULK        A0        A1        A2        PC
         1       1.8 0.0006385      0.303.4000E-137.0330E-07      0.30-6.900E-08
$       VCR       REF
       0.0       0.0
$      EPS1      EPS2      EPS3      EPS4      EPS5      EPS6      EPS7      EPS8
       0.0    -0.104    -0.161    -0.192    -0.224    -0.246    -0.271    -0.283
$      EPS9     EPS10
     -0.29     -0.40
$       P1        P2        P3        P4        P5        P6        P7        P8
       0.0   0.00020   0.00040   0.00060    0.0012    0.0020    0.0040    0.0060
$       P9       P10
    0.0080     0.041
*MAT_USER_DEFINED_MATERIAL_MODELS
$      MID        RO        MT       LMC       NHV    IORTHO     IBULK        IG
        11  1.800000        46        16        10         0         3         4
$    IVECT     IFAIL    ITHERM    IHYPER      IEOS
         0         0         0         0         0
$        E        MU      BULK         G      ALFA      BETA      GAMA     THETA
       0.0       0.0  0.0010646.3850e-046.4200e-05 3428.30005.8900e-06  0.182500
$        R         D         W        X0      TCUT      CONV     ITMAX
  5.000000 952.00000  0.214200       0.06.9000e-08  0.001000 60.000000   0.00e+0
*MAT_USER_DEFINED_MATERIAL_MODELS
$      MID        RO        MT       LMC       NHV    IORTHO     IBULK        IG
        12   2.05500        48        16         9         0         1         2
$    IVECT     IFAIL    ITHERM    IHYPER      IEOS
         0         0         0         0         1
$     BULK         G      ALFA      BETA      GAMA     THETA         R         D
  0.0100002.0000e-046.2500e-07 3643.00003.2000e-08  0.249000  5.320000   0.00884
$        W        X0      TCUT      CONV     ITMAX      YITA      FAI0     EXPON
  0.225000  0.001e-31.2000e-08  0.001000 60.000000  0.200e-1       1.2       1.0
*MAT_HIGH_EXPLOSIVE_BURN
$^M-2
$      MID        RO         D       PCJ      BETA         K         G      SIGY
         2     1.601    0.8193      0.28       0.0       0.0       0.0       0.0
*INITIAL_DETONATION
$      PID         X         Y         Z        LT
         2       0.0       0.0      -4.0
*MAT_NULL
$^M-3
$      MID        RO        PC        MU     TEROD     CEROD        YM        PR
         3   0.00129       0.0       0.0       0.0       0.0       0.0       0.0
$---+----1----+----2----+----3----+----4----+----5----+----6----+----7----+----8
$                                                                        $
$                                 EOS CARDS                              $
$                                                                        $
$---+----1----+----2----+----3----+----4----+----5----+----6----+----7----+----8
*EOS_JWL
$^EQUATION_2
$    EOSID         A         B        R1        R2     OMEGA        E0        V0
         2    6.0997    0.1295       4.5       1.4      0.25     0.090       1.0
*EOS_LINEAR_POLYNOMIAL
```

```
$^EQUATION_1
$    EOSID        C0        C1        C2        C3        C4        C5        C6
         1-0.0000010       0.0       0.0       0.0      0.40      0.40       0.0
$       E0        V0
 0.0000025       1.0
*EOS_GRUNEISEN
$^EQUATION_4
$    EOSID         C        S1        S2        S3     GAMAO         A        E0
         4     0.032      4.92       0.0       0.0      1.11       0.0       0.0
$       V0
       1.0
*EOS_USER_DEFINED
$^EQUATION_5
$    EOSID      EOST       LMC       NHV     IVECT        EO        VO      BULK
         5        21         6         6         0       0.0       1.0  0.002064
$        C        S1        S2        S3     GAMAO         A
     0.032      4.92       0.0       0.0      0.11       0.0
*EOS_USER_DEFINED
$^EQUATION_6
$    EOSID      EOST       LMC       NHV     IVECT        EO        VO      BULK
         6        23        34         6         0       0.0       1.0       0.0
$      As0       Aw0       Aa0        Rs        Rw        Ra        ks        kw
       0.7       0.2       0.1      2.65       1.0    0.0012       3.0       7.0
$       ka         C        S1        S2        S3     GAMAO         A       C-s
       1.4     0.032      4.92       0.0       0.0      0.11       0.0    0.6319
$     S1-s      S2-s      S3-s   GAMAO-s       A-s       C-w      S1-w      S2-w
      1.41       0.0       0.0       1.0       0.0     0.146       2.0       0.0
$     S3-w   GAMAO-w       A-w       C-a      S1-a      S2-a      S3-a   GAMAO-a
       0.0       0.6       0.0   0.02406    1.0602       0.0       0.0       0.4
$      A-a        P0
       0.0   1.0e-07
$---+----1----+----2----+----3----+----4----+----5----+----6----+----7----+----8
$                                                                             $
$                              SEGMENT SET CARDS                              $
$                                                                             $
$---+----1----+----2----+----3----+----4----+----5----+----6----+----7----+----8
*SET_SEGMENT
$^SEGMENT_SET 1
$      SID       DA1       DA2       DA3       DA4
         1       0.0       0.0       0.0       0.0
$       N1        N2        N3        N4        A1        A2        A3        A4
      3278      3292      7092      7086       0.0       0.0       0.0       0.0
      6870      6876      6900      6894       0.0       0.0       0.0       0.0
      .
      .
      .
      7816      7817      7799      7798       0.0       0.0       0.0       0.0
      7817      7818      7800      7799       0.0       0.0       0.0       0.0
$---+----1----+----2----+----3----+----4----+----5----+----6----+----7----+----8
$                                                                             $
$                                NODE SET CARDS                               $
$                                                                             $
$---+----1----+----2----+----3----+----4----+----5----+----6----+----7----+----8
*SET_NODE_LIST
$^
$      SID       DA1       DA2       DA3       DA4
         1       0.0       0.0       0.0       0.0
$     NID1      NID2      NID3      NID4      NID5      NID6      NID7      NID8
       121       122       123       124       129       130       135       136
       141       142       145       148       153       154       157       160
```

```
      .
      .
      .
      1665      1667      1675      1677      1679      1681      1683      1685
      7651      7667      7668      7672      7689      7691      7693      7722
      7724      7726      7728      7730      7746      7747      7751      7768
      7770      7772      7801      7803      7805      7807      7809
*SET_NODE_LIST
$^SPC CARD AT NODE SET 2
$      SID       DA1       DA2       DA3       DA4
         2       0.0       0.0       0.0       0.0
$     NID1      NID2      NID3      NID4      NID5      NID6      NID7      NID8
        13        14        15        16        23        24        31        32
        39        40        44        48        55        56        60        64
        .
        .
        .
        71        72        76        80        87        88        92        96
      7758      7760      7777      7779      7781      7783      7785
*SET_NODE_LIST
$^SPC CARD AT NODE SET 3
$      SID       DA1       DA2       DA3       DA4
         3       0.0       0.0       0.0       0.0
$     NID1      NID2      NID3      NID4      NID5      NID6      NID7      NID8
       213       214       223       232       241       250       259      3854
      3863      3872       472       473       482       491       500       509
       518      1261      1277      1293      1309      1325      1341      1740
      1756      1772      1788      1804      1820      3561      3577      4049
      4058      4067      4076      4085      4094      4383      4392      4401
      4410      4419      4428      4437      4446      4455      4464      5143
      5159      5175      5191      5207      5223      5624      5640      5656
      5672      5688      5704      7360      7376      7392      7597      7676
      7755
*SET_NODE_LIST
$^SPC CARD AT NODE SET 4
$      SID       DA1       DA2       DA3       DA4
         4       0.0       0.0       0.0       0.0
$     NID1      NID2      NID3      NID4      NID5      NID6      NID7      NID8
      2195      2920      2921      2945      2969      2993      3017      3041
      3065      3089      3113      3137      3161      3185      3209      3233
      .
      .
      .
      3580      3579      3585      3583      3581      3578
$---+----1----+----2----+----3----+----4----+----5----+----6----+----7----+----8
$                                                                              $
$                        BOUNDARY NON REFLECTING CARDS                         $
$                                                                              $
$---+----1----+----2----+----3----+----4----+----5----+----6----+----7----+----8
*BOUNDARY_NON_REFLECTING
$^NON-REFLECTING CARD 1
$     SSID        AD        AS
         1       0.0       0.0
$---+----1----+----2----+----3----+----4----+----5----+----6----+----7----+----8
$                                                                              $
$                              BOUNDARY SPC CARDS                              $
$                                                                              $
$---+----1----+----2----+----3----+----4----+----5----+----6----+----7----+----8
*BOUNDARY_SPC_SET_ID
$       ID
         1
```

```
$     NSID       CID      DOFX      DOFY      DOFZ     DOFRX     DOFRY     DOFRZ
         1         0         0         1         0         1         0         1
         2
         2         0         1         0         0         0         1         1
         3
         3         0         1         1         0         1         1         1
         4
         4         0         1         1         1         1         1         1
$---+----1----+----2----+----3----+----4----+----5----+----6----+----7----+----8
$                                                                               $
$                                  ALE CARDS                                    $
$                                                                               $
$---+----1----+----2----+----3----+----4----+----5----+----6----+----7----+----8
*ALE_MULTI-MATERIAL_GROUP
$^ALE_1
$     PSID    IDTYPE
         1         1
*ALE_MULTI-MATERIAL_GROUP
$^ALE_2
$     PSID    IDTYPE
         2         1
*ALE_MULTI-MATERIAL_GROUP
$^ALE_3
$     PSID    IDTYPE
         3         1
$---+----1----+----2----+----3----+----4----+----5----+----6----+----7----+----8
$                                                                               $
$                              NODE INFORMATION                                 $
$                                                                               $
$---+----1----+----2----+----3----+----4----+----5----+----6----+----7----+----8
*NODE
$    NID               X               Y               Z      TC      RC
       1        2.262741        2.262741             0.0     0.0     0.0
       2        2.041828        2.041828             0.0     0.0     0.0
       3        1.422222        2.380852             0.0     0.0     0.0
       .
       .
    7818        51.96153            30.0           110.0     0.0     0.0
$---+----1----+----2----+----3----+----4----+----5----+----6----+----7----+----8
$                                                                               $
$                            ELEMENTS INFORMATION                               $
$                                                                               $
$---+----1----+----2----+----3----+----4----+----5----+----6----+----7----+----8
$---+----1----+----2----+----3----+----4----+----5----+----6----+----7----+----8
$                                                                               $
$                              SOLID ELEMENTS                                   $
$                                                                               $
$---+----1----+----2----+----3----+----4----+----5----+----6----+----7----+----8
*ELEMENT_SOLID
$    EID     PID    NID1    NID2    NID3    NID4    NID5    NID6    NID7    NID8
       1       1       1       2       3       4       5       6       7       8
       2       1       4       3       9      10       8       7      11      12
       .
       .
       .
    6398       3    7737    7738    7720    7719    7816    7817    7799    7798
    6399       3    7738    7739    7721    7720    7817    7818    7800    7799
$---+----1----+----2----+----3----+----4----+----5----+----6----+----7----+----8
*END
```